

Institut für Theoretische Teilchenphysik
Karlsruher Institut für Technologie

Supersymmetric Flavour Changing Neutral Currents beyond Minimal Flavour Violation

zur Erlangung des akademischen Grades eines
Doktors der Naturwissenschaften

von der Fakultät für Physik des Karlsruher Instituts für Technologie genehmigte

Dissertation

von

Momchil Davidkov

Tag der mündlichen Prüfung: 22. Oktober 2010

Referent: Prof. Dr. U. Nierste

Korreferent: Prof. Dr. M. Steinhauser

CONTENTS

1	Introduction	3
2	The Effective Hamiltonian formalism	9
2.1	General definitions and scheme dependence	9
2.2	The Renormalisation Group Evolution	10
2.2.1	The Anomalous Dimension Matrix	10
2.3	The Evolution Matrix	16
2.3.1	Solution of the RG equation at LO	17
2.3.2	Solution of the RG equation at NLO	18
2.4	Evolution of the $\Delta B = 2$ effective Hamiltonian	20
2.4.1	The operator basis	20
2.4.2	Program for Evolution	21
2.5	Hadronic Matrix Elements	25
2.5.1	Hadronic Matrix Elements for $B-\bar{B}$ mixing	26
2.5.2	Hadronic Matrix Elements for $K-\bar{K}$ mixing	27
2.5.3	Hadronic Matrix Elements for $D-\bar{D}$ mixing	28
3	General aspects of meson mixing	29
4	Wilson coefficients for meson mixing processes in the MSSM	35
4.1	SM contribution	35
4.1.1	The pure SM CKM matrix	35
4.1.2	The mixing of neutral B mesons in the SM	39
4.1.3	Indirect CP violation in $K-\bar{K}$ mixing	43
4.1.4	Main aspects on the mixing of neutral D mesons	46
4.2	The SUSY contributions to the meson mixing processes	48

5	The inclusive decay $B \rightarrow X_s \gamma$	55
5.1	$B \rightarrow X_s \gamma$ in the SM	55
5.2	$B \rightarrow X_s \gamma$ in the MSSM	56
6	Method and general features of the analysis	59
6.1	General correlations between $B_s - \bar{B}_s$ and $B_d - \bar{B}_d$ mixing	60
6.2	Constraints on the mass splitting of left-handed squarks	69
7	Numerical analysis of δ_{23}^{uLL} and δ_{13}^{uLL}	77
7.1	The calculation procedure	80
7.2	The logical structure of the program	81
7.3	Results of the numerical analysis	83
8	Summary and outlook	85
A	Appendix	91
A.1	The Feynman rules for MSSM	91
A.1.1	Quark-squark-gluino vertices	91
A.1.2	Quark-squark-chargino vertices	92
A.1.3	Quark-squark-neutralino vertices	92
A.1.4	Quark-quark-charged Higgs vertices	93
A.2	Plots	94

1. INTRODUCTION

The objects of study of theoretical particle physics are the fundamental laws of nature. Its aim is to describe the elementary constituents of matter and their interactions within a theoretical framework which implies predictions for particle experiments. All the knowledge about the elementary particles and forces in nature is theoretically classified in the so called Standard Model (SM) of elementary particle physics. This $SU(3) \times SU(2) \times U(1)$ gauge theory of the strong and electroweak interactions developed by Glashow, Weinberg and Salam starting in 1967 describes almost all experimental results obtained at the elementary particle colliders until now with remarkable precision. Let me set a short example of the power of the Standard Model. Combining the most precise experimental measurement of the anomalous magnetic moment of the electron $g/2 = 1.001\,159\,652\,180\,85(76)$ [1] with high precision calculation in quantum electrodynamics, the most precisely tested part of the Standard Model, one obtains the value $\alpha_s^{-1} = 137.035\,999\,709(96)[0.70\text{ ppb}]$ [2] for the fine structure constant, with an amazing theoretical precision. Experiments based on atom recoil methods determine the fine structure constant independently of the anomalous magnetic moment of the electron. The atoms of the chemical elements Rubidium (Rb) and Caesium (Cs) are the most appropriate ones for the experimental determination of the fine structure constant. Comparing the results $\alpha^{-1}(Rb) = 137.035\,998\,78(91)[6.7\text{ ppb}]$ and $\alpha^{-1}(Cs) = 137.036\,000\,0(11)[8.0\text{ ppb}]$ with the theoretical value given above we find a difference from -1.0 and $+0.3$ standard deviations, respectively [2]. That comparison is known as the best test of the validity of the QED. The incredible theoretical and experimental accuracies demonstrate the impressive predictive power of the Standard Model.

However, there are many examples which show the discrepancy between the SM predictions and experimental results. Let me mention one of them. The difference between the SM theoretical prediction for the anomalous magnetic moment of the heavier “brother“ of the electron, the muon, and the experimental measurement for this quantity is more than 3 standard deviations. That means, the anomalous magnetic moment of the muon cannot be explained within the Standard Model with a probability of more than 99.6%. The aim of

the theoretical physicists is to develop a consistent theory with the smallest possible number of free parameters which explains the properties of the particles and the fundamental interactions in nature. Despite of its phenomenological success the Standard Model has several drawbacks: Some couplings develop Landau poles, the exact mechanism of electroweak symmetry breaking is not understood, the unification of strong and and electroweak interactions is incomplete, the hierarchy between the Planck, GUT and the electroweak scale and the strong CP problem are not addressed. Further, the SM cannot explain the observed dark matter in the universe nor the preponderance of matter over antimatter. One of the fundamental questions unaddressed in the early stages of the SM is the mechanism how the fermions obtain their masses. Seven years later, Weinberg and Salam incorporated the so called Higgs mechanism [4–6] into the electroweak theory of Glashow in order to provide a theoretical explanation of the masses of spin-one-half particles and gauge bosons [7,8]. In fact, the SM needs the Higgs mechanism for its predictive power. However, this is the only part of the theory which has not been experimentally confirmed yet. The search for the Higgs boson, the theoretically postulated particle which gives masses to the fermions and gauge bosons is the most important goal of today’s biggest discovery machine in the world, the Large Hadron Collider (LHC). Its prime purpose is the investigation of the mechanism of electroweak symmetry breaking and of the dynamics which stabilises the electroweak scale. General considerations of the latter aspect suggest New Physics (NP) with particle masses around or below 1 TeV. In order to provide a satisfactory explanation of different experimental observations and to solve conceptual problems of the Standard Model many approaches for incorporation of the Standard Model into a more general theory have been proposed. In fact, among various possible extensions of the Standard Model by far the most popular one is the Supersymmetry (SUSY), in particular, the so called Minimal Supersymmetric Standard Model (MSSM). The reason why the MSSM has become the most favoured extension of the Standard Model in the last decades is its capability to solve a very large spread of theoretical problems including gauge coupling unification, to give a rationale for a heavy top and light Higgs, to provide a method of unification of gravity with other gauge forces and finally to provide a dark matter candidate, the lightest supersymmetric particle. Increasing the precision of the theoretical predictions for the masses and other properties of the new particles in different possible scenarios of the Supersymmetry is very important for the searches of these particles at the high- p_T experiments of the LHC. One of the most important tasks of theoretical particle physics is therefore to identify and investigate the processes which are highly sensitive to contributions of supersymmetric particles in order

to test the Standard Model and to clarify where manifestation of Supersymmetry can show up and how to distinguish Supersymmetry from other possible theories beyond the Standard Model. Hopefully, in upcoming years the physics community will uncover the laws of nature governing the TeV scale.

In fact, Supersymmetry, in particular the minimal supersymmetric extension of the SM (MSSM) is the most favoured model of NP considered to explain the discrepancies between SM predictions and experiments. The MSSM predicts many new particles. The postulated superpartners of SM particles affect the physical processes and change the values of the observable quantities. The extent to which the theoretical prediction of a certain process is changed in a given model of NP depends on many parameters of the certain NP model, in particular, considering the MSSM, on the masses of the supersymmetric particles involved in the studied transition amplitude.

The prediction of the mass spectrum of the supersymmetric particles is a very important issue from phenomenological point of view as well as an essential topic in regard to the direct search for superparticles at the LHC. Therefore, the squark mass matrices have been the object of study of numerous analyses in the past. In view of the start of the LHC any improvement of the knowledge about the mass spectrum of the MSSM is important and timely.

The aim of this work is to constrain the parameters of the MSSM by considering processes which are highly sensitive to contributions from supersymmetric particles. Since meson mixing processes are known with good experimental accuracy and have small theoretical uncertainties, they are especially appropriate candidates for this purpose. The focus is set on generic physical relations which are mostly independent of boundary conditions. Such a physical relation stems from chargino boxes which correlate $B_d-\bar{B}_d$ mixing and $B_s-\bar{B}_s$ mixing through the CKM matrix elements involved in the meson mixing processes. Another very important theoretical issue is the relation between the left-handed up-type squark mass matrix and the left handed down-type one $M_{uLL}^2 = VM_{dLL}^2V^\dagger$ due to $SU(2)$ gauge symmetry in the left handed fermion sector. Since these mass matrices are not independent, the only way to avoid flavour off-diagonal mass insertions in the up and in the down sector simultaneously is to choose the up-type and the down-type mass mixing matrix proportional to the unit matrix. This is realised in the naive minimal flavour violating MSSM. In a more general definition of Minimal Flavour Violation (MFV) [64, 65] flavour

violation is postulated to stem solely from the Yukawa sector, resulting in FCNC transitions (which can now also be mediated by gluinos and neutralinos) proportional to products of CKM elements and Yukawa couplings. In addition, we take into account the numerical relation between the $B_s - \bar{B}_s$ mixing and $B_d - \bar{B}_d$ mixing transition due to the ratio of the decay constants and the bag parameters in the B_s and B_d system. In almost all the analyses of this type the $B_s - \bar{B}_s$ mixing and $B_d - \bar{B}_d$ mixing are treated independently from each other. However, these two processes are related to each other through the ratio of the decay constants of the B_s and B_d mesons. The numerical value of this ratio is known from lattice calculations to a much better precision than the quantities in the numerator and denominator themselves.

Studying in detail the experimental data and the analyses of the CKMfitter and Ufit collaborations which estimate the amount of New Physics in the meson mixing processes, we derive a general relations between fundamental parameters of the MSSM. Assuming a non diagonal elements in the LL part of the squark mass matrices the impact of the different SUSY contributions to the mixing phase in the B_s and B_d meson systems is investigated. We determine general relations between the masses of the squarks, the mass of the gluino and the off-diagonal elements of the squark mass matrices.

Performing an exhausting analysis of the meson mixing processes in the $K - \bar{K}$ and $D - \bar{D}$ systems, our aim has been to investigate the possible mass splitting between the left-handed squarks. We have considered different scenarios given by the choice of the form of the up-type and down-type mass mixing matrices. In contrast to previous analyses in which the electroweak supersymmetric contributions to the meson mixing processes have been neglected claiming their smallness in comparison to the gluino contribution we have found that this argumentation does not hold for gluino masses bigger then the squark masses. In this region of the MSSM parameter space the electroweak contributions can be even dominant and they have been included in our calculation as well.

The aim of our numerical analysis is to obtain constraints on the δ_{i3}^{uLL} mass insertions of the up-type squark mass matrix in the general MSSM. For this purpose, we first considered the $B_s - \bar{B}_s$ and $B_d - \bar{B}_d$ mixing processes calculating the electroweak and strong contributions in general MSSM. In an iterative procedure we pass through several constraints and obtain the allowed values for the mass insertions δ_{23}^{uLL} and δ_{33}^{uLL} . We take into account the charged Higgs contribution to the meson mixing box diagrams as well. Since these diagrams do not involve squarks their contribution affects the flavour changing process only in a MFV way. Yet through the resulting shift in the observable quantities the charged Higgs contribu-

tion influences the flavour changing parameters under study. With the obtained values for δ_{LL}^{u23} and δ_{LL}^{u13} we calculate the CP violating parameter ϵ_K which is used as an additional constraint on the studied mass insertions. The parameter ϵ_K which measures the CP violation in mixing in the Kaon system has not been considered by many analyses in the past. However, the value of the non perturbative parameter \hat{B}_K is known from recent lattice calculations with a good enough precision such that ϵ_K becomes an important quantity for NP searches or analysis which aim is the constraining of off-diagonal elements of the squark mass matrices. Further, we examine whether the branching ratio $\text{Br}(B \rightarrow X_s \gamma)$ which is very sensitive to NP effects satisfies its experimental bounds. In addition, we confront the obtained values for δ_{LL}^{u23} and δ_{LL}^{u13} with the $D-\bar{D}$ transition amplitude.

We start with the description of the main theoretical formalism in the next chapter. After that, we concentrate on the main features of our studies and describe in detail the performed analyses which aim has been the constraining of the MSSM parameter space, in particular, placing bounds on elements of the mass mixing matrices. In the last part of this work, we comment on the results of our analyses before we conclude and give a short outlook.

2. THE EFFECTIVE HAMILTONIAN FORMALISM

Theoretical predictions of several measurable quantities relevant in meson mixing phenomenology are usually studied in some effective theory obtained by using the so called Operator Product Expansion (OPE). A common feature of the OPE is the definition of local operators of the form (in the case of $\Delta B = 2$ transitions)

$$Q = C^{\alpha\beta\gamma\delta}(\bar{b}_\alpha\Gamma q_\beta)(\bar{b}_\gamma\Gamma q_\delta) \quad (2.1)$$

where Γ is a general Dirac matrix acting on spinor indices, $\alpha, \beta, \gamma, \delta$ are colour indices and the constant $C^{\alpha\beta\gamma\delta}$ is given by either $\delta^{\alpha\beta}\delta^{\gamma\delta}$ or $\delta^{\alpha\delta}\delta^{\beta\gamma}$.

The obtaining of physical amplitudes from the matrix elements of Q goes through the following three steps:

1. Matching of the full theory onto the effective one at some large energy scale.
2. Renormalisation-group evolution from the high energy scale to the low energy scale suitable for the calculation of the hadronic matrix elements.
3. Calculation of the hadronic matrix elements using non-perturbative methods.

2.1. General definitions and scheme dependence

The matrix elements of the effective Hamiltonian can be written as

$$\mathcal{A}_{\text{eff}} = \langle F|\mathcal{H}_{\text{eff}}|I\rangle = \sum_i \langle F|Q_i(\mu)|I\rangle C_i(\mu) \quad (2.2)$$

where the $\langle Q_i(\mu)\rangle$ are matrix elements of local operators and the $C_i(\mu)$ denote the corresponding effective couplings, the so called Wilson coefficients. In eq. (2.2) μ denotes the energy scale where the matching of the full theory onto the effective one is performed. In general, its value can be chosen arbitrarily. Through the OPE the problem of the calculation of transition amplitudes can be separated in two parts. The Wilson coefficients $C_i(\mu)$

which contain the short-distance (perturbative) effects are calculated using perturbation theory methods. Since the physics contributions from energy scales higher than μ are contained in $C_i(\mu)$, they are affected by the heavy particles involved in the problem i.e. W , Z -bosons and new particles of supersymmetric extensions of the SM. The calculation of the Wilson coefficients is performed at the high scale defined by the masses of the heavy particles. On the other hand, for the determination of the matrix elements $\langle Q_i(\mu) \rangle$ which summarise long-distance (non-perturbative) effects non-perturbative methods i.e. lattice QCD, QCD sum rules, chiral perturbation theory etc. are used. In this case the scale μ is usually chosen to be of the order of the decaying hadron. Since the matching condition requires the matching scale μ to be the same for the Wilson coefficients as well as for the hadronic matrix elements either the effective couplings $C_i(\mu)$ have to be evolved down to the scale of the matrix elements or vice versa. The evolution is done using Renormalisation Group (RG) equations. The transition amplitude \mathcal{A} does not depend on the matching scale μ . Therefore, the μ -dependence of the Wilson coefficients and the μ -dependence of the hadronic matrix elements have to cancel each other. For a very clear introductory explanation of the OPE in the context of the meson mixing phenomenology as well as of other important processes sensitive to NP effects we refer to [9].

2.2. The Renormalisation Group Evolution

The today's most precise determinations of the hadronic matrix elements are known from lattice gauge theory. These calculations are performed using so called Regularisation Independent renormalisation schemes (RI-MOM). However, in practical calculations of the Wilson coefficients in meson mixing processes Minimal Subtraction schemes (MS, $\overline{\text{MS}}$) appear to be more convenient. In order to solve the problem with the different scales mentioned above, the Renormalisation Group (RG) evolution has to be performed in a certain renormalisation scheme. In the following we concentrate on the RG evolution in context of the different renormalisation schemes and show the translation of the main results between the different schemes. The important results are summarised and explained. Our discussion is based on the theoretical approach discussed in ref. [11].

2.2.1. The Anomalous Dimension Matrix

The Renormalisation Group evolution follows from the requirement that the transition amplitude is independent of the matching scale μ . Adopting a vector notation for the

Wilson coefficients and the hadronic matrix elements we take the derivative of \mathcal{A}_{eff} in eq. (2.2) with respect to μ and obtain

$$\mu^2 \frac{d}{d\mu^2} \langle \vec{Q}^T(\mu) \rangle \vec{C}(\mu) + \langle \vec{Q}^T(\mu) \rangle \mu^2 \frac{d\vec{C}(\mu)}{d\mu^2} = 0. \quad (2.3)$$

The relation between the bare and the renormalised operators is given by

$$\langle \vec{Q}^B \rangle = \hat{Z} \langle \vec{Q}(\mu) \rangle. \quad (2.4)$$

The matrix \hat{Z} depends on the coupling constant $\alpha(\mu)$ and, in the most general renormalisation schemes like the Regularisation Independent (RI) scheme [10], on the gauge parameter λ as well. On the contrary, the minimal subtraction schemes $\overline{\text{MS}}$ and $\overline{\text{MS}}$ are gauge independent.

Since the bare operators do not depend on μ , it follows by taking the derivative with respect to μ of eq.(2.4)

$$\mu^2 \frac{d\hat{Z}}{d\mu^2} \langle \vec{Q}(\mu) \rangle + \hat{Z} \mu^2 \frac{d}{d\mu^2} \langle \vec{Q}(\mu) \rangle = 0. \quad (2.5)$$

From the last equation we easily obtain a differential equation for the renormalised operators

$$\mu^2 \frac{d}{d\mu^2} \langle \vec{Q}(\mu) \rangle = -\hat{Z}^{-1} \mu^2 \frac{d\hat{Z}}{d\mu^2} \langle \vec{Q}(\mu) \rangle \quad (2.6)$$

and define the *anomalous dimension matrix* (ADM) $\hat{\gamma}(\alpha(\mu))$ as

$$\hat{\gamma} \equiv 2\hat{Z}^{-1} \mu^2 \frac{d\hat{Z}}{d\mu^2}. \quad (2.7)$$

Inserting eq. (2.6) into eq. (2.3) we obtain the RG equation for the Wilson coefficients

$$\mu^2 \frac{d\vec{C}(\mu)}{d\mu^2} = \frac{\hat{\gamma}^T}{2} \vec{C}(\mu). \quad (2.8)$$

In order to find the expression of $\hat{\gamma}$ in dimensional regularisation, we define Z_g through

$$\alpha_0 = Z_g^2 \alpha(\mu) \mu^{2\epsilon} \quad (2.9)$$

where α_0 is the bare coupling and $\epsilon = (4 - D)/2$. Z_g is a composite function of μ , $Z_g = Z_g(\alpha(\mu))$.

Next, we apply the derivative operator with respect to μ on eq. (2.9). Since the bare coupling α_0 does not depend on the renormalisation point we find

$$\frac{d\alpha(\mu)}{d\ln\mu^2} = -\epsilon\alpha(\mu) - \alpha(\mu)\frac{2}{Z_g}\frac{Z_g}{d\ln\mu^2}. \quad (2.10)$$

With the definitions

$$\begin{aligned} \beta(\alpha(\mu), \epsilon) &\equiv \frac{d\alpha(\mu)}{d\ln\mu^2} \\ \beta(\alpha(\mu)) &\equiv -\alpha(\mu)\frac{2}{Z_g}\frac{Z_g}{d\ln\mu^2} \end{aligned} \quad (2.11)$$

eq. (2.10) can be written in the simple form

$$\beta(\alpha(\mu), \epsilon) = -\epsilon\alpha(\mu) + \beta(\alpha(\mu)) \quad (2.12)$$

where $\beta(\alpha(\mu))$ is expanded in $\alpha(\mu)$ as

$$\beta(\alpha(\mu)) = -\beta_0\frac{\alpha^2(\mu)}{4\pi} - \beta_1\frac{\alpha^3(\mu)}{(4\pi)^2} + \mathcal{O}(\alpha^4(\mu)). \quad (2.13)$$

Writing Z_g as an expansion in α and ϵ

$$Z_g = 1 + \sum_{i=1}^{\infty} \sum_{k=1}^i \left(\frac{\alpha}{4\pi}\right)^i \frac{1}{\epsilon^k} Z_{g,k}^{(i)} \quad (2.14)$$

it can be shown that the coefficients in the expansion of $\beta(\alpha(\mu))$ are related to the ones of the expansion of Z_g in eq. (2.13) through

$$\beta_i = -2(i+1)Z_{g,1}^{(i+1)}, \quad (2.15)$$

and consequently the bare parameter α_0 can be expressed through

$$\alpha_0 = \alpha \left[1 - \frac{\alpha}{4\pi} \frac{\beta_0}{\epsilon} + \mathcal{O}(\alpha^2) \right]. \quad (2.16)$$

Analogously, we introduce the gauge fixing parameter λ defined from the gauge fixing Lagrangian

$$\mathcal{L}_{\text{gauge fixing}} = -\frac{1}{2\lambda}(\partial^\mu G_\mu^a)(\partial^\nu G_\nu^a), \quad (2.17)$$

The gauge fixing parameter λ satisfies the RG equation

$$\lambda\beta_\lambda(\alpha(\mu)) \equiv \mu^2 \frac{d\lambda}{d\mu^2} = -\frac{\alpha}{4\pi}\beta_\lambda^0 + \mathcal{O}(\alpha^2). \quad (2.18)$$

In the following we denote by $\lambda = 0$ the Landau gauge and $\lambda = 1$ the Feynman gauge. Using eq. (2.18) we find the series expansion of λ_0 in the coupling constant α

$$\lambda_0 = \lambda \left[1 - \frac{\alpha}{4\pi} \frac{\beta_\lambda^0}{\epsilon} + \mathcal{O}(\alpha^2) \right]. \quad (2.19)$$

Further, we obtain from (2.7) the anomalous dimension matrix $\hat{\gamma}$

$$\hat{\gamma} = 2\hat{Z}^{-1} \left[\beta(\alpha, \epsilon) \frac{\partial \hat{Z}}{\partial \alpha} + \beta_\lambda(\alpha) \lambda(\alpha) \frac{\partial \hat{Z}}{\partial \lambda} \right]. \quad (2.20)$$

The renormalisation scheme in which the strong coupling constant α and the gauge parameter λ are renormalised can be chosen different from the renormalisation scheme in which the operators are renormalised [11]. In $\overline{\text{MS}}$ scheme the coefficients β_λ^0 , β_1 and β_0 in the series expansions eq. (2.13) and eq. (2.19) which depend on the number of colours N_c and the number of effective flavours n_f are given by

$$\begin{aligned} \beta_0 &= \frac{11N_c}{3} - \frac{2n_f}{3}, \\ \beta_1 &= \frac{34N_c^2}{3} - \frac{10N_cn_f}{3} - \frac{(N_c^2 - 1)n_f}{N_c} \end{aligned} \quad (2.21)$$

and

$$\beta_\lambda^0 = -\frac{13N_c}{6} + \frac{\lambda N_c}{2} + \frac{2n_f}{3}. \quad (2.22)$$

From eq. (2.20) by expanding $\hat{\gamma}$ and \hat{Z} as

$$\hat{\gamma} = \frac{\alpha}{4\pi} \hat{\gamma}^{(0)} + \left(\frac{\alpha}{4\pi} \right)^2 \hat{\gamma}^{(1)}, \quad (2.23)$$

$$\hat{Z} = 1 + \frac{\alpha}{4\pi} \hat{Z}^{(1)} + \left(\frac{\alpha}{4\pi} \right)^2 \hat{Z}^{(2)} \quad (2.24)$$

we derive the following relations between the coefficients $\gamma^{(i)}$ and $\hat{Z}^{(i)}$:

$$\hat{\gamma}^{(0)} = -2\epsilon \hat{Z}^{(1)}, \quad (2.25)$$

$$\hat{\gamma}^{(1)} = -4\epsilon \hat{Z}^{(2)} - 2\beta_0 \hat{Z}^{(1)} + 2\epsilon \hat{Z}^{(1)} \hat{Z}^{(1)} - 2\beta_\lambda^0 \lambda \frac{\partial \hat{Z}^{(1)}}{\partial \lambda}. \quad (2.26)$$

Further, $\hat{Z}^{(1)}$ can be expanded in inverse powers of ϵ

$$\hat{Z}^{(i)} = \sum_{j=0}^i \left(\frac{1}{\epsilon} \right)^j \hat{Z}_j^{(i)}. \quad (2.27)$$

The requirement that the ADM is finite as $\epsilon \rightarrow 0$ implies ($\hat{Z}_1^{(1)}$ is gauge invariant)

$$4\hat{Z}_2^{(2)} + 2\beta_0\hat{Z}_1^{(1)} - 2\hat{Z}_1^{(1)}\hat{Z}_1^{(1)} = 0. \quad (2.28)$$

In addition, we have

$$\hat{\gamma}^{(0)} = -2\hat{Z}_1^{(1)}, \quad (2.29)$$

$$\hat{\gamma}^{(1)} = -4\hat{Z}_1^{(2)} - 2\beta_0\hat{Z}_0^{(1)} + 2\left\{\hat{Z}_1^{(1)}, \hat{Z}_0^{(1)}\right\} - 2\beta_\lambda^0\lambda\frac{\partial\hat{Z}_0^{(1)}}{\partial\lambda}. \quad (2.30)$$

For the computation of the NLO ADM it is necessary to calculate the pole and finite part of $\hat{Z}^{(1)}$, the single pole of $\hat{Z}^{(2)}$, β_0 and β_λ^0 .

In order to determine the matrix elements of the ADM, the result of the calculation of the bare hadronic matrix elements is expanded as

$$\langle\vec{Q}_B\rangle = \left[1 + \frac{\alpha_0}{4\pi}\left(\hat{A}_0 + \frac{\hat{A}_1}{\epsilon}\right) + \left(\frac{\alpha_0}{4\pi}\right)^2\left(\hat{B}_0 + \frac{\hat{B}_1}{\epsilon} + \frac{\hat{B}_2}{\epsilon^2}\right)\right]\langle\vec{Q}^{(0)}\rangle \quad (2.31)$$

where $\langle\vec{Q}^{(0)}\rangle$ are the tree level matrix elements. For given generic renormalisation scheme the following relation between the bare and the renormalised matrix elements can be written

$$\langle\vec{Q}(\mu)\rangle = \hat{Z}^{-1}\langle\vec{Q}_B\rangle = \left(1 + \frac{\alpha}{4\pi}\hat{r}\right)\langle\vec{Q}^{(0)}\rangle. \quad (2.32)$$

The renormalisation scheme is defined by the choice of the matrix \hat{r} . The matrix \hat{A}_1 is gauge and regularisation independent. \hat{A}_0 can be written as

$$\hat{A}_0(\lambda_0) = \hat{A}_0(0) + \lambda_0\frac{\partial\hat{A}_0}{\partial\lambda_0} \quad (2.33)$$

and $\partial\hat{A}_0/\partial\lambda_0$ is regularisation independent as well. Inserting eq. (2.33) and eq. (2.31) into eq. (2.32) we can obtain a relation between \hat{Z} and \hat{A}_0 , \hat{A}_1 , \hat{B}_0 , \hat{B}_1 and \hat{B}_2

$$\hat{Z}_0^{(1)} = \hat{A}_0 - \hat{r}, \quad \hat{Z}_1^{(1)} = \hat{A}_1, \quad (2.34)$$

$$\hat{Z}_1^{(2)} = \hat{B}_1 - \hat{A}_1\hat{r} - \beta_0\hat{A}_0 - \beta_\lambda^0\lambda\frac{\partial\hat{A}_0}{\partial\lambda}, \quad (2.35)$$

$$\hat{Z}_2^{(2)} = \hat{B}_2 - \beta_0\hat{A}_1. \quad (2.36)$$

Further, we introduce the regularisation and renormalisation scheme independent quantity

$$\hat{G} = \hat{\gamma}^{(1)} - [\hat{r}, \hat{\gamma}^{(0)}] - 2\beta_0\hat{r} - 2\beta_\lambda^0\lambda\frac{\partial\hat{r}}{\partial\lambda}. \quad (2.37)$$

The first property is manifest if we rewrite \hat{G} in terms of the matrices \hat{A}_0 , \hat{A}_1 , \hat{B}_0 , \hat{B}_1 and \hat{B}_2

$$\hat{G} = -4 \left[\hat{B}_1 - \frac{1}{2} \{ \hat{A}_1, \hat{A}_0 \} - \frac{1}{2} \beta_0 \hat{A}_0 - \frac{1}{2} \beta_\lambda^0 \lambda \frac{\partial \hat{A}_0}{\partial \lambda} \right]. \quad (2.38)$$

where we have used

$$\hat{\gamma}^{(0)} = -2\hat{A}_1. \quad (2.39)$$

The renormalisation scheme independence is immediately proven by the absence of the matrix \hat{r} in eq. (2.38). The regularisation independence is also guaranteed because the renormalised operators (and therefore their evolution controlled by $\hat{\gamma}^{(1)}$) at fixed gauge and external states depend uniquely on the \hat{r} matrix which in turn does not depend on the regularisation.

The Regularisation Independent (RI) scheme is defined for given external states and fixed gauge λ by the condition

$$\langle \vec{Q}(\mu) \rangle_{p^2=-\mu^2, \lambda} = \langle \vec{Q} \rangle^{(0)}. \quad (2.40)$$

Therefore, in the RI scheme \hat{G} coincides with the two loop ADM. It is apparent that these condition can be implemented in any regularisation scheme and, in particular, in a purely non-perturbative way.

The renormalisation condition for the massless quark propagator is given by

$$\frac{i}{4} \left[\gamma^\rho \frac{\partial}{\partial p^\rho} S(p)_R^{-1} \right]_{p^2=-\mu^2} = 1. \quad (2.41)$$

The quark wave-function renormalisation constant can be written as

$$Z_q^{\text{RI}} = 1 - \frac{\alpha}{4\pi} C_F \lambda \left(\frac{1}{\epsilon} - \gamma + \ln(4\pi) + \frac{1}{2} \right). \quad (2.42)$$

Different choices of the wave-function renormalisation correspond to different choices of the external quark states in the calculation of four-point Green functions, and therefore to different definitions of the renormalised operators. Even if every choice is perfectly admissible, in the RI scheme the condition (2.41) guarantees that the vector and axial current satisfy automatically the Ward identities.

Finally, we shortly describe the recipe to obtain the NLO ADM in the RI scheme, $\hat{\gamma}_{\text{RI}}^{(1)}$. In dimensional regularisations evanescent operators must be included in eq. (2.30). This fact

complicates the calculation because products between the \hat{Z} matrices should be performed with indices running over the whole set of physical and evanescent operators. Only at the end of the calculation the $d \rightarrow 4$ limit can be taken. It has been shown in [12] that the relation between the NLO ADM and the one-loop and two-loop renormalisation matrices are valid diagram by diagram. Therefore, according to eq. (2.38) the two basic steps of the computation are the evaluation of the two-loop bare matrix elements and the subtraction of the one-loop diagrams corresponding to the internal subdiagrams, according to the chosen renormalisation prescription. In the RI scheme it is not necessary to isolate the evanescent operators from the four-dimensional basis because the counterterms of the evanescent and physical operators are subtracted from the two-loop matrix element with the same numerical coefficient 1/2 (see the combination $\hat{A}_1\hat{A}_0 + \hat{A}_0\hat{A}_1$ of eq. (2.38)). Moreover, in the subtraction procedure the double poles cancel and thus the projection on the physical basis cannot generate new single poles due to the evanescent operators that would alter the result. More details about the calculation of the NLO ADM in the RI scheme can be found in [11, 12].

In order to obtain $\hat{\gamma}^{(1)}$ in the $\overline{\text{MS}}$ scheme, it is possible to use eqs. (2.37-2.38) with $\hat{r}_{\overline{\text{MS}}} = \overline{A}_0$:

$$\hat{\gamma}_{\overline{\text{MS}}}^{(1)} = -4 \left[\hat{B}_1 - \overline{A}_1\overline{A}_0 - \frac{1}{2}\tilde{A}_1\tilde{A}_0 - \beta_0\overline{A}_0 - \beta_\lambda^0\lambda\frac{\partial\overline{A}_0}{\partial\lambda} \right]. \quad (2.43)$$

\overline{A}_i are the matrix elements restricted to the operators of the four-dimensional basis, and \tilde{A}_i those connecting the operators of the four-dimensional basis with the evanescent ones. $\hat{\gamma}_{\overline{\text{MS}}}^{(1)}$ can be also obtained using eqs. (2.38-2.43) by

$$\hat{\gamma}_{\text{RI}}^{(1)} = \hat{\gamma}_{\overline{\text{MS}}}^{(1)} - 2(\overline{A}_1\overline{A}_0 - \overline{A}_0\overline{A}_1) - 2\beta_0\overline{A}_0 - 2\beta_\lambda^0\lambda\frac{\partial\overline{A}_0}{\partial\lambda}. \quad (2.44)$$

2.3. The Evolution Matrix

In this subsection we summarise some basic aspects of the calculation of the evolution matrix and discuss in detail the issues of the regularisation and renormalisation dependence of the Wilson coefficients and of the corresponding operators.

In order to compute the Wilson coefficients at a large energy scale $\mu \sim M$, we have to consider the full set of current-current, box and penguin diagrams in the full theory, e.g. with propagating heavy particles, including the terms of $\mathcal{O}(\alpha)$.

Adopting the notation in [11] we write the renormalised amplitude in the full theory as

$$\mathcal{A}_{\text{full}} = \langle \vec{Q}^{(0)T} \rangle \left[\vec{T}^{(0)} + \frac{\alpha}{4\pi} \vec{T}^{(1)} \right]. \quad (2.45)$$

Equating eqs. (2.2) and (2.45) at the matching scale $\mu = M$ we obtain

$$\vec{C}(M) = \vec{T}^{(0)} + \frac{\alpha}{4\pi} \left(\hat{T}^{(1)} - \hat{r}^T \vec{T}^{(0)} \right) \quad (2.46)$$

$\vec{T}^{(1)}$ and \hat{r}^T depend on the external states.

2.3.1. Solution of the RG equation at LO

The Wilson coefficients $\vec{C}(\mu)$ are expressed in terms of their counter-parts computed at the large scale $\mu \sim M$ through the evolution matrix $\hat{W}(\mu, M)$

$$\vec{C}(\mu) = \hat{W}(\mu, M) \vec{C}(M). \quad (2.47)$$

The coefficients $\vec{C}(\mu)$ obey the RG equation

$$\left[\mu^2 \frac{\partial}{\partial \mu^2} + \beta(\alpha) \frac{\partial}{\partial \alpha} + \beta_\lambda \lambda \frac{\partial}{\partial \lambda} - \frac{\hat{\gamma}^T(\alpha, \lambda)}{2} \right] \vec{C}(\mu, \alpha(\mu), \lambda(\mu)) = 0, \quad (2.48)$$

where the term proportional to β_λ cancels an identical one embedded in $\hat{\gamma}^T$. In order to solve the RG equation (2.48), we consider the basis where the ADM $\hat{\gamma}_s^{(0)T}$ is diagonal. In this basis the Wilson coefficients are given by a rotation with the matrix V

$$\vec{C}' = V \vec{C}, \quad (2.49)$$

where V is the matrix which diagonalises $\hat{\gamma}_s^{(0)T}$:

$$V \hat{\gamma}_s^{(0)T} V^{-1} = \hat{\gamma}_D = \text{diag}(\gamma_{D_1}, \dots, \gamma_{D_n}). \quad (2.50)$$

Since $\hat{\gamma}^{(0)}$ does not depend on the gauge parameter λ , at LO eq. (2.48) can be written as

$$\beta(\alpha) \frac{dC'_i(\mu)}{d\alpha(\mu)} = \frac{\gamma_{D_i}(\alpha)}{2} C'_i(\mu). \quad (2.51)$$

Applying the method of separation of variables on the equation (2.51), it can be integrated in this basis from the lower scale μ to the larger scale M . We find

$$\int_{C'(\mu)}^{C'(M)} \frac{dC'_i}{C'_i} = \int_{\alpha(\mu)}^{\alpha(M)} \frac{\gamma_{D_i}(\alpha)}{2\beta(\alpha)} d\alpha. \quad (2.52)$$

Expanding $\hat{\gamma}$ and $\beta(\alpha)$ in α using eqs. (2.10 - 2.18), we obtain at LO

$$\int_{C'_i(\mu)}^{C'_i(M)} \frac{dC'_i}{C'_i} = -\frac{\gamma_{D_i}}{2\beta_0} \int_{\alpha(\mu)}^{\alpha(M)} \frac{d\alpha}{\alpha}. \quad (2.53)$$

The solution of eq. (2.53) is easily found

$$C'_i(\mu) = \left(\frac{\alpha(M)}{\alpha(\mu)} \right)^{\frac{\gamma_{D_i}}{2\beta_0}} C'_i(M). \quad (2.54)$$

Rotating eq. (2.54) to the initial basis, we obtain the following expression for the evolution matrix $\hat{W}(\mu, M)$ at LO

$$\hat{W}_{LO}(\mu, M) = \hat{V}^{-1} \left(\frac{\alpha(M)}{\alpha(\mu)} \right)^{\frac{\hat{\gamma}_{D_j}}{2\beta_0}} \hat{V}. \quad (2.55)$$

2.3.2. Solution of the RG equation at NLO

Now, we go one step further in perturbation theory. Our goal is to find the solution of the RG equation (2.48) at NLO. For this purpose we write

$$\hat{W}(\mu, M) = \hat{M}(\mu) \hat{W}_{LO}(\mu, M) \hat{M}^{-1}(M), \quad (2.56)$$

where \hat{W}_{LO} is the leading order evolution matrix given in eq. (2.55) and the NLO evolution is encoded in

$$\hat{M}(\mu) = 1 + \frac{\alpha(\mu)}{4\pi} \hat{J}(\lambda(\mu)). \quad (2.57)$$

Writting eq. (2.48) as a power expansion in α it takes the form

$$\frac{\beta_\lambda^0}{\alpha\beta_0} \lambda \frac{\partial \vec{C}'}{\partial \lambda} + \frac{d\vec{C}'}{d\alpha} = -\frac{1}{2\alpha\beta_0} \left[\hat{\gamma}_D + \frac{\alpha}{4\pi} \left(\hat{G} - \frac{\beta_1}{\beta_0} \hat{\gamma}_D \right) \right] \vec{C}' \quad (2.58)$$

where

$$\hat{G} \equiv V \hat{\gamma}^{(1)T} V^{-1}. \quad (2.59)$$

For the solution of eq. (2.58) we use the ansatz

$$\vec{C}'(\mu) = \left(\mathbf{1} + \frac{\alpha(\mu)}{4\pi} \hat{S}(\lambda) \right) \left(\frac{\alpha(M)}{\alpha(\mu)} \right)^{\frac{\hat{\gamma}_D}{2\beta_0}} \left(\mathbf{1} - \frac{\alpha(M)}{4\pi} \hat{S}(\lambda) \right) \vec{C}'(M). \quad (2.60)$$

Inserting eq. (2.60). into eq. (2.58), we find after neglecting terms of $\mathcal{O}(\alpha(M))$

$$\hat{S} + \frac{\beta_\lambda^0}{\beta_0} \lambda \frac{\partial \hat{S}}{\partial \lambda} - \left[\hat{S}, \frac{\hat{\gamma}_D}{2\beta_0} \right] = \frac{\beta_1}{2\beta_0^2} \hat{\gamma}_D - \frac{\hat{G}}{2\beta_0}. \quad (2.61)$$

Rotating back into the initial basis, we obtain from eq. (2.61)

$$\hat{J} + \frac{\beta_\lambda^0}{\beta_0} \lambda \frac{\partial \hat{J}}{\partial \lambda} - \left[\hat{J}, \frac{\hat{\gamma}^{(0)T}}{2\beta_0} \right] = \frac{\beta_1}{2\beta_0^2} \hat{\gamma}^{(0)T} - \frac{\hat{\gamma}^{(1)T}}{2\beta_0}. \quad (2.62)$$

where

$$\hat{J} = V^{-1} \hat{S} V. \quad (2.63)$$

The elements of \hat{S} are given by

$$S_{ij} = \delta_{ij} \frac{\beta_1}{2\beta_0^2} \gamma_{D_i} - \frac{G_{ij}}{2\beta_0 + \gamma_{D_i}^{(0)} - \gamma_{D_j}^{(0)}}. \quad (2.64)$$

They become divergent in case $2\beta_0 + \hat{\gamma}_{D_i}^{(0)} - \hat{\gamma}_{D_j}^{(0)} = 0$. In order to find a solution for \hat{S}_{ij} we let \hat{S} to be α -dependent. In this case one additional term in (2.61) appears, in particular, we find

$$\hat{S} - \left[\hat{S}, \frac{\hat{\gamma}_D^{(0)}}{2\beta_0} \right] = \frac{\hat{\gamma}_D^{(0)} \beta_1}{2\beta_0^2} - \frac{\hat{G}}{2\beta_0} - \alpha \frac{d\hat{S}}{d\alpha}. \quad (2.65)$$

Setting the denominator $2\beta_0 + \hat{\gamma}_{d_i}^{(0)} - \hat{\gamma}_{d_j}^{(0)} = 0$ implies $i \neq j$ and from eq. (2.65), we obtain

$$dS_{ij}(\alpha(\mu)) = -\frac{G_{ij}}{2\beta_0} \frac{d\alpha}{\alpha}. \quad (2.66)$$

Finally, after integration we have

$$S_{ij}(\alpha(\mu)) = \frac{G_{ij}}{2\beta_0} \ln \left(\frac{\alpha(M)}{\alpha(\mu)} \right) + S_{ij}(\alpha(M)). \quad (2.67)$$

The generated singularities cancel and the physical evolution matrix has no divergent entries. An explicit calculation shows that in practice divergences appear only in case of 3 active flavours [13]. Since in our case we want to evolve the Wilson coefficients calculated at the SUSY scale ($M_{\text{SUSY}} \sim 500 \text{ GeV}$) down to the mass of the bottom quark where the matrix elements of the effective operators are obtained from lattice calculations, we work with at least 5 effective flavours. Thus, the problem with divergent matrix elements does not appear in our calculation. In general, the problem can be avoided by introducing the

general solution of the RG equation. In ref. [13] the solution for the evolution matrix for QCD and electromagnetic renormalisation until $\mathcal{O}(\alpha)$ is given. The solution in case of only QCD renormalisation has the same form and the problem with the divergences does not appear because the solution can be written in a form such that for divergent denominator the numerator vanishes as well. For more details about the explicit calculation we refer to [13].

We note that \hat{W}_{LO} is renormalisation and regularisation scheme independent while $\lambda\partial\hat{J}/\partial\lambda$ is independent of the regularisation scheme but not of renormalisation scheme. For instance, it vanishes in any possible MS scheme.

After insertion of the expansion (2.46) in eq. (2.47) it follows

$$\vec{C}(\mu) = \left(\mathbf{1} + \frac{\alpha(\mu)}{4\pi} \hat{J} \right) \hat{U}(\mu, M) \left[\hat{T}^{(0)} - \frac{\alpha(M)}{4\pi} \left((\hat{J} + \hat{r}^T) \hat{T}^{(0)} - \hat{T}^{(1)} \right) \right]. \quad (2.68)$$

The combination $\hat{J}_{\text{RI}} \equiv \hat{J} + \hat{r}^T$ is renormalisation scheme independent. Indeed, using (2.38) and (2.62) we derive

$$\hat{J}_{\text{RI}} + \frac{\beta_\lambda^0}{\beta_0} \lambda \frac{\partial \hat{J}_{\text{RI}}}{\partial \lambda} - \left[\hat{J}_{\text{RI}}, \frac{\hat{\gamma}^{(0)T}}{2\beta_0} \right] = \frac{\beta_1}{2\beta_0^2} \hat{\gamma}^{(0)T} - \frac{\hat{G}^T}{2\beta_0}. \quad (2.69)$$

Since the r.h.s. of (2.69) contains only renormalisation scheme independent quantities (\hat{G} and $\hat{\gamma}^{(0)}$) the l.h.s. must be also renormalisation scheme independent which in turn implies that \hat{J}_{RI} has to be also independent of the renormalisation scheme.

2.4. Evolution of the $\Delta B = 2$ effective Hamiltonian

In the analysis of the meson mixing processes we calculate the Wilson coefficients in the SM as well as the supersymmetric contributions. In this section we describe the evolution of the Wilson coefficients relevant for the meson mixing processes from the SUSY scale down to the scale at which the hadronic matrix elements are computed in lattice gauge theory.

2.4.1. The operator basis

The relevant operators which enter the effective Hamiltonian for $\Delta F = 2$ flavour transitions are given by [62]

$$Q_1 = \bar{q}^\alpha \gamma_\mu P_L b^\alpha \bar{q}^\beta \gamma_\mu P_L b^\beta,$$

$$\begin{aligned}
Q_2 &= \bar{q}^\alpha P_L b^\alpha \bar{q}^\beta P_L b^\beta, \\
Q_3 &= \bar{q}^\alpha P_L b^\beta \bar{q}^\beta P_L b^\alpha, \\
Q_4 &= \bar{q}^\alpha P_L b^\alpha \bar{q}^\beta P_R b^\beta, \\
Q_5 &= \bar{q}^\alpha P_L b^\beta \bar{q}^\beta P_R b^\alpha,
\end{aligned} \tag{2.70}$$

together with the operators $\tilde{Q}_{1,2,3}$ which can be obtained from the operators $Q_{1,2,3}$ by the exchange $L \leftrightarrow R$. The left-handed and right-handed projectors are defined as $P_{R,L} = (1 \pm \gamma_5)/2$ while α and β are colour indices.

The ADM of $\Delta F = 2$ flavour transition takes part in several phenomenological applications. Apart from FCNCs in supersymmetric extensions of the SM, also the width difference $\Delta\Gamma_{B_s}$ at leading order in $1/m_b$ can be written in terms of $\Delta B = 2$ operators [15]. Corrections of order $1/m_b^3$ to the lifetime of heavy hadrons containing a b quark can be written in terms of four $\Delta B = 2$ operators as well [16]. Even if they mix with lower dimensional operators, the mixing matrix is triangular and the relevant sub-matrix involves the same computation required for the $\Delta B = 2$ ADM.

2.4.2. Program for Evolution

We give the analytic formulae for the evolution of the Wilson coefficients at the scale where the hadronic matrix elements are evaluated as a function of the initial conditions at the SUSY scale $C_i(M_{\text{SUSY}})$ and of $\alpha(M_{\text{SUSY}})$. Our calculation of the evolution matrix is based on the results given in chapter 5 of ref. [11] where the matrix elements of the ADM at one and two loop as well as the matrix elements of \hat{J} calculated in Feynman-gauge RI scheme (FRI scheme) can be found. Furthermore, following the recipe for the translation of \hat{J} between the FRI scheme the Landau-gauge renormalisation scheme (LRI scheme) and the $\overline{\text{MS}}$ renormalisation scheme we could crosscheck the results given in ref. [11] with the results in ref. [17] where the ADM is calculated directly in the $\overline{\text{MS}}$ renormalisation scheme. The ADMs in ref. [11] and ref. [17] are obtained in an operator basis different from the one defined in eq. (2.70) which is commonly used for calculations of the Wilson coefficients for meson mixing processes in SUSY. The two basis are related to each other by a Fierz transformation. Therefore, in order to obtain the right form of the matrices in the SUSY basis (2.70) we have to apply a Fierz transformation on the matrices given in refs. [11] and [17]. The so called Fierz basis in general form is given by [11]

$$Q_1^\pm = \frac{1}{2}(\overline{\Psi}_1^i \gamma_L^\mu \Psi_2^i)(\overline{\Psi}_3^j \gamma_{\mu L} \Psi_4^j) \pm (\Psi_2 \leftrightarrow \Psi_4),$$

$$\begin{aligned}
Q_2^\pm &= \frac{1}{2}(\overline{\Psi}_1 \gamma_L^\mu \Psi_2^i)(\overline{\Psi}_3^j \gamma_{\mu R} \Psi_4^j) \pm (\Psi_2 \leftrightarrow \Psi_4), \\
Q_3^\pm &= \frac{1}{2}(\overline{\Psi}_1 P_R \Psi_2^i)(\overline{\Psi}_3^j P_L \Psi_4^j) \pm (\Psi_2 \leftrightarrow \Psi_4), \\
Q_4^\pm &= \frac{1}{2}(\overline{\Psi}_1 P_L \Psi_2^i)(\overline{\Psi}_3^j P_L \Psi_4^j) \pm (\Psi_2 \leftrightarrow \Psi_4), \\
Q_5^\pm &= \frac{1}{2}(\overline{\Psi}_1 \sigma_L^{\mu\nu} \Psi_2^i)(\overline{\Psi}_3^j \sigma_{\mu\nu L} \Psi_4^j) \pm (\Psi_2 \leftrightarrow \Psi_4)
\end{aligned} \tag{2.71}$$

where $\sigma_K^{\mu\nu} = \frac{1}{2}[\gamma^\mu, \gamma^\nu] P_K$, $K \in \{L, R\}$. The $\Delta B = 2$ operators are obtained from the operators Q_i^+ by taking $\Psi_1 = \Psi_3 = b$ and $\Psi_2 = \Psi_4 = q$ while the operators Q_i^- vanish. In dimensional regularisation Fierz identities cannot be analytically continued in D dimensions. Therefore, in general evanescent operators have to be introduced. They are necessary to make a precise definition of the NDR- $\overline{\text{MS}}$ scheme but can be neglected in the RI schemes. In general, operators can mix under renormalisation. However, chiral symmetry forbids the mixing between some of the operators appearing in the basis (2.71). Therefore, in the Fierz basis the ADM has the form

$$\hat{\gamma}^\pm = \begin{pmatrix} A^\pm & 0 & 0 & 0 & 0 \\ 0 & B & \pm C & 0 & 0 \\ 0 & \pm D & E & 0 & 0 \\ 0 & 0 & 0 & F^\pm & G^\pm \\ 0 & 0 & 0 & H^\pm & I^\pm \end{pmatrix}, \tag{2.72}$$

and there is no mixing between Q^- and Q^+ . In particular, the correspondence between the operators of the Fierz basis (2.71) and the SUSY basis (2.70) is given by the transformation

$$\vec{Q}^{\text{SUSY}} = \hat{M} \vec{Q}^+ \tag{2.73}$$

with the matrix \hat{M} given by

$$\hat{M} = \begin{pmatrix} 1 & 0 & 0 & 0 & 0 \\ 0 & 0 & 0 & 1 & 0 \\ 0 & 0 & 0 & -\frac{1}{2} & \frac{1}{8} \\ 0 & 0 & 1 & 0 & 0 \\ 0 & -\frac{1}{2} & 0 & 0 & 0 \end{pmatrix}. \tag{2.74}$$

The ADM in the SUSY basis (2.70) $\hat{\gamma}^{\text{SUSY}}$ satisfies the relation

$$\hat{\gamma}^{\text{SUSY}} = \hat{M} \hat{\gamma}^+ \hat{M}^{-1}. \tag{2.75}$$

For the LO ADM $\gamma^{(0)\text{SUSY}}$ which is independent of the regularisation and of the renormalisation scheme we find after inserting the corresponding numerical values and performing a rotation from the Fierz basis to the SUSY basis

$$\gamma^{(0)\text{SUSY}} = \begin{pmatrix} 4 & 0 & 0 & 0 & 0 \\ 0 & -\frac{28}{3} & \frac{4}{3} & 0 & 0 \\ 0 & \frac{16}{3} & \frac{32}{3} & 0 & 0 \\ 0 & 0 & 0 & -16 & 0 \\ 0 & 0 & 0 & -6 & 2 \end{pmatrix}. \quad (2.76)$$

In order to solve the RG equations, we need to diagonalise the LO ADM $\gamma^{(0)\text{SUSY}}$. For the entries of the corresponding diagonal matrix γ_D we find

$$\gamma_D^{(0)\text{SUSY}} = \text{diag}(4, -9.68278, 11.0161, -16, 2). \quad (2.77)$$

The elements of the NLO ADM depend on the renormalisation scheme and the number of active flavours. Their analytical expressions obtained in the NDR $\overline{\text{MS}}$ scheme and in the FRI scheme can be found in refs. [17] and [11], respectively. Using the formal approaches in the analyses [11] and [17], we could obtain and translate the relevant matrices between the different renormalisation schemes and have found a full agreement between the results. Schematically, we show the two possible ways for the determination of the matrices in the different renormalisation schemes on the example of the matrix \hat{J} :

$$\begin{aligned} \hat{J}_{\text{FRI}}^{\text{Fierz}} &\longrightarrow \hat{J}_{\text{LRI}}^{\text{Fierz}} \longrightarrow \hat{J}_{\text{LRI}}^{\text{SUSY}} \\ \hat{J}_{\overline{\text{MS}}}^{\text{Fierz}} &\longrightarrow \hat{J}_{\text{LRI}}^{\text{Fierz}} \longrightarrow \hat{J}_{\text{LRI}}^{\text{SUSY}}. \end{aligned}$$

Starting from the FRI scheme in the Fierz basis, we translate the matrices to the LRI scheme. Then the results are transformed to the SUSY basis according to ref. [11]. On the other hand, we use the results of the calculation in $\overline{\text{MS}}$ renormalisation scheme of ref. [17], transform them to the LRI scheme and then change the operator basis from the Fierz basis to the SUSY basis. Both approaches are completely equivalent.

Further, we introduce the quantity

$$\eta \equiv \frac{\alpha(M_{\text{SUSY}})}{\alpha(m_t)} \quad (2.78)$$

where m_t denotes the mass of the top quark, and write every entry in the evolution matrix at NLO as

$$\hat{W}(\mu, M)_{mn} = \sum_i \left(b_i^{(mn)} + \eta c_i^{(mn)} \right) \eta^{a_i}, \quad (2.79)$$

where b_i and c_i are the so called “magic“ numbers. In the case of $B-\bar{B}$ mixing, the $C_i(M_{\text{SUSY}})$ are evolved down to the hadronic scale $\mu = m_b$ at which the hadronic matrix elements are calculated using lattice QCD methods. Studying $K-\bar{K}$ mixing or $D-\bar{D}$ mixing we have to go even more lower in the energy scale, to $\mu = 2.0 \text{ GeV}$ and to $\mu = 2.8 \text{ GeV}$, respectively. The constants a_i in eq. (2.79) are given by

$$a_i = \frac{\hat{\gamma}_{D_i}^{(0)}}{2\beta_0} = (-1.14286, 0.78687, -0.69163, 0.28571, 0.14286)_i. \quad (2.80)$$

By the evolution of the Wilson coefficients from the scale M_{SUSY} down to the scale μ the threshold at m_t is passed at which the number of active flavours n_f changes by one unit from 6 to 5. Therefore, the evolution of the Wilson coefficients at NLO is performed using eq. (2.47) in two steps, first from M_{SUSY} down until m_t where $n_f = 6$, and after this from m_t to $\mu = m_b$ with 5 active flavours. Since we apply two times (2.47) after each other terms proportional to $\alpha(m_t)^2$ and $\alpha(m_b)\alpha(m_t)$ can appear which are of $\mathcal{O}(\alpha^2)$. We have restricted our working precision up to $\mathcal{O}(\alpha)$ and have neglected the contribution of terms of $\mathcal{O}(\alpha^2)$ to the matrix elements of the evolution matrix.

With the numerical input in table (4.1) the magic numbers $b_i^{(mn)}$ and $c_i^{(mn)}$ for the non-vanishing matrix elements are the following:

$$\begin{aligned} b_i^{(11)} &= (0.868, 0, 0, 0, 0), & c_i^{(11)} &= (-0.016, 0, 0, 0, 0), \\ b_i^{(22)} &= (0, 1.820, 0.012, 0, 0), & c_i^{(22)} &= (0, -0.157, -0.003, 0, 0), \\ b_i^{(23)} &= (0, -0.477, 0.183, 0, 0), & c_i^{(23)} &= (0, -0.012, 0.008, 0, 0), \\ b_i^{(32)} &= (0, -0.050, 0.036, 0, 0), & c_i^{(32)} &= (0, 0.010, -0.012, 0, 0), \\ b_i^{(33)} &= (0, 0.013, 0.549, 0, 0), & c_i^{(33)} &= (0, 0.001, 0.030, 0, 0), \\ b_i^{(44)} &= (0, 0, 0, 2.719, 0), & c_i^{(44)} &= (0, 0, 0, -0.377, 0.006), \\ b_i^{(45)} &= (0, 0, 0, 0.906, -0.235), & c_i^{(45)} &= (0, 0, 0, -0.193, -0.006), \\ b_i^{(54)} &= (0, 0, 0, 0.073, 0), & c_i^{(54)} &= (0, 0, 0, 0, -0.017), \\ b_i^{(55)} &= (0, 0, 0, 0.024, 0.868), & c_i^{(55)} &= (0, 0, 0, 0, 0.019). \end{aligned} \quad (2.81)$$

In order to calculate the $K-\bar{K}$ mixing amplitude we have to evolve the Wilson coefficients down to the scale $\mu = 2.0 \text{ GeV}$ at which the corresponding hadronic matrix elements are

extracted from lattice simulations. In this case we find the magic numbers:

$$\begin{aligned}
b_i^{(11)} &= (0.816, 0, 0, 0, 0), & c_i^{(11)} &= (-0.015, 0, 0, 0, 0), \\
b_i^{(22)} &= (0, 2.275, 0.010, 0, 0), & c_i^{(22)} &= (0, -0.188, -0.003, 0, 0), \\
b_i^{(23)} &= (0, -0.596, 0.155, 0, 0), & c_i^{(23)} &= (0, -0.015, 0.006, 0, 0), \\
b_i^{(32)} &= (0, -0.042, 0.029, 0, 0), & c_i^{(32)} &= (0, 0.012, -0.010, 0, 0), \\
b_i^{(33)} &= (0, 0.011, 0.438, 0, 0), & c_i^{(33)} &= (0, 0.001, 0.025, 0, 0), \\
b_i^{(44)} &= (0, 0, 0, 3.890, 0), & c_i^{(44)} &= (0, 0, 0, -0.507, 0.005), \\
b_i^{(45)} &= (0, 0, 0, 1.297, -0.212), & c_i^{(45)} &= (0, 0, 0, -0.259, -0.006), \\
b_i^{(54)} &= (0, 0, 0, 0.127, 0), & c_i^{(54)} &= (0, 0, 0, 0, -0.016), \\
b_i^{(55)} &= (0, 0, 0, 0.042, 0.824), & c_i^{(55)} &= (0, 0, 0, 0, 0.018).
\end{aligned} \tag{2.82}$$

The hadronic matrix elements involved in the $D-\bar{D}$ mixing process are known at the scale $\mu = 2.8 \text{ GeV}$. Therefore, we evolve the Wilson coefficients to that scale as well. In this case the magic numbers are given by:

$$\begin{aligned}
b_i^{(11)} &= (0.838, 0, 0, 0, 0), & c_i^{(11)} &= (-0.016, 0, 0, 0, 0), \\
b_i^{(22)} &= (0, 2.059, 0.011, 0, 0), & c_i^{(22)} &= (0, -0.174, -0.003, 0, 0), \\
b_i^{(23)} &= (0, -0.540, 0.167, 0, 0), & c_i^{(23)} &= (0, -0.013, 0.007, 0, 0), \\
b_i^{(32)} &= (0, -0.046, 0.032, 0, 0), & c_i^{(32)} &= (0, 0.011, -0.011, 0, 0), \\
b_i^{(33)} &= (0, 0.012, 0.484, 0, 0), & c_i^{(33)} &= (0, 0.001, 0.027, 0, 0), \\
b_i^{(44)} &= (0, 0, 0, 3.315, 0), & c_i^{(44)} &= (0, 0, 0, -0.445, 0.006), \\
b_i^{(45)} &= (0, 0, 0, 1.105, -0.222), & c_i^{(45)} &= (0, 0, 0, -0.227, -0.006), \\
b_i^{(54)} &= (0, 0, 0, 0.992, 0), & c_i^{(54)} &= (0, 0, 0, 0, -0.017), \\
b_i^{(55)} &= (0, 0, 0, 0.033, 0.843), & c_i^{(55)} &= (0, 0, 0, 0, 0.019).
\end{aligned} \tag{2.83}$$

2.5. Hadronic Matrix Elements

The matrix elements of the operators in eq. (2.70) can be computed from first principles only in the framework of the lattice QCD. While the operators in eq. (2.70) have both parity even and parity odd parts, only the parity even parts contribute to the matrix elements relevant for the meson mixing processes. The strong interaction preserve parity and consequently

$$\langle \bar{M} | Q_i | M \rangle = \langle \bar{M} | \tilde{Q}_i | M \rangle, \quad i = 1, 2, 3 \tag{2.84}$$

where M denotes a B , K or D meson. Usually, one defines the dimensionless B -parameters as a measure of the deviation of the matrix elements from their expression in the vacuum insertion approximation (VIA), in particular

$$B_i(\mu) = \frac{\langle \bar{M} | Q_i | M \rangle}{\langle \bar{M} | Q_i | M \rangle_{\text{VIA}}} . \quad (2.85)$$

The matrix elements in a given renormalisation scheme RS are defined as [19, 62]

$$\langle Q_i^{\text{RS}}(\mu) \rangle = b_i \chi_i f_M^2 M_M^2 B_i^{M, \text{RS}}(\mu) \quad (2.86)$$

where

$$\begin{aligned} b_i &= \left(\frac{2}{3}, -\frac{5}{12}, \frac{1}{12}, \frac{1}{2}, \frac{1}{6} \right)_i, \\ \chi_1 &= 1, \\ \chi_i &= \left[\frac{M_M}{m_q(\mu) + m_{\bar{q}}(\mu)} \right]^2 \text{ for } i \in [2, 5]. \end{aligned} \quad (2.87)$$

The matrix elements of all the non-SM operators are chirally enhanced by the ratio of the meson mass over the sum of the masses of its quark constituents. In order to determine the numerical values of the B -parameters, numerical simulations of a quenched and unquenched QCD on the lattice have been performed. The results of recent QCD lattice calculations are reviewed in ref. [20].

2.5.1. Hadronic Matrix Elements for $B - \bar{B}$ mixing

In the case of $B - \bar{B}$ mixing we use the B -parameters obtained in a lattice calculation of a quenched QCD reported in ref. [18]. Lattice simulations can be made up to the c quark mass or some heavier mass but present computational resources do not allow a direct study of the b quark. The calculation in ref. [18] has been performed in the range of heavy-light pseudoscalar masses [1.7, 2.4] GeV, and then extrapolated to the physical point m_{B_d} guided by Heavy Quark Effective Theory (HQET) scaling laws. The numerical values of the B -parameters involved in the $B_d - \bar{B}_d$ and $B_s - \bar{B}_s$ mixing amplitudes are given by

$$\begin{aligned} B_i^{B_d, \text{RI}} &= [0.87(4)_{-4}^{+5}, 0.82(3)(4), 1.02(6)(9), 1.16(3)_{-7}^{+5}, 1.91(4)_{-7}^{+22}]_i, \\ B_i^{B_s, \text{RI}} &= [0.86(2)_{-4}^{+5}, 0.83(2)(4), 1.03(4)(9), 1.17(2)_{-7}^{+5}, 1.94(3)_{-7}^{+23}]_i \end{aligned} \quad (2.88)$$

in the LRI scheme [18]. For the determination of the numerical values of the hadronic matrix elements the knowledge of the B_d and B_s decay constants f_{B_d} and f_{B_s} is necessary. In

our calculation we use the averages of lattice QCD inputs for the CKM fits performed by the CKMfitter collaboration [21]. According to the CKMfitter group the average value of the decay constant f_{B_s} is given by

$$f_{B_s} = (228 \pm 3 \pm 17) \text{ MeV} \quad (2.89)$$

where the first error is statistical and the second systematical. Lattice calculations allow the determination of the ratio

$$\xi = \frac{f_{B_s} \sqrt{B_1^{B_s}}}{f_{B_d} \sqrt{B_1^{B_d}}} \quad (2.90)$$

with much better precision than the decay constants themselves. Furthermore, the decay constant f_{B_s} is determined more precisely than f_{B_d} . Therefore, by the calculation of the $B_s - \bar{B}_s$ and $B_d - \bar{B}_d$ transition amplitudes we use the ratio of the decay constants

$$\frac{f_{B_s}}{f_{B_d}} = 1.199 \pm 0.008 \pm 0.023 \quad (2.91)$$

determined from the CKMfitter group [21] by analysing various lattice simulations, and the decay constant f_{B_s} . In eq. (2.91) again the first error is the statistical and the second the systematical one as before. In ref. [18] the operators are defined without the factor 1/2 in the projectors i.e. $O_1 = \bar{q}^i \gamma^\mu (1 - \gamma_5) b^i \bar{q}^j \gamma_\mu (1 - \gamma_5) b^j$. Taking this fact into account we obtain for the hadronic matrix elements with the definition of the operators given in (2.70) the following mean values at the scale $\mu = 4.6 \text{ GeV}$:

$$\begin{aligned} \langle Q_i^{B_d, \text{RI}} \rangle &= (0.8593, -0.6809, 0.1690, 1.1518, 0.6366)_i, \\ \langle Q_i^{B_s, \text{RI}} \rangle &= (0.5846, -0.4520, 0.1125, 0.7673, 0.4211)_i. \end{aligned} \quad (2.92)$$

2.5.2. Hadronic Matrix Elements for $K - \bar{K}$ mixing

For the calculation of the $K - \bar{K}$ transition amplitude we use the B -parameters presented in ref. [20] where the results of many quenched and unquenched lattice simulations with different lattice spacing are collected and analysed in context of the relevant errors. The parameter B_1^K which is involved in the SM $K - \bar{K}$ mixing amplitude has been computed in several lattice calculations while a calculation of the B -parameters of the full operator basis (2.70) has been performed only in three lattice studies until now [95–97]. All of them have been performed within the quenched approximation. However, the authors of the analysis

[20] do not recommend to use the number for B_1^K obtained in the three lattice simulations mentioned above which determine the B -parameters for all the operators. Instead, they refer to the result of lattice calculations whose goal has been the computation of B_1^K only which is known more precisely than the other B -parameters. Finally, the average values of the B -parameters in the RI-MOM scheme at the scale $\mu = 2 \text{ GeV}$ are given by [20]

$$B_i^{K,\text{RI}} = [0.54(5), 0.7(2), 1.0(4), 0.9(2), 0.6(1)]_i. \quad (2.93)$$

Together with the decay constant $f_K = (155.5 \pm 0.3 \pm 1.9) \text{ MeV}$ [21] and $(m_s^{\text{RI}} + m_d^{\text{RI}}) = (135 \pm 18) \text{ MeV}$ [20] we obtain the following mean values for the hadronic matrix elements involved in $K-\bar{K}$ mixing at $\mu = 2 \text{ GeV}$:

$$\langle Q_i^{K,\text{RI}} \rangle = (0.00864, -0.09520, 0.02720, 0.14689, 0.03264)_i. \quad (2.94)$$

2.5.3. Hadronic Matrix Elements for $D-\bar{D}$ mixing

As stated in ref. [20] in the case of $D-\bar{D}$ mixing the involved hadronic matrix elements can be obtained from the lattice results presented in [18] as well. This work provides numerical results for heavy-light mesons with masses $1.75(9) \text{ GeV}$ and $2.02(10) \text{ GeV}$, respectively. Thus, the B -parameters for the D mesons can be obtained by extrapolating to the physical point m_D between the two sets of results. The authors of ref. [20] add in the final averages an additional systematic uncertainty of 10%. This decision is motivated by the fact that the results in ref. [18] are obtained from a single quenched simulation in lattice QCD. Finally, the B -parameters relevant for $D-\bar{D}$ mixing in the RI-MOM scheme at the scale $\mu = 2.8 \text{ GeV}$ are given by

$$B_i^{D,\text{RI}} = [0.85(9), 0.82(9), 1.07(12), 1.10(11), 1.37(14)]_i. \quad (2.95)$$

With the averages for the decay constant $f_{D_s} = (246.3 \pm 1.1 \pm 5.3) \text{ MeV}$ and for the ratio $f_{D_s}/f_D = 1.186 \pm 0.0046 \pm 0.01$ [21] we find the mean values for the hadronic matrix elements

$$\langle Q_i^{D,\text{RI}} \rangle = (0.3398, -0.4402, 0.1149, 0.7087, 0.2942). \quad (2.96)$$

3. GENERAL ASPECTS OF MESON MIXING

In this chapter we describe the general formalism of meson mixing. It can be applied to all cases of meson mixing processes in particular to $B-\bar{B}$ mixing, $K-\bar{K}$ mixing or $D-\bar{D}$ mixing. In the next chapter we focus on the three meson mixing processes mentioned above and discuss the specific issues of each one and the main differences between them from phenomenological point of view. For a more detailed description of the phenomenon of meson mixing we refer to [9], [23, 24] and references therein.

The meson-antimeson mixing is a Flavour Changing Nuclear Current (FCNC) process. In the SM FCNC transitions are forbidden at tree level. At one loop level the flavour changing W^\pm and G^\pm vertices make FCNC processes possible. The meson mixing is an effect of fourth order flavour-changing weak interaction which is described in the SM by the box diagrams shown in fig. 4.2. The charged Higgs vertices have to be taken into account by performing the calculation in R_ξ gauge while they are absent by choosing an unitary gauge. In following we focus on the time evolution of a meson or antimeson state. The calculation of the box diagrams in the SM as well as the supersymmetric contributions will be discussed in chapters 4.1.2 and 4.2.

Meson-antimeson mixing means that a neutral meson state $|M\rangle$ initially created as $|M\rangle$ or $|\bar{M}\rangle$ becomes a superposition of $|M\rangle$ and $|\bar{M}\rangle$ with time elapsing. Assuming first no meson-antimeson mixing which is fulfilled in the case of charged mesons the time evolution of a meson state $|M\rangle$ is described by the Schrödinger equation

$$i\frac{d}{dt}|M(t)\rangle = \left(M_M - i\frac{\Gamma_M}{2}\right)|M\rangle \quad (3.1)$$

where M_M is the mass and Γ_M stays for the total decay width of the meson. With $|M\rangle$ we denote the meson state at the initial time $t = 0$, $|M(0)\rangle = |M\rangle$. The solution of eq. (3.1) is given by

$$|M(t)\rangle = e^{i\left(M_M - i\frac{\Gamma_M}{2}\right)t}|M\rangle \quad (3.2)$$

Eq. (3.2) describes the usual exponential time evolution of a stable state with energy $E = M_M$ as well as the process of decaying of the meson following an exponential law. Thus, the probability the meson not to have decayed at time t is given by

$$|\langle M|M(t)\rangle|^2 = e^{-\Gamma_M t}. \quad (3.3)$$

In case of meson-antimeson mixing the time evolution of a meson or an antimeson state produced at time $t = 0$ is more complicated. An initially created meson or antimeson is a quantum superposition of the states $|M\rangle$ and $|\bar{M}\rangle$ at the time $t > 0$:

$$|M(t)\rangle = a(t)|M\rangle + b(t)|\bar{M}\rangle. \quad (3.4)$$

In the basis $\{|M\rangle, |\bar{M}\rangle\}$ we can write the two-dimensional Schrödinger equation

$$i\frac{d}{dt}|M(t)\rangle = \mathcal{M}|M(t)\rangle \quad (3.5)$$

with the matrix $\mathcal{M} \in \mathbb{C}^{2 \times 2}$. Further, we use the property of every matrix to be written as a sum of a hermitian and an antihermitian one and decompose \mathcal{M} as

$$\mathcal{M} = \hat{M} - i\frac{\hat{\Gamma}}{2} \quad (3.6)$$

where the mass matrix \hat{M} and the decay matrix $\hat{\Gamma}$ have been introduced which are both hermitian. According to the CPT theorem [25–27] the states $|M\rangle$ and $|\bar{M}\rangle$ have identical masses and total decay widths. This requirement enforces the equality of the diagonal elements of \mathcal{M} . Then, it follows

$$\hat{M}_{11} = \hat{M}_{22}, \quad \hat{\Gamma}_{11} = \hat{\Gamma}_{22}. \quad (3.7)$$

We find the time evolution of the flavour eigenstates $|M(t)\rangle$ and $|\bar{M}(t)\rangle$ starting from the time evolution of the mass eigenstates $|M_1(t)\rangle$ and $|M_2(t)\rangle$. Because of the special form of the matrix \mathcal{M} with equal diagonal elements we can make the following ansatz for the matrix Q which diagonalises it

$$Q = \begin{pmatrix} p & p \\ q & -q \end{pmatrix}. \quad (3.8)$$

For the inverse matrix Q^{-1} it follows

$$Q^{-1} = \frac{1}{2pq} \begin{pmatrix} q & p \\ q & -p \end{pmatrix}. \quad (3.9)$$

Thus, the mass eigenstates and the flavour eigenstates are related to each other through

$$\begin{aligned} |M_1\rangle &= p|M\rangle + q|\overline{M}\rangle, \\ |M_2\rangle &= p|M\rangle - q|\overline{M}\rangle \end{aligned} \quad (3.10)$$

with $|p|^2 + |q|^2 = 1$ and \mathcal{M} is diagonalised as

$$Q^{-1} \mathcal{M} Q = \text{diag} \left(M_{M_1} - i \frac{\Gamma_{M_1}}{2}, M_{M_2} - i \frac{\Gamma_{M_2}}{2} \right). \quad (3.11)$$

Since the mass eigenstates do not mix with elapsing time their time evolution is described by eq. (3.1) which is valid for the time evolution of charged particles. We can write

$$i \frac{d}{dt} |M_j(t)\rangle = \left(M_{M_j} - i \frac{\Gamma_{M_j}}{2} \right) |M_j(t)\rangle, \quad j \in \{1, 2\}. \quad (3.12)$$

The solution is analogous to the one given in eq. (3.2):

$$|M_j(t)\rangle = e^{i \left(M_{M_j} - i \frac{\Gamma_{M_j}}{2} \right) t} |M_j\rangle, \quad j \in \{1, 2\}. \quad (3.13)$$

Having obtained the time evolution of the mass eigenstates we can transform it to the flavour eigenstate basis. Inverting eq. (3.10) we find

$$\begin{aligned} |M(t)\rangle &= \frac{1}{2p} (|M_1(t)\rangle + |M_2(t)\rangle), \\ |\overline{M}(t)\rangle &= \frac{1}{2q} (|M_1(t)\rangle - |M_2(t)\rangle). \end{aligned} \quad (3.14)$$

In order to write the formulae in a more simple form, we adopt the following definitions for the mass and width differences and the average mass and width of the mass eigenstates:

$$\begin{aligned} m &\equiv \frac{M_{M_1} + M_{M_2}}{2}, & \Gamma &\equiv \frac{\Gamma_{M_1} + \Gamma_{M_2}}{2}, \\ \Delta M &\equiv M_{M_2} - M_{M_1}, & \Delta \Gamma &\equiv \Gamma_{M_1} - \Gamma_{M_2}. \end{aligned} \quad (3.15)$$

Further, we define the functions [23, 24]

$$\begin{aligned} g_+(t) &= e^{-i \left(m - \frac{\Gamma}{2} \right) t} \left[\cosh \left(\frac{\Delta \Gamma}{4} t \right) \cos \left(\frac{\Delta m}{2} t \right) - i \sinh \left(\frac{\Delta \Gamma}{4} t \right) \sin \left(\frac{\Delta m}{2} t \right) \right], \\ g_-(t) &= e^{-i \left(m - \frac{\Gamma}{2} \right) t} \left[-\sinh \left(\frac{\Delta \Gamma}{4} t \right) \cos \left(\frac{\Delta m}{2} t \right) + i \cosh \left(\frac{\Delta \Gamma}{4} t \right) \sin \left(\frac{\Delta m}{2} t \right) \right] \end{aligned} \quad (3.16)$$

Finally, after inserting in eq. (3.14) the time evolution of the mass eigenstates given in eq. (3.13) considering the definitions in (3.15 - 3.16), the time evolution of the flavour

eigenstates can be written in a compact form

$$\begin{aligned} |M(t)\rangle &= g_+(t)|M\rangle + \frac{q}{p}g_-(t)|\bar{M}\rangle, \\ |\bar{M}(t)\rangle &= \frac{p}{q}g_-(t)|M\rangle + g_+(t)|\bar{M}\rangle. \end{aligned} \quad (3.17)$$

Since $g_{\pm}(t)$ does not vanish for $t > 0$ if $\Delta\Gamma \neq 0$ an initially produced meson $|M\rangle$ will never transform into a pure antimeson state $|\bar{M}\rangle$ or back into a pure $|M\rangle$. The meson-antimeson oscillation process can be easily illustrated by means of eq. (3.17). The time dependent probabilities $P_{MM}(t)$ and $P_{M\bar{M}}(t)$ to find a meson or an antimeson when at the initial time $t = 0$ a meson has been created are given by

$$\begin{aligned} P_{MM} &= |g_+(t)|^2 = \frac{e^{-\Gamma t}}{2} \left[\cosh\left(\frac{\Delta\Gamma}{2}t\right) + \cos(\Delta m t) \right], \\ P_{M\bar{M}} &= \left| \frac{q}{p}g_-(t) \right|^2 = \frac{e^{-\Gamma t}}{2} \left[\cosh\left(\frac{\Delta\Gamma}{2}t\right) - \cos(\Delta m t) \right]. \end{aligned} \quad (3.18)$$

We plot these probabilities in case of $B_d - \bar{B}_d$, $B_s - \bar{B}_s$, and $D - \bar{D}$ mixing in fig. 3.1. As a numerical input of the quantities ΔM_d , $\Delta\Gamma_d$, ΔM_s , $\Delta\Gamma_s$ and τ_B the values given in table 4.1 have been used. In case of $D - \bar{D}$ mixing we obtained the relevant quantities taking into account the input parameters given in table 4.2. In the $B_s - \bar{B}_s$ system we see a lot of oscillations in the shown time interval. On the contrary, the $B_d - \bar{B}_d$ oscillations happen much slower. In fact, the first minimum of $P_{B_s B_s}$ is at $t = 0.18$ ps while the probability $P_{B_d B_d}$ is not minimal until $t = 6.20$ ps. The D mesons decay so fast that there is no sufficient time during their lifetime for a creation of an antimeson component.

At this point it is important to clarify which quantities relevant for the meson-antimeson mixing process are independent of phase conventions and have therefore a physical meaning. The multiplication of either $|M\rangle$ or $|\bar{M}\rangle$ by an arbitrary complex phase factor will affect the phases of the matrix elements M_{12} , Γ_{12} as well as the phase of q/p . In fact, $|M_{12}|$, $|\Gamma_{12}|$ and their relative phase

$$\phi = \arg\left(-\frac{M_{12}}{\Gamma_{12}}\right) \quad (3.19)$$

are invariant under phase transformations. These are the physical observables which appeared in our discussion of the meson-antimeson mixing formalism until now.

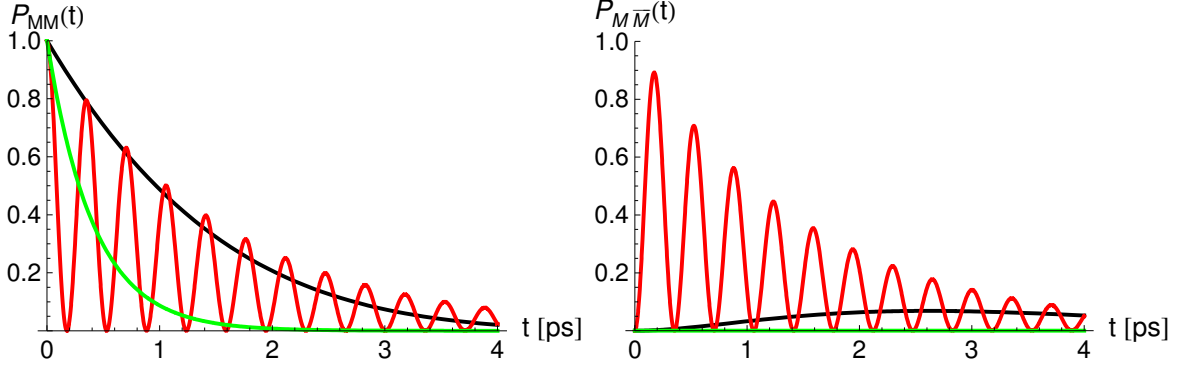


Figure 3.1: Time evolution of an initially created meson (left plot) or antimeson (right plot) for the $B_d - \bar{B}_d$ system (black line), $B_s - \bar{B}_s$ system (red line) and $D - \bar{D}$ system (green line). In the right plot $P_{D\bar{D}}$ coincides with the x-axis.

Our approach for constraining supersymmetric parameters is based on the comparison between the theoretical estimate of the mass differences in the B_d and B_s meson systems and the corresponding measured values of these quantities under the assumption that NP only enters at the loop level through additional particles running in the loops. For this reason $\Delta F = 2$ transitions which in the SM are mediated by box diagrams can be sensitive probes of NP. The matrix elements M_{12} and Γ_{12} are related to the dispersive and absorptive parts of the $\Delta F = 2$ transitions. Γ_{12} can be written as a product of tree-level $\Delta F = 1$ amplitudes so that NP is not likely to alter its value. In this sense it is important to find the relation between ΔM and the meson mixing amplitude M_{12} . For that purpose we turn back to the eigenvalue problem (3.11) and denote the two eigenvalues of the matrix \mathcal{M} by λ_1 and λ_2 . Solving the secular equation

$$(\mathcal{M}_{11} - \lambda_{1,2}) - \mathcal{M}_{12}\mathcal{M}_{21} = 0 \quad (3.20)$$

we obtain a relation between the eigenvalues

$$(\lambda_1 - \lambda_2)^2 = 4\mathcal{M}_{12}\mathcal{M}_{21}. \quad (3.21)$$

Equating the real and imaginary part of the l.h.s and r.h.s of eq. (3.21) separately leads to a relation between the mass difference, the total width difference, the decay amplitude and the total width:

$$\begin{aligned} (\Delta M)^2 - \left(\frac{\Delta\Gamma}{2}\right)^2 &= 4|M_{12}|^2 - |\Gamma_{12}|^2, \\ (\Delta M)(\Delta\Gamma) &= -4 \operatorname{Re}(M_{12}\Gamma_{12}^*) = 4|M_{12}||\Gamma_{12}|\cos\phi. \end{aligned} \quad (3.22)$$

For the $B-\bar{B}$ system it is experimentally known that $\Delta\Gamma \ll \Delta M$. On the other hand, SM calculations show that $\Gamma_{12} \ll \Delta M$ is valid as well. Therefore, from eq. (3.22) it follows

$$\begin{aligned}\Delta M &\simeq 2|M_{12}|, \\ \Delta\Gamma &\simeq 2|\Gamma_{12}|\cos\phi.\end{aligned}\tag{3.23}$$

Equation (3.23) is valid also in the case of $K-\bar{K}$ mixing, in which $\Delta\Gamma > \Delta M$, but $\phi \approx 0$.

4. WILSON COEFFICIENTS FOR MESON MIXING PROCESSES IN THE MSSM

In this chapter we discuss the meson mixing processes in the neutral B , D and Kaon systems. We explain the specific features of the meson mixing phenomenon in the three cases mentioned above. We focus on the computation of the Wilson coefficients in the SM as well as on the supersymmetric contributions.

4.1. SM contribution

Each of the Wilson coefficients corresponding to the operators basis given in eq. (2.70) can be written as

$$C_i = C_i^{\text{SM}} + C_i^{\text{SUSY}} \quad (4.1)$$

In eq. (4.1) the first term represents contributions from the SM and the second one summarises the contributions from supersymmetric particles.

The SM contribution to the meson mixing processes is described only by the operator Q_1 given in eq. (2.70) which corresponds to the situation that all external particles of the boxes are left-handed. In this section we summarise and discuss the basic results regarding the $B - \bar{B}$, $K - \bar{K}$ and $D - \bar{D}$ mixing in the SM. For a more detailed description of the phenomenon of meson mixing we refer to [9, 23, 24] and references therein.

4.1.1. The pure SM CKM matrix

The flavour violation process in the SM is governed by the CKM matrix elements. Since our goal is to place constraints on parameters of SUSY particles which can affect the meson mixing amplitudes, the separation of the pure SM contribution from the contribution caused by SUSY particles is extremely important. However, the CKM matrix elements are

measured using processes which cannot be always free of NP effects. Therefore, one has to find a way to determine the CKM matrix elements involved in the calculation of the SM part of the Wilson coefficients, if possible without, or with the minimal possible amount of NP contributions.

Within the SM a great variety of processes characterised by a very different dynamics are sensitive to the same four independent parameters of the CKM matrix defined in the so called Standard parametrisation by

$$V = \begin{pmatrix} c_{12}c_{13} & s_{12}c_{13} & s_{13}e^{-i\delta} \\ -s_{12}c_{23} - c_{12}s_{23}s_{13}e^{i\delta} & c_{12}c_{23} - s_{12}s_{23}s_{13}e^{i\delta} & s_{23}c_{13} \\ s_{12}s_{23} - c_{12}c_{23}s_{13}e^{i\delta} & -c_{12}s_{23} - s_{12}c_{23}s_{13}e^{i\delta} & c_{23}c_{13} \end{pmatrix} \quad (4.2)$$

with $c_{ij} = \cos\theta_{ij}$ and $s_{ij} = \sin\theta_{ij}$. In the presence of NP this is no longer true even in minimally flavour violating extensions of the SM. Taking into account the smallness of $s_{13} \approx \mathcal{O}(10^{-3})$ and $s_{23} \approx \mathcal{O}(10^{-2})$ which implies $c_{13} = 1 = c_{23}$ the four independent parameters are given by

$$s_{12} = |V_{us}|, \quad s_{13} = |V_{ub}|, \quad s_{23} = |V_{cb}| \quad \text{and} \quad \delta. \quad (4.3)$$

In order to write the results of theoretical calculations in a more transparent form and to exhibit the experimentally found hierarchy $s_{13} \ll s_{23} \ll s_{12} \ll 1$ the so called Wolfenstein parametrisation [28] of the CKM matrix is very useful. In this parametrisation each element of the CKM matrix is written as a power series expansion of the small parameter $\lambda = |V_{us}|$. In particular,

$$V = \begin{pmatrix} 1 - \frac{\lambda^2}{2} & \lambda & (\rho - i\eta)A\lambda^3 \\ -\lambda & 1 - \frac{\lambda^2}{2} & A\lambda^2 \\ (1 - \rho - i\eta)A\lambda^3 & -A\lambda^2 & 1 \end{pmatrix} + \mathcal{O}(\lambda^4). \quad (4.4)$$

The relation between the independent parameters (4.3) in the Standard parametrisation and the parameters λ , A , ρ and η used in the Wolfenstein parametrisation is given by

$$s_{12} = \lambda, \quad s_{23} = A\lambda^2, \quad s_{13}e^{-i\delta} = A\lambda^3(\rho - i\eta). \quad (4.5)$$

The unitarity relation $V_{ij}V_{kj}^* = \delta_{ik}$ creates various relations between the CKM matrix elements. The most important one follows from the multiplication of the first and the third column of the CKM matrix. In particular, we find

$$V_{ud}V_{ub}^* + V_{cd}V_{cb}^* + V_{td}V_{tb}^* = 0. \quad (4.6)$$

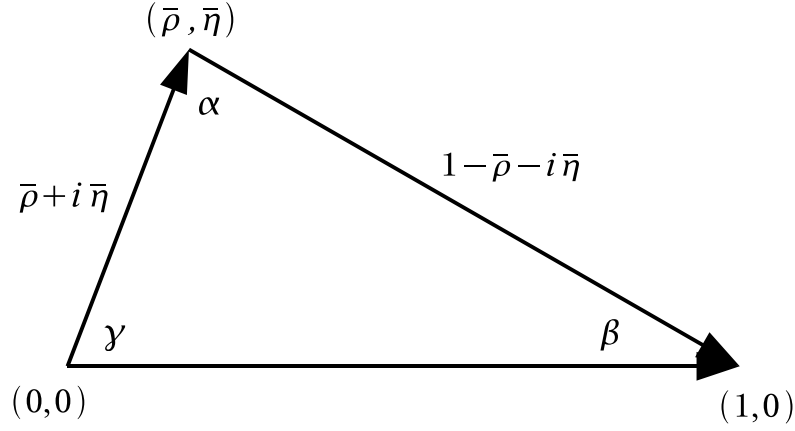


Figure 4.1: The unitarity triangle.

This equation involves the only two complex elements in the expansion until $\mathcal{O}(\lambda^4)$ in the Wolfenstein parametrisation. The representation of eq. (4.6) in the complex $(\bar{\rho}, \bar{\eta})$ -plane shown in fig. 4.1 where the axis are defined as [98]

$$\bar{\rho} = \rho \left(1 - \frac{\lambda^2}{2}\right), \quad \bar{\eta} = \eta \left(1 - \frac{\lambda^2}{2}\right) \quad (4.7)$$

is the so called unitarity triangle (UT). With

$$\bar{\rho} + i\bar{\eta} = -\frac{V_{ud}V_{ub}^*}{V_{cd}V_{cb}^*} \quad (4.8)$$

we obtain from eq. (4.6)

$$[(\bar{\rho} + i\bar{\eta}) + (-1) + (1 - \bar{\rho} - i\bar{\eta})] \quad (4.9)$$

which is shown in fig. 4.1. Since eq. (4.9) is invariant under phase transformations, the sides and angles of the UT are physical observables.

The sides and angles of the UT can be expressed using trigonometric relations through the Wolfenstein parameters as follows:

$$\begin{aligned} \sin(2\alpha) &= \frac{2\bar{\eta}(\bar{\eta}^2 + \bar{\rho}^2 - \bar{\rho})}{(\bar{\rho}^2 + \bar{\eta}^2)[(1 - \bar{\rho})^2 + \bar{\eta}^2]}, \\ \sin(2\beta) &= \frac{2\bar{\eta}(1 - \bar{\rho})}{(1 - \bar{\rho})^2 + \bar{\eta}^2}, \\ \sin(2\gamma) &= \frac{2\bar{\rho}\bar{\eta}}{\bar{\rho}^2 + \bar{\eta}^2}, \end{aligned}$$

$$\begin{aligned}
R_b &= \left| \frac{V_{ud}V_{ub}^*}{V_{cd}V_{cb}^*} \right| = \sqrt{\bar{\rho}^2 + \bar{\eta}^2}, \\
R_t &= \left| \frac{V_{td}V_{tb}^*}{V_{cd}V_{cb}^*} \right| = \sqrt{(1 - \bar{\rho})^2 + \bar{\eta}^2}.
\end{aligned} \tag{4.10}$$

We insert the parameters

$$\rho = \frac{s_{13}}{s_{12}s_{23}} \cos \delta, \quad \eta = \frac{s_{13}}{s_{12}s_{23}} \sin \delta \tag{4.11}$$

which we easily derive from (4.5) in the equation for $\sin(2\gamma)$ and find $\gamma = \delta$. To an excellent accuracy the angles β and γ of the UT are directly linked to the phases of the complex elements V_{td} and V_{ub} . We find the relations

$$\begin{aligned}
V_{td} &= |V_{td}|e^{-i\beta} = R_t A \lambda^3 e^{-i\beta}, \\
V_{ub} &= |V_{ub}|e^{-i\gamma} = R_b A \lambda^3 e^{-i\gamma}.
\end{aligned} \tag{4.12}$$

For all predictions within the SM we assume unitarity of the CKM matrix and calculate all CKM elements from the four parameters

$$|V_{us}|, \quad |V_{cb}|, \quad |V_{ub}|, \quad \gamma. \tag{4.13}$$

The numerical input values are given in table 4.1. This set of parameters can be determined entirely from tree level decays and are consequently independent of NP contributions. Our strategy to extract γ without NP contributions includes the combination of the informations from $B \rightarrow J/\psi K_S$ and $B \rightarrow \pi^+\pi^-$ decays. These transitions can be affected by NP in the electromagnetic penguins only which is a very unlikely scenario. We discard this possibility and assume that decays to be completely governed by the SM. Both decays provide information about the mixing induced CP asymmetry $\mathcal{A}_{\text{CP}}^{\text{mix}}$. The relevant relations are

$$\begin{aligned}
\mathcal{A}_{\text{CP}}^{\text{mix}}(B \rightarrow J/\psi K_S) &= -\sin(\phi_d) \\
\mathcal{A}_{\text{CP}}^{\text{mix}}(B \rightarrow \rho\rho) &= \sin(2\gamma + \phi_d)
\end{aligned} \tag{4.14}$$

where ϕ_d is the $\bar{B}_d - B_d$ mixing phase. In the SM the $B_d - \bar{B}_d$ mixing phase $\phi_d = 2\beta$ but in the presence of NP it can be affected by an additional phase ϕ_d^{NP} . In this case we can write

$$\phi_d = 2\beta + \phi_d^{\text{NP}}. \tag{4.15}$$

α (dir. meas.)	$89.0^{\circ+4.4^{\circ}}_{-4.2^{\circ}}$ [22]	$ V_{cb} $	$(41.17^{+0.38}_{-1.17}) \cdot 10^{-3}$ [22]
β (dir. meas.)	$21.15^{\circ+0.90^{\circ}}_{-0.88^{\circ}}$ [22]	$ V_{ub} $	$(3.51^{+0.14}_{-0.16}) \cdot 10^{-3}$ [22]
$ V_{us} = \lambda = s_{12}$	0.22544 ± 0.00095 [22]	$\alpha_s(M_Z)$	0.119 ± 0.003
G_F	$1.16637 \cdot 10^{-5} \text{ GeV}^{-2}$	$\alpha(M_Z)$	$1/127.9$
M_{B_d}	$(5.2794 \pm 0.0005) \text{ GeV}$ [85]	M_{B_s}	$(5.3696 \pm 0.0024) \text{ GeV}$ [85]
$m_b(\overline{m}_b)$	$(4.248 \pm 0.051) \text{ GeV}$ [86]	$m_t(\overline{m}_t)$	$(165.02 \pm 1.16 \pm 0.11) \text{ GeV}$ [22]
M_W	$(80.423 \pm 0.039) \text{ GeV}$	s_W	$\sqrt{0.2397}$
$\Delta M_{B_d}^{\text{exp}}$	$(0.507 \pm 0.005) \text{ ps}^{-1}$ [85]	$\Delta M_{B_s}^{\text{exp}}$	$(17.77 \pm 0.10 \pm 0.07) \text{ ps}^{-1}$ [90, 91]
$f_{B_s}^{\text{th}}$	$(228 \pm 3 \pm 17) \text{ MeV}$ [21]	$f_{B_s}^{\text{th}}/f_{B_d}^{\text{th}}$	$(1.199 \pm 0.008 \pm 0.023)$ [21]
f_D^{th}	$(212 \pm 14) \text{ MeV}$ [20]	f_K^{th}	$155.5 \pm 0.3 \pm 1.9 \text{ MeV}$ [21]
$\Delta\Gamma_{B_d}^{\text{th}}$	$26.7^{+5.8}_{-6.5} \cdot 10^{-4} \text{ ps}^{-1}$ [69]	$\Delta\Gamma_{B_s}^{\text{th}}$	$0.088 \pm 0.017 \text{ ps}^{-1}$ [69]

Table 4.1: Values of the experimental and theoretical quantities used as an input parameters.

Using the unitarity relation $\gamma = \pi - \alpha - \beta$ and the experimental information about the the measured quantities $\beta^{\text{exp}} = \beta + \phi_d/2$ and $\alpha^{\text{exp}} = \alpha - \phi_d/2$ we can determine γ from the equation

$$\gamma = \pi - \alpha^{\text{exp}} - \beta^{\text{exp}}. \quad (4.16)$$

In eq. (4.16) the the NP phase ϕ_d^{NP} cancels because it affects the measured quantities β^{exp} and α^{exp} with opposite sign. With the numbers given in table 4.1 we find

$$\gamma = 1.23918^{+0.10996}_{-0.12566} \left(71.0^{\circ+6.3^{\circ}}_{-7.2^{\circ}} \right) \quad (4.17)$$

which is the pure SM value of the angle γ .

4.1.2. The mixing of neutral B mesons in the SM

For the mixing of the neutral B mesons in the SM we consider the box diagrams shown in fig. 4.2. In case of $B_d - \overline{B}_d$ mixing the incoming and outgoing quarks are b and d while for $B_s - \overline{B}_s$ mixing the d quark is replaced by a s quark. Choosing an unitary gauge the particles running in the loop are represented by two W bosons and two up-type quarks. Performing the calculation in a general R_ξ gauge the contribution of the charged Pseudo-Goldstone bosons has to be taken into account as well. Our goal is to calculate

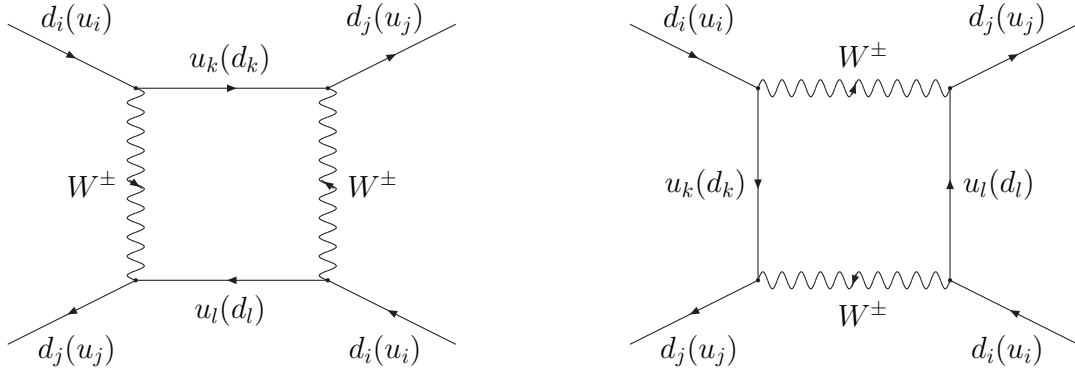


Figure 4.2: The box diagrams describing meson-antimeson mixing in the SM in the unitary gauge. In case of $B - \bar{B}$ and $K - \bar{K}$ mixing the incoming and outgoing quarks are of down-type and up-type quarks are involved in the loop. For $D - \bar{D}$ mixing the situation is the opposite - incoming and outgoing up-type quarks and down-type quarks running in the loop. In R_ξ gauge additional box diagrams involving charged Pseudo-Goldstone bosons have to be considered.

the mass differences ΔM_s and ΔM_d for the $B_s - \bar{B}_s$ and $B_d - \bar{B}_d$ system, respectively. It has been already pointed out that in the calculation procedure of meson-antimeson transition amplitudes we have to deal with low energy QCD which makes the application of perturbative methods impossible. In order to solve this problem, we have to extract the SM Wilson coefficient C_1^{SM} by matching the transition amplitude calculated in the full theory onto the one calculated in the effective theory. Then, the multiplication of the effective coupling C_1^{SM} by the corresponding hadronic matrix element $\langle \bar{B}_{d,s} | Q_1 | B_{d,s} \rangle$ at the same scale gives the transition amplitude. At this point it should be mentioned that the fact whether the CKM matrix elements and/or the mass of the W boson belong to the Wilson coefficient or not is a question of convention. In our treatment all factors which multiply the effective operator Q_1 are contained in the corresponding Wilson coefficient C_1^{SM} .

In the calculation of the transition amplitude one has to take the sum over all box diagrams which involve all possible combinations of two up-type quarks running in the loop. Thus, the transition amplitude can be written as

$$A = \sum_{i,j=u,c,t} V_{jb} V_{jq}^* V_{kb} V_{kq}^* A_{ij}(m_i^2, m_j^2) \quad (4.18)$$

where A_{ij} is the contribution if a certain box diagram which involves up quarks with flavours

i and j . A_{ij} is a symmetric function in the quark masses m_i and m_j . The calculation of the box diagrams in the full theory involves an integration over the loop momentum. The loop integral is finite. It can be written as a sum of master integrals using partial fraction decomposition. The master integrals contain divergences which are regularised by the method of dimensional regularisation and the divergent terms cancel in the sum. In general we encounter no problems with divergences by performing the integration. Further, using the relation

$$\sum_{i=u,c,t} V_{jb}V_{jq}^* = 0 \quad (4.19)$$

which follows from the unitarity of the CKM matrix i.e. with $j = u$ the expression for the transition amplitude can be simplified. In particular, eq. (4.19) implies vanishing transition amplitude A in case of equal quark masses. The vanishing of FCNC in the limit of equal quark masses as a consequence of the unitarity of the CKM matrix is known as Glashow-Iliopoulos-Maiani (GIM) suppression [29]. In the meson-antimeson mixing processes we encounter once more the GIM mechanism which has successfully explained the small branching ratio of the decay channel $K^0 \rightarrow \pi^+\pi^-$ predicting the existence of the charm quark.

Further, we neglect the contributions of the u -quark loops treating the u quark as a massless particle and find for the Wilson coefficient at LO

$$C_1^{\text{SM}} = \frac{g_2^4}{(16\pi)^2 M_W^2} [\lambda_{tq}^2 4S_0(x_t) + \lambda_{cq}\lambda_{tq} 4S_0(x_c, x_t)], \quad (4.20)$$

with the well known Inami-Lim-functions [30]

$$S_0(x_t) = \frac{x_t^3 - 11x_t^2 + 4x_t}{4(x_t - 1)^2} + \frac{3x_t^3 \ln x_t}{2(x_t - 1)^3}, \quad (4.21)$$

$$S_0(x_c, x_t) = x_c \left(-\frac{3x_t^2 \ln x_t}{4(x_t - 1)^2} + \frac{3x_t}{4(x_t - 1)} + \ln \frac{x_t}{x_c} \right), \quad (4.22)$$

and the definitions $x_i = m_i^2/M_W^2$, $\lambda_{iq} = V_{ib}V_{iq}^*$ for $i \in \{u, c, t\}$. In order to describe the mixing of neutral B_d mesons one has to make the choice $q = d$ while in case of $B_s - \bar{B}_s$ mixing q is identified with the s quark. Because of the small ratio $x_c = \mathcal{O}(10^{-4})$ the contribution of the second term in eq. (4.20) proportional to $S_0(x_c, x_t) = \mathcal{O}(x_c)$ is very tiny in comparison to the contribution of two top quarks in the loop and can be neglected. Finally, with the Fermi constant $G_F = g_2^2/4\sqrt{2}M_W^2$, the Wilson coefficient C_1^{SM} can be written as

$$C_1^{\text{SM}} = \frac{G_F^2 M_W^2}{4\pi^2} \lambda_{qt}^2 S_0(x_t). \quad (4.23)$$

In order to check the result of the calculation we have obtained the Wilson coefficient C_1^{SM} performing the calculation in the unitary gauge as well as in the R_ξ gauge. We found a full agreement between the results of the calculations in the different gauges and a full agreement with the results in the literature. Note that the Wilson coefficient given in eq. (4.23) is four times bigger than the one given in eqs. (3.17) and (3.19) in ref. [9]. The reason for this difference is the definition of the operators in ref. [9]. In particular, the projectors $P_{R,L}$ are defined without the factor $1/2$. The factor 4 included in the definition of the hadronic matrix elements is compensated by the factor $1/4$ in the Wilson coefficients such that there is no difference between the transition amplitudes calculated in this work and the ones given in ref. [9] and other previous works.

Now we turn back to the problem described in Ch. 2, namely, the different scales of the Wilson coefficient and the hadronic matrix elements. We have to take care about the fact that the Wilson coefficient C_1^{SM} is extracted at the scale $\mu = M_W$ while the hadronic matrix elements are obtained from lattice calculations at the scale $\mu = m_b$. In order to calculate the transition amplitude it is necessary to perform an RG evolution of either the Wilson coefficient C_1^{SM} down to the scale $\mu = m_b$ or of the corresponding hadronic matrix element up to the scale of the W boson mass $\mu = M_W$. In contrast to the evolution of the Wilson coefficients in the case of the supersymmetric contributions to the meson mixing processes which is performed in the RI-MOM renormalisation scheme, we follow for the SM contribution to the $B-\bar{B}$ mixing process the established treatment in the literature in the $\overline{\text{MS}}$ renormalisation scheme. Since the operator Q_1 does not mix with other operators under renormalisation, the evolution of the Wilson coefficient is described by a single factor. One usually writes

$$C_1^{\text{SM}}(m_b) = \hat{\eta}_B C_1^{\text{SM}}(M_W) \quad (4.24)$$

where $\hat{\eta}_B$ is obtained from NLO calculation and can be written as a product of two factors, $\hat{\eta}_B = \eta_B b_B(m_b)$ [31]. In this way the heavy scale and the low scale are separated. The scale dependence of the factor $b_B(m_b)$ cancels in the product with the hadronic matrix element which depends on m_b as well. Numerically, it is found $\hat{\eta}_B = 0.837$ in the $\overline{\text{MS}}$ -NDR scheme. More details on this topic can be found in [31] and [32].

Finally, writing the $|\Delta B| = 2$ Hamiltonian as

$$\mathcal{H}^{|\Delta B=2|} = \frac{G_F}{4\pi^2} M_W^2 (V_{tb} V_{tq}^*)^2 \hat{\eta} Q_1(m_b) + h.c. \quad (4.25)$$

we obtain for the transition amplitude M_{12}^{SM} taking into account the parametrisation of the hadronic matrix elements given in eq. (2.86) the expression

$$M_{12}^{\text{SM}} = \langle B | \mathcal{H}^{|\Delta B=2|} | \bar{B} \rangle = \frac{G_F^2}{6\pi^2} M_W^2 \lambda_{tq}^2 S_0(x_t) \hat{\eta} M_{B_q}^2 f_{B_q}^2 B_1(m_b). \quad (4.26)$$

4.1.3. Indirect CP violation in $K-\bar{K}$ mixing

The case of the mixing of neutral K mesons can be theoretically treated in analogous way as the mixing in the B meson system. However, in the $K-\bar{K}$ mixing some specific features appear which will be the main subject of the following discussion.

The Kaon mixing is described by the operator Q_1 with incoming and outgoing d and s quarks. The $K-\bar{K}$ transition is a $|\Delta S| = 2$ process. Because of the different external states compared to the ones in the case of $B_d-\bar{B}_d$ and $B_s-\bar{B}_s$ mixing, we encounter different combinations of CKM matrix elements by the computation of all the box diagrams involving the up-type quarks of the three generations in the loop. In contrast to the $B-\bar{B}$ mixing process where the top contribution is dominant, now the function $S(x_t)$ is highly suppressed by factor $(V_{ts}V_{td}^*)^2 \approx \mathcal{O}(\lambda^{10})$. On the contrary, even if the corresponding loop functions of the charm-charm and charm-top contributions are small, they are multiplied only by a CKM factor of $\mathcal{O}(\lambda)$. Therefore, the top quark loop becomes comparable in size with the ones with two charm quarks and with one charm quark and one top quark. Thus, the latter cannot be neglected as this has been the case in the neutral B meson system.

The effective $|\Delta S| = 2$ Hamiltonian can be written as [31]

$$\mathcal{H}_{\text{eff}}^{|\Delta S|=2} = \frac{G_F}{4\pi^2} M_W^2 [(V_{cs}V_{cd}^*)^2 \eta_{cc} x_c + (V_{ts}V_{td}^*)^2 \eta_{tt} S_0(x_t) + 2V_{cs}V_{cd}^* V_{ts}V_{td}^* \eta_{ct} S_0(x_c, x_t)] b_K(m_K) Q_1 + h.c. \quad (4.27)$$

with the coefficients η_{tt} , η_{ct} and η_{cc} which describe short-distance QCD effects. At NLO the QCD coefficients are given by [31, 33–35]

$$\begin{aligned} \eta_{cc} &= (1.44 \pm 0.35) \left(\frac{1.3 \text{ GeV}}{m_c} \right)^{1.1}, \\ \eta_{ct} &= 0.47 \pm 0.05, \\ \eta_{tt} &= 0.57 \pm 0.01. \end{aligned} \quad (4.28)$$

For the $K - \bar{K}$ transition amplitude one obtains

$$M_{12}^{\text{SM}} = \frac{G_F}{4\pi^2} M_W^2 f_K^2 \hat{B}_K m_K [(V_{cs}V_{cd}^*)^2 \eta_{cc} x_c + (V_{ts}V_{td}^*)^2 \eta_{tt} S_0(x_t) + 2V_{cs}V_{cd}^*V_{ts}V_{td}^* \eta_{ct} S_0(x_c, x_t)] \quad (4.29)$$

with the definition of the hadronic matrix elements given in eq. (2.86) and the renormalisation group invariant factor $\hat{B}_K = B_K b(m_K)$. In contrast to the situation in $B - \bar{B}$ mixing, the K meson decay constant f_K is well known from experiments. The factor \hat{B}_K is determined by lattice calculations (see Ch. 2.5.2). Calculating $\Delta M_K^{\text{SM}} = 2|M_{12}^{\text{SM}}|$ with the usual effective field theory methods, the obtained result differs from the experimentally measured value of the same quantity by roughly 30%. In fact, eq. (4.29) contains only the so called short distance contributions to the $K - \bar{K}$ transition amplitude. However, the $K - \bar{K}$ mixing can occur through two $|\Delta S| = 1$ transitions as well. This so called long distance contribution cannot be calculated from first principles.

In our analysis we constrain MSSM parameters through their effects on the indirect CP violation in the neutral Kaon system. In particular, the supersymmetric particles contributing with new box diagrams to the $K - \bar{K}$ transition amplitude affect the quantity ϵ_K which measures the CP violation in mixing in the $K - \bar{K}$ mixing process. CP violation in mixing of neutral mesons arises from the fact that the CP eigenstates are different from the mass eigenstates. Following the general analysis of the meson-antimeson mixing in Ch. (3), we replace the mass eigenstates in eq. (3.10) $|M_1\rangle$ and $|M_2\rangle$ with $|K_S\rangle$ and $|K_L\rangle$, respectively. The indices "L = long" and "S = short" have been chosen in the past according to the decay of neutral Kaons to $\pi^+\pi^-$ or $\pi^0\pi^0$. A K meson state $|K\rangle$ is a quantum superposition of the lighter mass eigenstate $|K_S\rangle$ and the heavier mass eigenstate $|K_L\rangle$. Defining

$$\bar{\epsilon} = \frac{1 + \frac{q}{p}}{1 - \frac{q}{p}} \quad (4.30)$$

eq. (3.10) can be written as

$$\begin{aligned} |K_S\rangle &= \frac{1 + \bar{\epsilon}}{2\sqrt{1 + |\epsilon|^2}} |K^0\rangle - \frac{1 - \bar{\epsilon}}{2\sqrt{1 + |\epsilon|^2}} |\bar{K}^0\rangle, \\ |K_L\rangle &= \frac{1 + \bar{\epsilon}}{2\sqrt{1 + |\epsilon|^2}} |K^0\rangle + \frac{1 - \bar{\epsilon}}{2\sqrt{1 + |\epsilon|^2}} |\bar{K}^0\rangle. \end{aligned} \quad (4.31)$$

With the CP transformation $CP|K^0\rangle = -|\bar{K}^0\rangle$, $CP|\bar{K}^0\rangle = -|K^0\rangle$ we introduce the CP-even and CP-odd eigenstates $|K_+\rangle$ and $|K_-\rangle$ as

$$|K_+\rangle = \frac{1}{\sqrt{2}} (|K^0\rangle - |\bar{K}^0\rangle),$$

$$|K_-\rangle = \frac{1}{\sqrt{2}} \left(|K^0\rangle + |\bar{K}^0\rangle \right). \quad (4.32)$$

Expressing the mass eigenstates through the CP eigenstates we obtain

$$|K_S\rangle = \frac{|K_+\rangle + \bar{\epsilon}|K_-\rangle}{\sqrt{1 + |\bar{\epsilon}|^2}}, \quad |K_L\rangle = \frac{|K_-\rangle + \bar{\epsilon}|K_+\rangle}{\sqrt{1 + |\bar{\epsilon}|^2}}. \quad (4.33)$$

Equation (4.33) shows in explicit way that the mass eigenstates are an admixture of the CP eigenstates. The limit of CP conservation is given by $\bar{\epsilon} = 0$ and in this case $|K_S\rangle$ becomes the CP-odd eigenstate and $|K_L\rangle$ the CP-even one. Considering the decay of a neutral Kaon to a CP even final state represented by two pions or to a CP odd final state combination of three pions one realises that under the assumption of CP conservation the decays $K_L \rightarrow \pi\pi$ and $K_S \rightarrow \pi\pi\pi$ are forbidden. Since the ratio $|q/p| \approx 1$ in the $B-\bar{B}$ and $K-\bar{K}$ systems the phase dependent quantity $\bar{\epsilon}$ is small. Therefore, $|K_L\rangle$ is "almost" a CP odd eigenstate and $|K_S\rangle$ "almost" a CP even one. This is the reason for the big difference in the lifetimes of the mass eigenstates. However, since $\bar{\epsilon} \neq 0$ the mass eigenstates $|K_L\rangle$ and $|K_S\rangle$ can decay CP violating to two or three pion states, respectively. The CP violation in mixing is described by the parameter

$$\epsilon_K = \frac{A(K_L \rightarrow (\pi\pi)_{I=0})}{A(K_S \rightarrow (\pi\pi)_{I=0})} \quad (4.34)$$

where I denotes the strong isospin. This quantity can be expressed entirely through the mass difference ΔM_K , $\Delta\Gamma_K$ and ϕ which are physical observables. The result reads up to corrections of $\mathcal{O}(\phi^2)$ [23, 24]

$$\epsilon_K = \frac{\phi}{2} \frac{2\Delta M_K}{\sqrt{(\Delta M_K)^2 + (\Delta\Gamma_K)^2}} e^{i\phi_\epsilon} \quad (4.35)$$

with the phase ϕ_ϵ of ϵ_K given by

$$\phi_\epsilon = \arctan \frac{2\Delta M_K}{\Delta\Gamma_K} \approx 43^\circ. \quad (4.36)$$

Expressing eq. (4.34) in terms of M_{12} one finds

$$\phi = 2 \left(\frac{\text{Im}M_{12}}{\Delta M_K^{\text{exp}}} + \xi_K \right) \quad (4.37)$$

where ξ_K is introduced as

$$\xi_K = \frac{1}{2} \frac{\text{Im} [A [K^0 \rightarrow (\pi\pi)_{I=0}]]}{\text{Re} [A [K^0 \rightarrow (\pi\pi)_{I=0}]]} \quad (4.38)$$

defined in the CKM phase convention with V_{us}, V_{ud} real. Numerically, it has been found $\xi_K \approx -1.7 \cdot 10^{-4}$ [36]. Equation (4.36) implies

$$\sin \phi_\epsilon = \frac{2 \Delta M_K}{\sqrt{(\Delta M_K)^2 + (\Delta \Gamma_K)^2}}, \quad (4.39)$$

and finally, inserting this result in eq. (4.35), we obtain

$$\epsilon_K = \left(\frac{\text{Im} M_{12}}{\Delta M_K^{exp}} + \xi_K \right) \sin \phi_\epsilon e^{i\phi_\epsilon}. \quad (4.40)$$

Because of the experimental observation $2 \Delta M_K \approx \Delta \Gamma_K$ the phase of ϵ_K is very close to 45° . In fact, the measured value is $\phi_\epsilon = 43.52^\circ \pm 0.05^\circ$ [37]. The impact of the ratio ξ_K on the result of ϵ_K is of $\mathcal{O}(5\%)$ [36]. With the result for the $K-\bar{K}$ transition amplitude given in eq. (4.29) one finds [36]

$$|\epsilon_K^{\text{SM}}| = C_\epsilon [|V_{cb}|^2 (1 - \bar{\rho}) \eta_{tt} S_0(x_t) + \eta_{ct} S_0(x_c, x_t) - \eta_{cc} x_c] \quad (4.41)$$

with the factor C_ϵ given by

$$C_\epsilon = \frac{G_F^2 f_K^2 M_W^2 m_K \kappa_\epsilon \hat{B}_K \lambda^2 \bar{\eta}^2 |V_{cb}|^2}{6\sqrt{2} \pi^2 \Delta M_K} \quad (4.42)$$

where $\bar{\rho}, \bar{\eta}$ are the Wolfenstein parameters introduced in eq. (4.4). The constant $\kappa_\epsilon = 0.92 \pm 0.02$ parametrises the suppression effect caused by ξ_K . More details about the explicit derivation of these results as well as on the meson mixing of neutral K mesons in general can be found in [9, 23, 24, 36] and references therein.

4.1.4. Main aspects on the mixing of neutral D mesons

The $D-\bar{D}$ mixing is a $\Delta C = 2$ FCNC process. It is described by the same box diagrams as in the case of meson mixing in the B or K sector, but, in contrast to the situation with the mixing of neutral B and K mesons, the incoming and outgoing quarks are the up-type quarks u and c and the quarks involved in the loop are the ones of the down-type quark sector. Because of the absence of a heavy quark in the loop as this is the case in $B-\bar{B}$ and $K-\bar{K}$ mixing due to the top quark contribution, the GIM cancellation works much more efficiently. The $D-\bar{D}$ transition amplitude in the SM is very small, and therefore, highly sensitive to NP effects. NP contributions can be of the same order of magnitude or even larger than the SM one which makes the mixing of neutral D mesons a very interesting process regarding the indirect search of physics beyond the SM. However, the

large long distance effects which have been mentioned in the analysis of the $K-\bar{K}$ mixing appear in the D sector as well. Since these effects given by K, π intermediate states have non-perturbative nature and cannot be calculated by analytical methods the distinguishing of the SM contributions from the pure NP ones is hardly possible. The poor control over the long distance contributions impairs an effective use of $D-\bar{D}$ mixing as a test of the SM.

The third family contribution which would be enhanced by the large mass m_b is suppressed by a very small CKM factor resulting in a relative box contribution of $\mathcal{O}(10^{-3})$ and in a correspondingly suppressed amount of CP violation in the SM. Therefore,

$$\Delta M_D^{\text{SM}} \sim \frac{(m_s^2 - m_d^2)^2}{m_c^2} \quad (4.43)$$

with a GIM suppression $\sim (m_s^2 - m_d^2)/M_W^2$ and an additional suppression $\sim (m_s^2 - m_d^2)/m_c^2$ which comes from the fact that the external momentum of $\mathcal{O}(m_c)$ is communicated to the light quarks in the loops. Usually, in the description of $D-\bar{D}$ mixing in addition to the phase ϕ defined in eq. (3.19) the physical quantities

$$x_{12} \equiv \frac{2M_{12}}{\Gamma}, \quad y_{12} = \frac{\Gamma_{12}}{\Gamma}, \quad (4.44)$$

are introduced. The relation between these parameters and the experimentally measured quantities

$$x \equiv \frac{m_1 - m_2}{\Gamma} = \frac{\Delta M_D}{\Gamma}, \quad y \equiv \frac{\Gamma_2 - \Gamma_1}{2\Gamma} = \frac{\Delta\Gamma}{2\Gamma} \quad (4.45)$$

is given by

$$\begin{aligned} x_{12}^2 &= \frac{x^4 \cos^2 \phi + y^4 \sin^2 \phi}{x^2 \cos^2 \phi - y^2 \sin^2 \phi}, \\ \sin^2 \phi_{12} &= \frac{(x^2 + y^2)^2 \cos^2 \phi \sin^2 \phi}{x^4 \cos^2 \phi + y^4 \sin^2 \phi}. \end{aligned} \quad (4.46)$$

From the values of the $D-\bar{D}$ mixing parameters x , y , and ϕ obtained by the Heavy Flavour Averaging Group (HFAG) [38] by fitting the present experimental data, we obtain the numerical value of $|M_{12}|$. Expanding x_{12} given in eq. (4.46) in the presumably small parameter ϕ , we find

$$x_{12} = x + \frac{(x^2 + y^2)y^2}{2x^3} \phi^2 + \mathcal{O}(\phi^4). \quad (4.47)$$

Parameter	1σ	95% CL
x	$(0.98_{-0.26}^{+0.24}) \cdot 10^{-2}$	$[0.46, 1.44] \cdot 10^{-2}$
y	$(0.83 \pm 0.16) \cdot 10^{-2}$	$[0.51, 1.14] \cdot 10^{-2}$
ϕ	$(-8.5_{-7.0}^{+7.4} \text{°})$	$[-22.1 \text{°}, 6.3 \text{°}]$
$ M_{12} $	$(11.95_{-3.17}^{+2.93}) \text{ ps}^{-1}$	$[5.61, 17.56] \text{ ps}^{-1}$
ΔM_D	$(2.39_{-0.63}^{+0.59}) \cdot 10^{-2} \text{ ps}^{-1}$	$[1.12, 3.51] \cdot 10^{-2} \text{ ps}^{-1}$
$\Delta\Gamma_D$	$(4.04 \pm 0.07) \cdot 10^{-2} \text{ ps}^{-1}$	$[2.49, 5.56] \cdot 10^{-2} \text{ ps}^{-1}$

Table 4.2: The final results for the $D-\bar{D}$ mixing parameters $|M_{12}|$, ΔM_D and $\Delta\Gamma_D$ obtained from the parameters x , y and ϕ allowing for CP violation (HFAG) [38]. For the determination of ΔM_D and $\Delta\Gamma_D$ the D^0 mean life time $\tau_{D^0} = (410.1 \pm 1.5) \cdot 10^{-3} \text{ ps}$ [85] has been used.

We calculate $|M_{12}|$ using the D^0 life time $\tau_{D^0} = \Gamma_{D^0}^{-1} = 410.1 \cdot 10^{-3} \text{ ps}$ [85] and neglecting the term proportional to ϕ^2 whose contribution is of $\mathcal{O}(1\%)$ and therefore much smaller than the experimental accuracy. The result as well as the numerical values of the input parameters are given in table (4.2). For more phenomenological details about the mixing of neutral D mesons we refer to [39, 40] and references therein.

In our numerical analysis of the flavour violating supersymmetric parameters we will calculate the contributions of supersymmetric particles to box diagrams in case of $D-\bar{D}$ mixing. Since the spectrum of the MSSM contains heavy particles the calculation can be performed by neglecting the momenta of the external quarks. Unfortunately, this is not true in the SM where the momenta of the incoming and outgoing quarks can be comparable with masses of the light quarks in the loop and, therefore, have to be taken into account. Comparing the pure supersymmetric result for $|M_{12}|$ with the experimentally obtained value given in table (4.2) we can estimate to which extent the measured value of $|M_{12}|$ can be explained through the contribution from the MSSM.

4.2. The SUSY contributions to the meson mixing processes

If nature has chosen Supersymmetry as the right extension of the SM, box diagrams with supersymmetric particles will be involved in meson mixing as well (see fig. 4.3). In particular, the Wilson coefficients corresponding to all the operators given in eq. (2.70) would be different from zero in general. The Wilson coefficient C_i^{SUSY} in eq. (4.1) can be written as



Figure 4.3: Feynman diagrams describing meson-antimeson oscillations in the MSSM. The crossed diagrams (second row) are needed only if the fermion in the loop is a Majorana particle.

a sum of the Wilson coefficients stemming from box diagrams where the FCNC transition is mediated by supersymmetric particles:

$$C_i^{\text{SUSY}} = C_i^{H^\pm} + C_i^{\tilde{\chi}^\pm} + C_i^{\tilde{g}} + C_i^{\tilde{g}\tilde{\chi}^0} + C_i^{\tilde{\chi}^0}. \quad (4.48)$$

The additional contributions arise from boxes with charged Higgs and up-type quarks ($C_i^{H^\pm}$), charginos and up-type squarks ($C_i^{\tilde{\chi}^\pm}$), gluinos and down-type squarks ($C_i^{\tilde{g}}$), mixed gluino, neutralino and down-type squarks ($C_i^{\tilde{g}\tilde{\chi}^0}$), and neutralinos and down-type squarks ($C_i^{\tilde{\chi}^0}$). The complete list of the Feynman rules for the MSSM vertices and their derivation from the Lagrangian can be found in [41–43]. Note that for the derivation of the MSSM Feynman rules different conventions are adopted in the literature. For the calculation of the Wilson coefficients in the MSSM C_i^{SUSY} in this work the Feynman rules given in the appendix have been used. In following we present the convention which we have used in our analysis of the MSSM with R-parity and softly broken SUSY.

The squark superfield matter multiplets contain scalar and fermionic superpartners given by

$$Q^I = \left\{ \begin{pmatrix} \tilde{u}^I \\ \tilde{d}^I \end{pmatrix}_L, \begin{pmatrix} u^I \\ d^I \end{pmatrix}_L \right\}, \quad U_c^I = \{(\tilde{u}_R^I)^*, (u_L^I)^c\}, \quad D_c^I = \{(\tilde{d}_R^I)^*, (d_L^I)^c\}. \quad (4.49)$$

In the SM flavour violation appears through the non-diagonal Yukawa matrices. The $U(3) \times U(3) \times U(3)$ global symmetry of the quark gauge sector allows the diagonalisation of the the up and down Yukawa matrices by performing a rotation of the quark fields in the flavour

space. For the diagonalisation of the two Yukawa matrices by a biunitary transformations four unitary matrices are necessary but according to the $[U(3)]^3$ symmetry of the quark gauge sector only three matrices are available. This fact arises in the appearance of the CKM matrix which contains all the flavour violation in the SM in the basis in which both the up and down Yukawa matrices are diagonal. Applying the same transformations on the superfields in the MSSM one obtains the so called Super-CKM (SCKM) basis. In the SCKM basis the squark mass matrices still have off-diagonal entries. The unitary matrices acting on the superfield to diagonalise the quark mass matrices are

$$Q_i^I \rightarrow V_{Q_i}^{IJ} Q_i^J, \quad U_c^I \rightarrow V_U^{*IJ} U_c^J, \quad D_c^I \rightarrow V_D^{*IJ} D_c^J. \quad (4.50)$$

After performing this transformations one obtains the following relation between the diagonal Yukawa and quark mass matrices

$$\hat{m}_u = \frac{v_2}{\sqrt{2}} \hat{Y}_u, \quad \hat{m}_d = \frac{v_1}{\sqrt{2}} \hat{Y}_d. \quad (4.51)$$

The mass mixing matrices for the up-type and down-type squarks are given by

$$\begin{aligned} \mathcal{M}_U^2 &= \begin{pmatrix} (M_U^2)_{LL} + m_u^2 - \frac{\cos 2\beta}{6}(M_Z^2 - 4M_W^2)\mathbb{1} & (M_U^2)_{LR} - \mu \cot \beta m_u \\ (M_U^2)_{LR}^\dagger - \mu^* \cot \beta m_u & (M_U^2)_{RR} + m_u^2 + \frac{2\cos 2\beta}{3}M_Z^2 \sin^2 \theta_W \end{pmatrix}, \\ \mathcal{M}_D^2 &= \begin{pmatrix} (M_D^2)_{LL} + m_d^2 - \frac{\cos 2\beta}{6}(M_Z^2 + 2M_W^2)\mathbb{1} & (M_D^2)_{LR} - \mu \tan \beta m_d \\ (M_D^2)_{LR}^\dagger - \mu^* \tan \beta m_d & (M_D^2)_{RR} + m_d^2 - \frac{\cos 2\beta}{3}M_Z^2 \sin^2 \theta_W \end{pmatrix} \end{aligned} \quad (4.52)$$

where θ_W is the Weinberg angle and the flavour changing entries are contained in the 3×3 matrices in the flavour space

$$\begin{aligned} (M_U^2)_{LL} &= V_{Q_1} m_Q^2 V_{Q_1}^\dagger, & (M_U^2)_{RR} &= V_U m_U^2 V_U^\dagger, & (M_U^2)_{LR} &= V_{Q_1} m_Q^2 V_U^\dagger \\ (M_D^2)_{LL} &= V_{Q_2} m_Q^2 V_{Q_2}^\dagger, & (M_D^2)_{RR} &= V_D m_U^2 V_D^\dagger, & (M_D^2)_{LR} &= V_{Q_1} m_Q^2 V_D^\dagger. \end{aligned} \quad (4.53)$$

The hermiticity of the squark mass matrices implies $M_{Q_{LL}}^2 = M_{Q_{LL}}^{2\dagger}$, $M_{Q_{LR}}^2 = M_{Q_{RL}}^{2\dagger}$ and $M_{Q_{RR}}^2 = M_{Q_{RR}}^{2\dagger}$. Then, in order to have the squark mass matrices in diagonal form a second redefinition of the up-type and down-type squark fields is necessary. We transform the squark fields from the flavour-chirality basis to the mass eigenstates basis by the rotations

$$\begin{aligned} \tilde{u}_L^i &= (Z_U^\dagger)^{ik} U^k, & \tilde{d}_L^i &= (Z_D^\dagger)^{ik} D^k, \\ \tilde{u}_R^i &= (Z_U^\dagger)^{(i+3)k} U^k, & \tilde{d}_R^i &= (Z_D^\dagger)^{(i+3)k} D^k, \end{aligned} \quad (4.54)$$

where the index $i = 1, 2, 3$ and $k = 1, \dots, 6$. This relations define the unitary matrices $Z_Q \in \mathbb{C}^{6 \times 6}$ which diagonalise the mass mixing matrices M_Q^2 . Using the transformation given in eq. (4.54) we obtain

$$(M_D^2)^D = Z_D M_D^2 Z_D^\dagger, \quad (M_U^2)^D = Z_U M_U^2 Z_U^\dagger, \quad (4.55)$$

where $(M_U^2)^D$ and $(M_D^2)^D$ are the diagonal up-type and down-type squark mass matrices. In the MSSM there is a nontrivial mixing between the charged gauginos, the winos, and the charged higgsinos as well as between the neutral gauginos, the bino and the photino, and the neutral higgsinos. For this reason the charginos and neutralinos are the mass eigentates obtained by the diagonalisation of the so called chargino and neutralino mass mixing matrices. The charginos are two Dirac fermions $\tilde{\chi}_{1,2}^\pm$ whose masses are the two eigenvalues of the chargino mass matrix:

$$\begin{pmatrix} M_{\tilde{\chi}_1^\pm} & 0 \\ 0 & M_{\tilde{\chi}_2^\pm} \end{pmatrix} = \hat{U}^\dagger \begin{pmatrix} M_2 & \sqrt{2} M_W s_\beta \\ \sqrt{2} M_W c_\beta & \mu \end{pmatrix} \hat{V} \quad (4.56)$$

Since the chargino mixing matrix is not necessarily hermitian, it is diagonalised by a biunitary transformation with the unitary matrices $\hat{U}, \hat{V} \in \mathbb{C}^{2 \times 2}$. The higgsino mass parameter μ and the gaugino mass parameter M_2 which appear in the soft SUSY breaking part of the supersymmetric Lagrangian are free parameters of the model. In the interaction eigenstate basis the charged higgsino components of the chargino fields couple to squarks and quarks with the Yukawa couplings which are proportional to m_q/M_W . Because of the smallness of the quark masses in comparison to the mass of the W boson which is true for all quarks except for the mass of the top quark the dominant contribution arises through the squark-quark-wino weak interaction and through the squark-top-higgsino Yukawa interaction. All other Yukawa couplings are negligible due to their proportionality to the mass of the corresponding light quark.

Neutralinos are four Majorana fermions $\tilde{\chi}_{1,\dots,4}^0$ with a symmetric mass matrix which is diagonalised as

$$\begin{pmatrix} M_{\tilde{\chi}_1^0} & & & 0 \\ & \ddots & & \\ & & & M_{\tilde{\chi}_4^0} \\ 0 & & & \end{pmatrix} = \hat{Z}_N^\dagger \begin{pmatrix} M_1 & 0 & -c_\beta s_W m_Z & s_\beta s_W m_Z \\ 0 & M_2 & c_\beta c_W m_Z & -s_\beta c_W m_Z \\ -c_\beta s_W m_Z & c_\beta c_W m_Z & 0 & -\mu \\ s_\beta s_W m_Z & -s_\beta c_W m_Z & -\mu & 0 \end{pmatrix} \hat{Z}_N$$

where the angle β is defined through the ratio of the vacuum expectation values i.e. $\beta = \arctan(v_u/v_d)$. In eq. (4.57) the abbreviations $c_\beta = \cos \beta$, $s_\beta = \sin \beta$, $c_W = \cos \theta_W$, and $s_W = \sin \theta_W$ have been used as well. The matrix \hat{Z}_N is a unitary complex matrix, $\hat{Z}_N \in \mathbb{C}^{4 \times 4}$. The quantity $\tan \beta = v_u/v_d$ is a free parameter in the MSSM.

In the MSSM an additional contribution to the flavour changing processes can occur through the charged Higgs bosons in the box diagrams. The reason for this fact is that the Higgs sector of the MSSM is extended by an additional Higgs doublet. In the SM there are two possibilities to write Lorentz-invariant fermion mass terms in the Lagrangian - these are the so called Dirac and Majorana mass terms. Unfortunately, these terms are not invariant under transformations according to the electroweak gauge group $SU(2)_L \times U(1)_Y$. Including such terms in the SM Lagrangian leads to an explicit breaking of the local $SU(2)_L \times U(1)_Y$ symmetry of the SM Lagrangian density. Moreover, mass terms for the gauge fields are not allowed by the gauge symmetry as well. However, in nature fermions and the gauge bosons of the weak interaction are massive particles and the SM Lagrangian has to be properly modified in order to describe these obvious experimental finds. The solution to this problem is given by the spontaneous symmetry breaking of the $SU(2)_L \times U(1)_Y$ gauge group to the electromagnetic gauge group $U(1)_{em}$ by introducing of a scalar field, the so called Higgs field. The Higgs field is a $SU(2)_L$ dublet and has a specially chosen potential such that its vacuum expectation value is different from zero. In this way one finds in the Lagrangian of the SM mass terms for the gauge bosons proportional to the positive vacuum expectation value of the Higgs field. The masses of the fermions arise through Yukawa-type interaction between the left handed lepton and quark doublets, their right-handed singlet partners and the Higgs field. In a special choice of the gauge, the so called unitary gauge which is realised by performing a local $SU(2)$ transformation on the Higgs doublet, three of the four scalar fields in the Higgs doublet can be removed. These are the nonphysical Pseudo-Goldstone bosons which appear by the spontaneous breaking of the electroweak gauge symmetry to the electromagnetic gauge symmetry. The Pseudo-Goldstone bosons become the third, longitudinal degree of freedom of the massive vector bosons after the spontaneous symmetry breaking. One field remains, this is the SM Higgs field. However, in the MSSM the situation is more complicated. The MSSM is an extension of the so called two Higgs doublet models. That means, at least two Higgs doublets have to be introduced in order to have gauge invariant mass terms of the fermions and gauge bosons in the supersymmetric Lagrangian. The introduction of two Higgs doublets is necessary because of

a special property - the holomorphy - of the superpotential. The two Higgs doublets ensure the cancellation of anomalies related to the Higgsinos in the model as well. We will not go further into details on this topic and refer for a more comprehensive explanation of the Higgs sector of the MSSM to [41, 92–94] and references therein. In the MSSM the two Higgs doublets comprise eight additional degrees of freedom. After spontaneous symmetry breaking five of them appear as physical Higgs bosons. Three of the physical Higgses are neutral particles while the remaining two carry an electric charge.

The charged Higgs bosons H_1^+ and H_2^+ which affect the processes on which we focus in this work are related to the initial Higgs fields by the transformation

$$\begin{pmatrix} H_2^{1*} \\ H_1^2 \end{pmatrix} = Z_H \begin{pmatrix} H_1^+ \\ H_2^+ \end{pmatrix}. \quad (4.57)$$

The matrix Z_H is given by

$$Z_H = \frac{1}{\sqrt{v_u^2 + v_d^2}} \begin{pmatrix} v_u & -v_d \\ v_d & v_u \end{pmatrix} \quad (4.58)$$

where v_u and v_d are the vacuum expectation values. With the ratio $\tan\beta = v_u/v_d$ the matrix Z_H in eq. (4.58) can be written in a more convenient form

$$Z_H = \begin{pmatrix} \sin\beta & -\cos\beta \\ \cos\beta & \sin\beta \end{pmatrix}. \quad (4.59)$$

Finally, the masses of the two physical charged Higgs scalars H^\pm are given by

$$M_{H_1^\pm}^2 = M_W^2 + m_{H_u}^2 + m_{H_d}^2 + 2|\mu|^2. \quad (4.60)$$

where $m_{H_u}^2$ and $m_{H_d}^2$ are soft terms for the corresponding Higgs doublets. The gaugino masses $M_{1,2}$ are assumed real as well as the Higgs sector parameter μ . In fact, if one allows non-trivial phases in $M_{1,2}$, they are communicated to the gaugino diagonalisation matrices, which in turn enter the Feynman rules for charginos and neutralinos. One would then have new sources of CP violation. The same argument applies to the Higgs sector parameter μ . The strong, electroweak and charged Higgs vertices involved in the box diagrams given in fig. 4.3 can be found in the appendix.

5. THE INCLUSIVE DECAY $B \rightarrow X_s \gamma$

The inclusive radiative decay $B \rightarrow X_s \gamma$ is a rare loop mediated process which involves the third quark generation. Therefore, these transitions are very sensitive to NP contributions and play a crucial role in the indirect searches for NP. The theoretical SM prediction is known up to NNLO precision in QCD [44]. The branching ratio of the $B \rightarrow X_s \gamma$ decay has been experimentally measured by CLEO, BaBar and Belle collaborations [45–51]. Thus, the comparison of the experimental data with the theoretical prediction by including the supersymmetric contributions to the SM result is a powerful strategy for constraining the parameter space of various extensions of the SM [53–55] and, in particular, the supersymmetric parameter space.

5.1. $B \rightarrow X_s \gamma$ in the SM

The $B \rightarrow X_s \gamma$ transition is a $|\Delta F| = 1$ process which is governed by the so called magnetic penguins shown in the Feynman diagram in fig. 5. In the SM where the $b \rightarrow s$ quark transition is mediated by a W boson a crucial role plays the magnetic γ -penguin. In the loop the top quark contribution is the dominant one. The effective Hamiltonian in the SM at the scale $\mu = m_b$ is can be written as

$$\mathcal{H}_{\text{eff}}^{\text{SM}} = -\frac{4G_F}{\sqrt{2}} V_{ts}^* V_{tb} \sum_{i=1}^8 C_i(\mu) Q_i(\mu). \quad (5.1)$$

To an excellent accuracy the relevant operators are given by

$$\begin{aligned} Q_2 &= \bar{s}^\alpha \gamma_\mu P_L c^\alpha \bar{c}^\beta \gamma_\mu P_L b^\beta, \\ Q_7 &= \frac{e m_b}{16\pi^2} \bar{s}^\alpha \sigma_{\mu\nu} F^{\mu\nu} P_R b^\alpha, \\ Q_8 &= \frac{g_3 m_b}{16\pi^2} \bar{s}^\alpha \sigma_{\mu\nu} G_a^{\mu\nu} T_{\alpha\beta}^a P_R b^\beta. \end{aligned} \quad (5.2)$$

The contribution of the other operators is suppressed and can be neglected. Q_2 is the dominant current-current operator while the operators Q_7 and Q_8 correspond to the magnetic

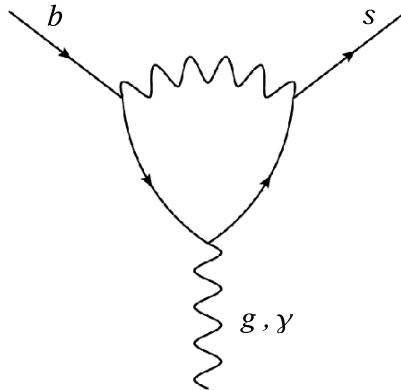


Figure 5.1: $|\Delta F| = 1$ penguin diagram relevant for the $B \rightarrow X_s \gamma$ process. In the SM (in unitary gauge) up-type quarks and W bosons are involved in the loop. In the MSSM additional contributions stemming from gluinos or neutralinos and down-type squarks, charginos and up-type squarks and charged Higgs bosons and up-type quarks are present.

γ -penguin and to the magnetic gluon-penguin shown in fig. 5, respectively. The calculation of the branching fraction $\text{Br}(B \rightarrow X_s \gamma)$ in the SM is done by first evaluating the corresponding Wilson coefficients at the higher scale $\mu \approx M_W, m_t$ by matching of the effective theory result onto the one obtained in the full theory calculation. Furthermore, considering the operator mixing under renormalisation, the RG equations are derived in order to perform an evolution of the Wilson coefficients down to the low energy scale $\mu \approx m_b$. In the last step the on-shell $B \rightarrow X_s \gamma$ amplitudes are evaluated [44]. The obtained SM value for the branching ratio of the inclusive $B \rightarrow X_s \gamma$ process is given by $\text{Br}(B \rightarrow X_s \gamma) = (3.15 \pm 0.23) \cdot 10^{-4}$. The indicated error has been obtained by adding in quadrature the non-perturbative (5%), parametric (3%), higher-order perturbative (3%), and the interpolation ambiguity (3%) uncertainties. For more details about the calculation of the $B \rightarrow X_s \gamma$ branching ratio at NLO we refer to [52]. Details about the NNLO SM contribution can be found in [44].

5.2. $B \rightarrow X_s \gamma$ in the MSSM

Considering the possible interactions and the particle content of the MSSM we find a new contributions to the $b \rightarrow s \gamma$ process. In particular, they stem from exchange of up-type

quarks and a charged Higgs boson, of down-type squarks and a gluino or neutralino, and of up-type squark and a chargino. The SUSY contributions are described by $|\Delta B| = |\Delta S| = 1$ effective magnetic and chromomagnetic operators as well as by new four quark operators. Considering operators up to dimension six allows the matching of the charged Higgs, chargino and neutralino penguins onto the SM magnetic and chromomagnetic operators Q_7 and Q_8 given in eq. (5.2), and onto their counterparts

$$\begin{aligned} Q'_7 &= \frac{e \overline{m}_b}{16\pi^2} \overline{s}^\alpha \sigma_{\mu\nu} F^{\mu\nu} P_L b^\alpha \\ Q'_8 &= \frac{g_3 \overline{m}_b}{16\pi^2} \overline{s}^\alpha \sigma_{\mu\nu} G_a^{\mu\nu} T_{\alpha\beta}^a P_L b^\beta \end{aligned} \quad (5.3)$$

which are obtained from Q_7 and Q_8 by replacing $P_R \rightarrow P_L$. In supersymmetric scenarios which do not assume extremely large values for $\tan\beta$ the contributions to the Wilson coefficients corresponding to the operators given in eq. (5.3) from charged Higgs bosons and charginos are small in comparison to C_7 and C_8 and vanish in the limit of massless strange quark. The neutralino contributions to all Wilson coefficients involve the same elements of the down-type squark mass matrix as the gluino contribution. However, the gluinos couple with the strong coupling constant g_3 while the neutralino vertices involve the weak coupling constant g_2 . Thus, the gluino contribution which is proportional to g_3^2 dominates the neutralino contribution which is proportional to g_2^2 by far. In fact, compared to the other contributions stemming from SUSY particles the neutralino contribution turns out to be inessential [56].

The gluino contribution is described by the effective Hamiltonian [56]

$$\mathcal{H}_{\text{eff}}^{\tilde{g}} = \sum_i C_{i,\tilde{g}}(\mu) Q_{i,\tilde{g}}(\mu) + \sum_i \sum_{q=u,\dots,b} C_{i,\tilde{g}}^q(\mu) Q_{i,\tilde{g}}^q(\mu) \quad (5.4)$$

The second term in eq. (5.4) includes four-quark scalar, vector and tensor operators $Q_{i,\tilde{g}}^q$. At one loop level the scalar and tensor operators mix into the magnetic and chromomagnetic operators of dimension six [57, 58] and, therefore, have to be taken into account by performing the calculation. However, the mixing mentioned above turns out to be numerically small. Thus, the contribution of the operators $Q_{i,\tilde{g}}^q$ can be neglected [56]. The dipole operators $Q_{i,\tilde{g}}$ in which the chirality flip is induced by the b -quark mass are given by

$$\begin{aligned} Q_{7b,\tilde{g}} &= eg_3^2(\mu) \overline{m}_b(\mu) \overline{s}^\alpha \sigma_{\mu\nu} F^{\mu\nu} P_R b^\alpha, \\ Q'_{7b,\tilde{g}} &= eg_3^2(\mu) \overline{m}_b(\mu) \overline{s}^\alpha \sigma_{\mu\nu} F^{\mu\nu} P_L b^\alpha, \\ Q_{8b,\tilde{g}} &= g_3^3(\mu) \overline{m}_b(\mu) \overline{s}^\alpha \sigma_{\mu\nu} G_a^{\mu\nu} T_{\alpha\beta}^a P_R b^\beta, \\ Q'_{8b,\tilde{g}} &= g_3^3(\mu) \overline{m}_b(\mu) \overline{s}^\alpha \sigma_{\mu\nu} G_a^{\mu\nu} T_{\alpha\beta}^a P_L b^\beta. \end{aligned} \quad (5.5)$$

There are also gluino-induced operators where the chirality violation is signalled by the charm quark mass. These operators are obtained from the ones given in eq. (5.5) by replacing $\overline{m}_b(\mu)$ by $\overline{m}_c(\mu)$. The operators where the chirality flip is induced by the gluino mass read

$$\begin{aligned}
Q_{7\tilde{g},\tilde{g}} &= e g_3^2(\mu) \overline{s}^\alpha \sigma_{\mu\nu} F^{\mu\nu} P_R b^\alpha, \\
Q'_{7\tilde{g},\tilde{g}} &= e g_3^2(\mu) \overline{s}^\alpha \sigma_{\mu\nu} F^{\mu\nu} P_L b^\alpha, \\
Q_{8\tilde{g},\tilde{g}} &= g_3^3(\mu) \overline{s}^\alpha \sigma_{\mu\nu} G_a^{\mu\nu} T_{\alpha\beta}^a P_R b^\beta, \\
Q'_{8\tilde{g},\tilde{g}} &= g_3^3(\mu) \overline{s}^\alpha \sigma_{\mu\nu} G_a^{\mu\nu} T_{\alpha\beta}^a P_L b^\beta.
\end{aligned} \tag{5.6}$$

In our calculation we use the Wilson coefficients obtained in the model independent analysis of $B \rightarrow X_s \gamma$ based on a leading-log QCD calculation in the MSSM [56]. The Wilson coefficients for all the supersymmetric contributions mentioned above can be found in the appendix of [56].

6. METHOD AND GENERAL FEATURES OF THE ANALYSIS

In the past many analyses have been done in order to constrain off-diagonal elements of the squark mass matrix. In the first studies [60, 62, 80] the framework of the so called mass insertion approximation (MIA) [63] has been used. The main advantage of the mass insertion method is given by the fact that the full diagonalisation of the sfermion mass matrices is not necessary. It is enough to compute only ratios of the off-diagonal over diagonal elements of the sfermion mass matrices in order to test the SUSY model under consideration in the FCNC sector. Usually, the off-diagonal elements of the mass mixing matrix are written as an expansion in off-diagonal mass insertions

$$\delta_{ij}^{qXY} = (\delta^{qYX})_{ji}^* = \frac{\Delta_{ij}^{\tilde{q}XY}}{\tilde{M}^2}, \quad \tilde{M}^2 \equiv \frac{1}{6} \sum_k [\mathcal{M}_{\tilde{q}}^2]_{kk}. \quad (6.1)$$

where $\Delta_{ij}^{\tilde{q}XY}$ are off-diagonal elements of the mass mixing matrices and the indices $q \in \{u, d\}$ and $X, Y \in \{L, R\}$ denote the up-type and down-type mass mixing matrix and the certain 3×3 blocks defined in eq. (4.53), respectively. Adopting the MIA the mechanism of flavour violation mediated by soft SUSY breaking terms is linearised. With this technique the results can be written in a more transparent and manageable form. However, the MIA is valid only under the assumption that the off-diagonal entries in the squark mass matrices are small compared to the diagonal ones. In this work we use results in MIA only for the purpose of clear explanation and better understanding of general relations. The numerical analysis is performed by an exact diagonalisation of the squark mass matrix.

In the next sections we first investigate analytically the correlation between the $B_s - \bar{B}_s$ and $B_d - \bar{B}_d$ mixing processes in the general MSSM. Our aim is to create general relations between the SUSY contributions to the meson mixing processes and to explore their impact on the $B_s - \bar{B}_s$ and $B_d - \bar{B}_d$ mixing phases. Then we concentrate on the main features of

our numerical analysis which has been performed to constrain off-diagonal elements of the up-type mass-mixing matrix, in particular the mass insertions δ_{23}^{uLL} and δ_{13}^{uLL} .

6.1. General correlations between $B_s - \bar{B}_s$ and $B_d - \bar{B}_d$ mixing

In the SM we can write the $B - \bar{B}$ mixing transition amplitude neglecting the small charm-quark contribution as

$$M_{12}^{q\text{SM}} = C_q S_0(x_t) (V_{tb} V_{tq}^*)^2 \quad (6.2)$$

where we combine all the couplings and factors coming from non-perturbative QCD in the constant C and $S_0(x_t)$ is the well-known Inami-Lim-function introduced in eq. (4.22). The ratio of the $B_s - \bar{B}_s$ and $B_d - \bar{B}_d$ transition amplitudes is given by

$$\frac{M_{12}^{s\text{SM}}}{M_{12}^{d\text{SM}}} = \left(\frac{V_{tb} V_{ts}^*}{V_{tb} V_{td}^*} \right)^2 \xi^2 \approx \frac{\xi^2}{\lambda^2 R_t^2} e^{-2i\beta} \approx \mathcal{O}(40) e^{-2i\beta} \quad (6.3)$$

where $R_t = |V_{td}|/\lambda|V_{cb}|$ and ξ is the ratio defined in eq. (2.90). We neglect the small $B_s - \bar{B}_s$ mixing phase $2\beta_s = 2\eta\lambda^2 + \mathcal{O}(\lambda^4)$ originating from the phase of the CKM element V_{ts} . Equation (6.3) shows that in the SM the $B_d - \bar{B}_d$ transition amplitude is suppressed roughly by a factor 40 compared with the $B_s - \bar{B}_s$ transition amplitude.

We define of the ratio of the NP contributions to the SM contribution

$$\Delta_{\text{NP}}^q \equiv \frac{M_{12}^{q\text{NP}}}{M_{12}^{q\text{SM}}} \quad (6.4)$$

where $M_{12}^{q\text{SM}}$ and $M_{12}^{q\text{NP}}$ are understood as the pure SM result and the sum of the different SUSY contributions i.e. originating from chargino box diagrams, gluino box diagrams etc., respectively. Thus, the NP contribution to M_{12}^q can be parametrised as [69]

$$1 + |\Delta_{\text{NP}}^q| e^{i\phi_{\text{NP}}^q} = |\Delta^q| e^{i\phi_{\Delta}^q} \quad (6.5)$$

The difference between the phase of the SM amplitude and the phase of the NP contribution arises as ϕ_{NP}^q in eq. (6.5). From eq. (6.5) it follows

$$\tan \phi_{\Delta}^q = \frac{|\Delta_{\text{NP}}^q| \sin \phi_{\text{NP}}^q}{|\Delta_{\text{NP}}^q| \cos \phi_{\text{NP}}^q + 1}. \quad (6.6)$$

Expressing the NP phase as a function of the complex parameter Δ^q we obtain

$$\tan \phi_{\text{NP}}^q = \frac{|\Delta^q| \sin \phi_{\Delta}^q}{|\Delta^q| \cos \phi_{\Delta}^q - 1}. \quad (6.7)$$

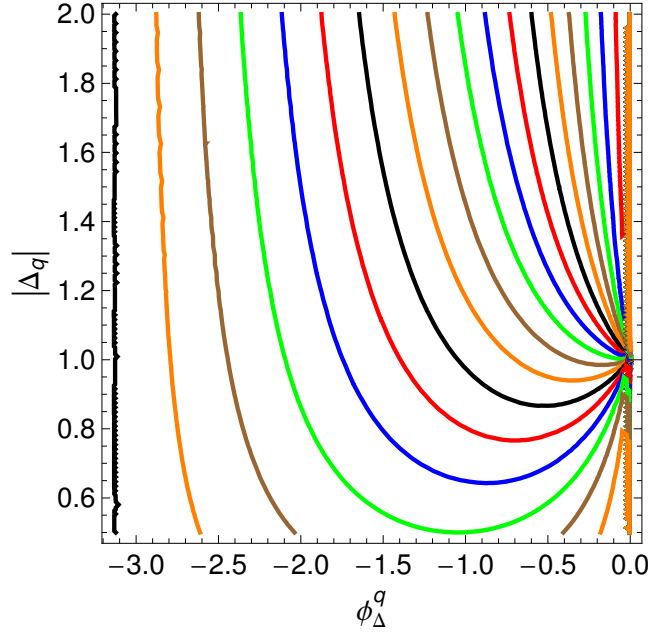


Figure 6.1: The absolute value and the phase of Δ^q for different values of ϕ_{NP}^q starting from the left with $\phi_{\text{NP}}^q = -180^\circ$ and increasing it in steps of 10° to the right until $\phi_{\text{NP}}^q = 0^\circ$.

In fig. 6.1 we graphically show the relation between the absolute value and the phase of Δ^q for different values of ϕ_{NP}^q .

Through the chargino boxes there is a generic correlation between the NP contribution to the $B_s - \bar{B}_s$ and $B_d - \bar{B}_d$ mixing processes. This can be demonstrated in a simple way by considering a simple chargino box diagram. If we allow a huge NP contribution to $B_s - \bar{B}_s$ mixing coming from additional flavour violation caused from the mass insertion δ_{23}^{uLL} the chargino box diagram can be expressed as

$$M_{12}^{q\tilde{\chi}^\pm} \sim f_{\tilde{\chi}^\pm}(m_i^2, m_j^2, m_k^2, m_l^2)(\delta_{23}^{uLL})^2 (V_{tb}V_{cq}^*)^2 \quad (6.8)$$

with the loop function $f_{\tilde{\chi}^\pm}(m_i^2, m_j^2, m_k^2, m_l^2)$ depending on the masses of the involved particles in the loop. The ratio of the NP contribution to the $B_s - \bar{B}_s$ and $B_d - \bar{B}_d$ mixing process reads now

$$\frac{M_{12}^{s\tilde{\chi}^\pm}}{M_{12}^{d\tilde{\chi}^\pm}} = \left(\frac{V_{cs}^*}{V_{cd}^*}\right)^2 \xi^2 = \frac{\xi^2}{\lambda^2} \quad (6.9)$$

and is of the same order as in the SM. With the definition in eq. (6.4) we obtain the relation

$$\Delta_{\text{NP}}^{d\tilde{\chi}^\pm} = \Delta_{\text{NP}}^{s\tilde{\chi}^\pm} \frac{e^{-2i\beta}}{R_t^2} \quad (6.10)$$

which let us conclude that a big NP contribution in the $B_s - \bar{B}_s$ system implies a big NP contribution in the $B_d - \bar{B}_d$ system as well. However, the opposite statement is not true. If we allow a large NP effect in the $B_d - \bar{B}_d$ mixing induced through the mass insertion δ_{13}^{uLL} the NP contribution is given by

$$M_{12}^{q\tilde{\chi}^\pm} \sim f_{\tilde{\chi}^\pm}(m_i^2, m_j^2, m_k^2, m_l^2)(\delta_{13}^{uLL})^2 (V_{tb}V_{uq}^*)^2 \quad (6.11)$$

Thus, one finds for the ratio of the NP contribution to the $B_s - \bar{B}_s$ and $B_d - \bar{B}_d$ mixing process

$$\frac{M_{12}^{s\tilde{\chi}^\pm}}{M_{12}^{d\tilde{\chi}^\pm}} = \left(\frac{V_{us}^*}{V_{ud}^*}\right)^2 \zeta^2 = \lambda^2 \zeta^2. \quad (6.12)$$

With this result we obtain

$$\Delta_{\text{NP}}^{s\tilde{\chi}^\pm} = \Delta_{\text{NP}}^{d\tilde{\chi}^\pm} R_t^2 \lambda^4 e^{2i\beta}. \quad (6.13)$$

Equation (6.13) demonstrates that a big NP effect in $B_d - \bar{B}_d$ mixing does not imply an effect of the same order in the $B_s - \bar{B}_s$ system as well.

The CKMfitter collaboration has performed an analysis in order to constrain the parameters Δ^s and Δ^d in the $B_s - \bar{B}_s$ and $B_d - \bar{B}_d$ meson systems [70]. The plot obtained for $B_d - \bar{B}_d$ mixing is shown in fig. 6.2. We extract the allowed 68.3% CL, 95.45% CL and 99.73% CL regions for the NP phases ϕ_Δ^s and ϕ_Δ^d which can be found in table 6.1. While the NP phase ϕ_Δ^d cannot exceed -20.0° even for the 99.73% CL region for the NP phase ϕ_Δ^s all negative values are allowed. This fact leads to the conclusion that the NP contribution in the $B_d - \bar{B}_d$ system is much more constrained than the NP contribution to the $B_s - \bar{B}_s$ system. Since eq. (6.10) relates the SUSY contributions in the neutral B_d and B_s meson systems assuming that the box diagrams are affected only by additional exchange of charginos in the loops we can translate the 1σ and 2σ regions from the $\text{Im} \Delta^d - \text{Re} \Delta^d$ plot to the corresponding one valid in the case of B_s mesons. From eq. (6.10) it follows

$$\Delta^s \tilde{\chi}^\pm = 1 + \left(\Delta^d \tilde{\chi}^\pm - 1\right) R_t^2 e^{2i\beta}. \quad (6.14)$$

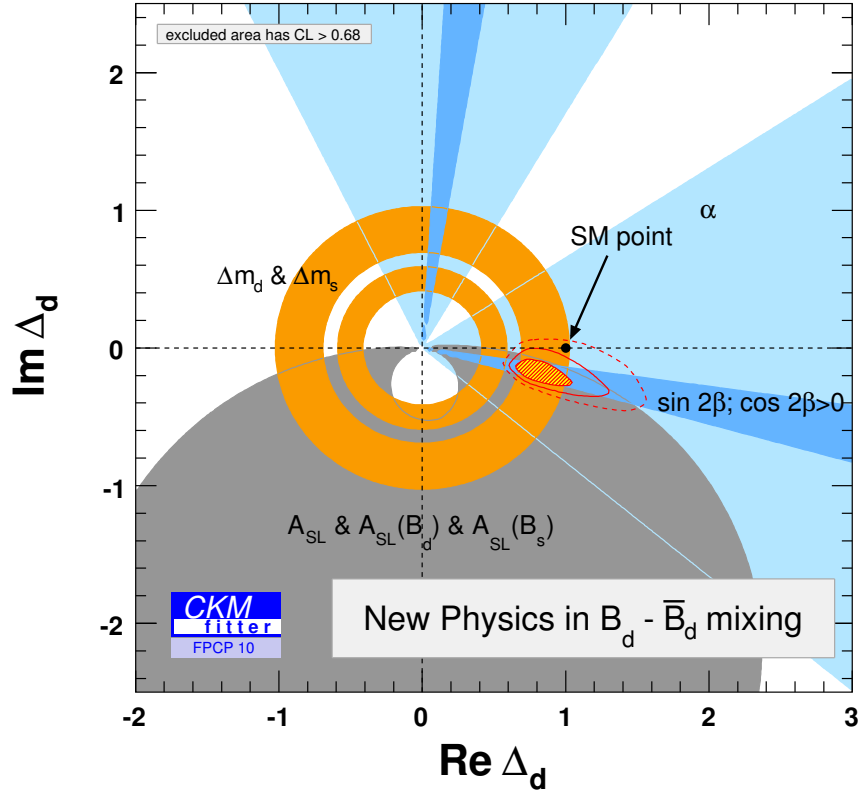


Figure 6.2: Constraints on NP in $B_d - \bar{B}_d$ system from the CKMfitter collaboration [70].

We parametrise the 68.3% CL, 95.45% CL and 99.73% CL contours in the plot in fig. 6.2 and depict them according to eq. (6.14) in the original $\text{Im } \Delta^s - \text{Re } \Delta^s$ plot obtained from the CKMfitter collaboration. The result of this procedure is shown in fig. 6.3. The outer black dashed line corresponds to the 99.73% CL region while the inner solid line represents the 95.45% CL and cross-hatched area corresponds to the 68.3% CL region in fig. 6.2. One can see that the 95.45% CL and the 99.73% CL regions obtained by translating the allowed 95.45% CL and the 99.73% CL regions in the $\text{Im } \Delta^d - \text{Re } \Delta^d$ plot overlaps with the 99.73% CL regions in the $\text{Im } \Delta^s - \text{Re } \Delta^s$ plot. However, there is no intersection between the 68.3% CL regions. The black hatched areas in fig. 6.3 show the region in which the NP in the $B_s - \bar{B}_s$ mixing process can be explained through a supersymmetric chargino contribution. However, looking at fig. 6.3 we realise how small is that region. It covers only the upper part of the 95.45% CL and 99.73% CL regions. We find that the maximal negative value of the phase ϕ_Δ^s which can be caused by a chargino contribution is -20.4° at 99.73% CL. For all points in the $\text{Im } \Delta^s - \text{Re } \Delta^s$ plot which are outside the back hatched regions

	68.3% CL	95.45% CL
ϕ_{Δ}^s	$[-67.2^{\circ}, -27.0^{\circ}] \cup [-150.2^{\circ}, -108.1^{\circ}]$	$[-86.7^{\circ}, -11.1^{\circ}] \cup [-165.4^{\circ}, -91.3^{\circ}]$
ϕ_{Δ}^d	$[-16.1^{\circ}, -5.9^{\circ}]$	$[-18.2^{\circ}, 0.0^{\circ}]$
99.73% CL		
ϕ_{Δ}^s	$[-182.0^{\circ}, 5.9^{\circ}]$	
ϕ_{Δ}^d	$[4.6^{\circ}, -20.0^{\circ}]$	

Table 6.1: The allowed regions at 68.3% CL, 95.45% CL and 99.73% CL for the NP phases ϕ_{Δ}^s and ϕ_{Δ}^d extracted from the analysis of the CKMfitter collaboration [70].

an additional source of flavour violation is necessary.

Until now we have not considered the gluino contribution. Because of the $SU(2)$ gauge symmetry in the left handed fermion sector in general the gluino contribution is present as well. If we assume a very heavy gluino the gluino contribution becomes very small. That is the case on which we focused in our discussion so far. In this case although the gluino contribution is present it is highly suppressed and can be neglected. In following we will concentrate on the situation when the gluino contribution affects the meson mixing processes as well.

Since the quark-squark-gluino vertices do not involve CKM elements a non-diagonal entries in the down-type squark mass matrix are the only source of flavour violation there. Because of the $SU(2)$ gauge symmetry of the left handed fermion fields the up-type and the down-type squark mass matrices are related to each other by the equation

$$M_{dLL}^2 = V^{\dagger} M_{uLL}^2 V. \quad (6.15)$$

Assuming only the mass insertions δ_{23}^{uLL} and δ_{13}^{uLL} to be different from zero and the mass insertions δ_{23}^{dLL} and δ_{13}^{dLL} in the down sector which induce a gluino contribution to the $B_d - \bar{B}_d$ and $B_s - \bar{B}_s$ meson mixing processes are related to the mass insertions in the up sector by the equations

$$\delta_{13}^{dLL} = \sum_i (M_{uLL}^2)_{ii} V_{i3} V_{i1}^* + \delta_{23}^{uLL} V_{tb} V_{cd}^* + (\delta_{23}^{uLL})^* V_{cb} V_{td}^* + \delta_{13}^{uLL} V_{tb} V_{ud}^* + (\delta_{13}^{uLL})^* V_{ub} V_{td}^* \quad (6.16)$$

$$\delta_{23}^{dLL} = \sum_i (M_{uLL}^2)_{ii} V_{i3} V_{i2}^* + \delta_{23}^{uLL} V_{tb} V_{cs}^* + (\delta_{23}^{uLL})^* V_{cb} V_{ts}^* + \delta_{13}^{uLL} V_{tb} V_{us}^* + (\delta_{13}^{uLL})^* V_{ub} V_{ts}^*.$$

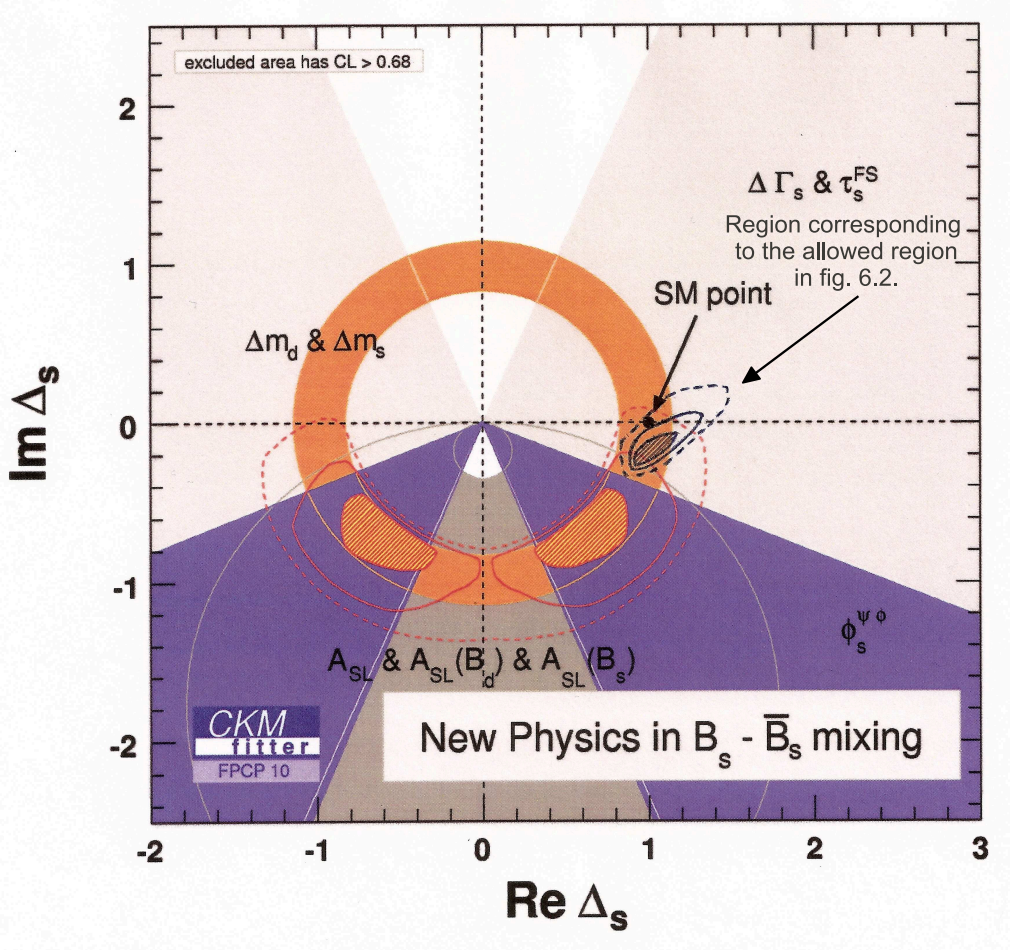


Figure 6.3: Constraints on NP in $B_s - \bar{B}_s$ system from the CKMfitter collaboration [70]. The black regions correspond to the 68.3% CL, 95.45% CL and 99.73% CL regions in fig. 6.2 according to eq. (6.14).

If M_{uLL}^2 is diagonal the flavour changing in the chargino box diagram is from MFV type. In this case the dominant NP contribution comes from the gluino box diagrams. The gluino mediated transition amplitudes can be written as

$$M_{12}^{q\bar{g}} = K f_{\bar{g}}(m_{\bar{g}}^2, m_i^2, m_j^2) (\delta_{q3}^{dLL})^2 \quad (6.17)$$

where we combine all the constants and non-perturbative QCD factors in the constant K and $f_{\bar{g}}(m_{\bar{g}}^2, m_i^2, m_j^2)$ is the sum of the loop functions multiplied by the corresponding factors. Taking into account the unitarity of the CKM matrix we obtain from eq. (6.16):

$$\delta_{13}^{dLL} = -\lambda \delta_{23}^{uLL} + A \lambda^3 \left\{ R_t e^{i\beta} \left[\frac{(M_{uLL}^2)_{33} - (M_{uLL}^2)_{11}}{\tilde{M}^2} \right] - \left[\frac{(M_{uLL}^2)_{22} - (M_{uLL}^2)_{11}}{\tilde{M}^2} \right] \right\}$$

$$\delta_{23}^{dLL} = \delta_{23}^{uLL} + A\lambda^2 \left[\frac{(M_{uLL}^2)_{22} - (M_{uLL}^2)_{33}}{\tilde{M}^2} \right] - \frac{A\lambda^4}{2} \left[\frac{(M_{uLL}^2)_{22} - (M_{uLL}^2)_{11}}{\tilde{M}^2} \right] \quad (6.18)$$

where we have used the Wolfenstein parametrisation of the CKM matrix given in eq. (4.4) and \tilde{M}^2 is the average squark mass defined in eq. (6.1). Relating the gluino contributions to the B_d and B_s system to each other gives

$$\frac{M_{12}^{d\tilde{g}}}{M_{12}^{s\tilde{g}}} = \frac{1}{\xi^2} \left(\frac{\delta_{13}^{dLL}}{\delta_{23}^{dLL}} \right)^2 \quad (6.19)$$

Inserting the expressions given in eq. (6.18) in eq. (6.19) by requiring the same mass for the first two diagonal elements in the up-type squark mass matrix and expanding the result in the Wolfenstein parameter λ we obtain

$$\frac{M_{12}^{d\tilde{g}}}{M_{12}^{s\tilde{g}}} = \frac{\lambda^2}{\xi^2} \left[1 + \frac{2A\lambda^2 (R_t e^{i\beta} - 1) (M_{uLL}^2)_{33} - (M_{uLL}^2)_{11}}{\delta_{23}^{uLL} \tilde{M}^2} + \mathcal{O}(\lambda^4) \right]. \quad (6.20)$$

With this result considering the ratio of $B_d - \bar{B}_d$ and $B_s - \bar{B}_s$ mixing amplitudes in the SM given in eq. (6.3) we find

$$\Delta_{\text{NP}}^{d\tilde{g}} = \Delta_{\text{NP}}^{s\tilde{g}} \frac{e^{-2i\beta}}{R_t^2} \left[1 + \frac{2A\lambda^2}{(\delta_{23}^{uLL})^2} (R_t e^{i\beta} - 1) \frac{(M_{uLL}^2)_{33} - (M_{uLL}^2)_{11}}{\tilde{M}^2} \right] \quad (6.21)$$

Then, we obtain the following relation between the NP contribution in the B_d and B_s sector stemming from chargino and gluino box diagrams:

$$\Delta_{\text{NP}}^{d\tilde{\chi}^\pm} + \Delta_{\text{NP}}^{d\tilde{g}} = \frac{e^{-2i\beta}}{R_t^2} \left\{ \Delta_{\text{NP}}^{s\tilde{\chi}^\pm} + \Delta_{\text{NP}}^{s\tilde{g}} \frac{2A\lambda^2}{(\delta_{23}^{uLL})^2} (R_t e^{i\beta} - 1) \frac{(M_{uLL}^2)_{33} - (M_{uLL}^2)_{11}}{\tilde{M}^2} \right\} \quad (6.22)$$

If the diagonal elements of M_{uLL}^2 are equal or the difference $(M_{uLL}^2)_{33} - (M_{uLL}^2)_{11}$ is small and its contribution can be neglected we obtain the same relation as in case of the pure chargino contribution given in eq. (6.10):

$$\Delta_{\text{NP}}^{d\tilde{g}} = \Delta_{\text{NP}}^{s\tilde{g}} \frac{e^{-2i\beta}}{R_t^2} \quad (6.23)$$

In this case eq. (6.22) leads to

$$\Delta_{\text{NP}}^{d\tilde{\chi}^\pm} + \Delta_{\text{NP}}^{d\tilde{g}} = \left(\Delta_{\text{NP}}^{s\tilde{\chi}^\pm} + \Delta_{\text{NP}}^{s\tilde{g}} \right) \frac{e^{-2i\beta}}{R_t^2} \quad (6.24)$$

From eq. (6.18) it follows that the mass insertion δ_{23}^{dLL} induced through the SU(2) relation eq. (6.15) and the mass insertion δ_{23}^{uLL} have the same imaginary part. Their real parts differ in case of an up-type squark mass matrix with not equal diagonal elements.

Considering eq. (6.17) we realise that $\phi_{\text{NP}}^{s\tilde{g}} = 2 \arg \delta_{23}^{dLL} - 2\beta_s$. With $\phi_{\text{NP}}^{s\tilde{\chi}^\pm} = 2 \arg \delta_{23}^{uLL} - 2\beta_s$ and neglecting the small phase β_s we obtain from eq. (6.18)

$$\tan \frac{\phi_{\text{NP}}^{s\tilde{g}}}{2} = \frac{|\delta_{23}^{uLL}| \sin \frac{\phi_{\text{NP}}^{s\tilde{\chi}^\pm}}{2}}{|\delta_{23}^{uLL}| \cos \frac{\phi_{\text{NP}}^{s\tilde{\chi}^\pm}}{2} + \frac{A\lambda^2}{M^2} [(M_{uLL}^2)_{22} - (M_{uLL}^2)_{33}]} \quad (6.25)$$

Equation (6.25) demonstrates the relation between the difference of the diagonal elements of (M_{uLL}^2) and the phases $\phi_{\text{NP}}^{s\tilde{\chi}^\pm}$ and $\phi_{\text{NP}}^{s\tilde{g}}$. If the diagonal elements of the up-type mass mixing matrix are equal the NP phases of the chargino and gluino contributions are equal as well.

Equation (6.24) shows that if the up-type squark mass matrix contains equal diagonal elements it is not possible to explain the points outside the black hatched region in fig. 6.3 through the flavour violating effects induced by the mass insertion δ_{23}^{uLL} only. In this case eq. (6.14) holds for the chargino and gluino contribution separately as well as for their sum and each point from the $\text{Im } \Delta^d - \text{Re } \Delta^d$ plot is translated according to eq. (6.14) to the $\text{Im } \Delta^s - \text{Re } \Delta^s$ plot as it is shown for the the 68.3% CL, 95.45% CL and 99.73% CL regions in fig. 6.3. However, looking at the general relation eq. (6.22) we see that the black hatched region in the $\text{Im } \Delta^s - \text{Re } \Delta^s$ plane can be enlarged if there is a mass difference between the diagonal elements of the up-type squark mass matrix. In this case a phase difference between the gluino and chargino contribution appears as well (see eq. (6.25)). If the mass difference between the diagonal elements of M_{uLL}^2 is not sufficient to provide the necessary amount of flavour violation in order to explain a certain point in fig. 6.3 the black hatched region can be enlarged further by choosing in addition the mass insertion δ_{13}^{uLL} to be non-zero. The LR sectors of the squark mass matrices are not related to each other as this is the case for the LL sectors due to $\text{SU}(2)$ gauge symmetry. Allowing matrix elements of the LR sectors to contribute to the flavour violation in the meson mixing processes the black hatched region could cover any desired region in $\text{Im } \Delta^s - \text{Re } \Delta^s$ plot.

In our numerical analysis assuming a non diagonal M_{uLL}^2 with equal diagonal elements the entries of the down-type squark mass matrix generated through the $\text{SU}(2)$ relation have a simple form

$$\begin{aligned} \delta_{23}^{dLL} &= \delta_{23}^{uLL} + \mathcal{O}(\lambda^2), \\ \delta_{13}^{dLL} &= -\lambda \delta_{23}^{uLL} + \mathcal{O}(\lambda^5). \end{aligned} \quad (6.26)$$

As already discussed, in this case the phases of the mass insertions in the down-type squark sector are to a very good approximation equal to the phases of the mass insertions in the

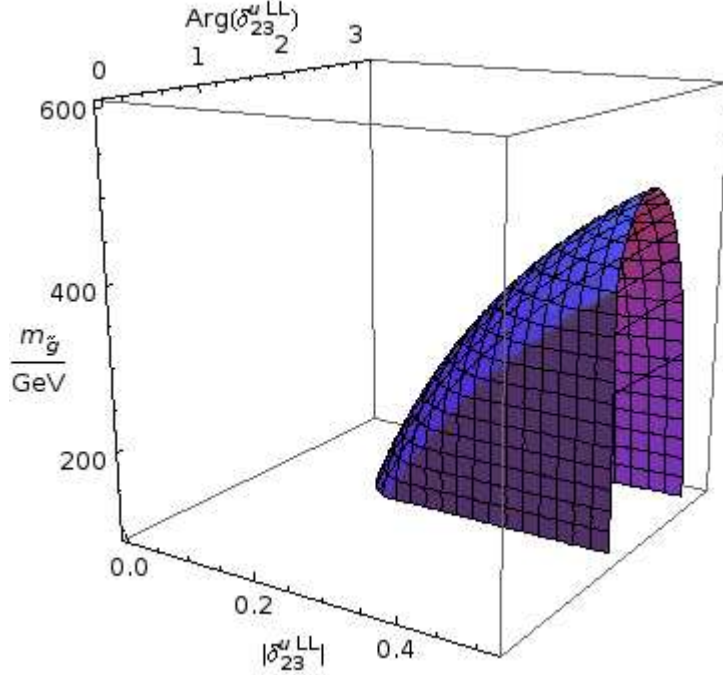


Figure 6.4: Relation between the gluino mass and the mass insertion δ_{23}^{uLL} for $B_s - \bar{B}_s$ mixing. $|\delta_{23}^{uLL}|$ is limited to 0.52 by the choice of the minimal squark mass eigenstate bigger than 350 GeV. $\phi_\Delta^s = -30^\circ$, $f_{B_s} = 0.228$ GeV.

up-type squark sector and eq. (6.6) creates a relation between the gluino mass, the mass insertion δ_{23}^{dLL} and the phase ϕ_Δ^q . In fig. 6.4 we show the surfaces in a 3-dimensional plot for $\text{Abs}(\delta_{23}^{uLL})$, $\text{Arg}(\delta_{23}^{uLL})$ and $m_{\tilde{g}}$ on which this condition is satisfied in $B_s - \bar{B}_s$ mixing. The plot contains not only the gluino contribution but the chargino and charged Higgs contributions as well. All diagonal elements of M_{uLL}^2 are set to $(500 \text{ GeV})^2$. The range of δ_{23}^{uLL} is chosen such that the minimal squark mass eigenstate is bigger than 350 GeV. Since $|\Delta_{\text{NP}}^{s\tilde{g}}|$ depends on the gluino mass, the absolute value of the mass insertion $|\delta_{23}^{uLL}|$ and on the squark masses one can obtain an upper limit on gluino mass $m_{\tilde{g}}$ from the maximal value of $|\Delta_{\text{NP}}^{s\tilde{g}}|$ for a given value of the mass insertion and a given set of squark masses. We choose all squark masses to be equal and show the relation between $|\Delta_{\text{NP}}^{s\tilde{g}}|$ and $m_{\tilde{g}}$ for a certain squark mass and different $|\delta_{23}^{uLL}|$ in fig. A.3 and for a certain $|\Delta_{\text{NP}}^{s\tilde{g}}|$ and different squark masses in fig. A.2 in the appendix. In all plots we see that the gluino contribution vanishes for $m_{\tilde{g}} \approx 1.5 m_{\tilde{q}}$ where $m_{\tilde{q}}$ is the value of all diagonal elements in the up-type squark mass matrix. The reason for this effect is the cancellation between the

crossed and uncrossed box diagrams in fig. 4.3. This is an important issue which has not been taken into account by most analyses, which have disregarded the electroweak SUSY contributions, claiming that they are suppressed by the factor g_2^4/g_3^4 in comparison to the gluino contribution. However, from the plots shown in fig. A.2 and fig. A.3 we see that this statement is true only for gluino masses smaller than the squark masses. In the opposite case, the electroweak contributions can be dominant and their omission is not justified. We will examine this topic in detail in the next chapter where we concentrate on the mass splitting between left-handed squarks.

6.2. Constraints on the mass splitting of left-handed squarks

The squark mass matrices in the down sector and in the up sector provide with their off-diagonal elements additional sources of flavour violation. In order to satisfy the bounds from FCNCs it has been noted already in very early analyses of the MSSM that a super GIM mechanism is necessary [76]. If the up-type squark mass matrix of the left-handed squarks contains big off-diagonal elements a flavour off-diagonal entries of the same order are generated through the SU(2) relation eq. (6.15) in the down-type squark mass matrix. The same statement is true for the reversed situation assuming down-type squark LL mass mixing matrix containing big off-diagonal elements. As we have shown in the previous section the off-diagonal matrix elements induced through the SU(2) gauge symmetry in the left handed fermion sector are proportional to the mass difference between the diagonal elements in the squark mass matrices. Therefore, in order to avoid off-diagonal entries which would spoil the experimental bounds on observables involving FCNC effects usually the left-handed squarks are assumed to be with degenerate masses. We have examined the mass splitting between the left-handed squarks by imposing constraints from $D-\bar{D}$ and $K-\bar{K}$ mixing. In following we explain the main features of our approach. The complete analysis with all the results for different values of the relevant MSSM parameters can be found in [77].

The $D-\bar{D}$ and $K-\bar{K}$ mixing are FCNC processes which are highly sensitive to transitions between the first two squark generations in the up-type and down-type squark sector. The neutral Kaon system probes NP in the down-type squark sector while the mixing of neutral D mesons is affected by flavour changing parameters in the up-type squark sector. Considering the SUSY contributions to the $D-\bar{D}$ and $K-\bar{K}$ mixing processes we can

place constraints on the involved flavour changing SUSY parameters.

The $K - \bar{K}$ mass difference ΔM_K and the indirect CP violation parameter ϵ_K are both small and in agreement with their SM predictions. In the SM the $K - \bar{K}$ transition amplitude is suppressed due to the rather precise GIM mechanism and the additional suppression of the top quark contribution by small CKM factors. Therefore, the meson mixing in the Kaon system is appropriate for testing NP models and obtaining bounds on NP parameters especially in the MSSM. This statement is true for the mixing of neutral D mesons as well. $D - \bar{D}$ mixing was experimentally discovered in 2007 by the BaBar [66] and Belle [67, 68] collaborations. Short-distance SM effects are strongly CKM suppressed and the long-distance contributions cannot be calculated perturbatively. Therefore, conservative estimates assume for the SM contribution a range up to the absolute measured value of the mass difference. However, due to the small measured mass difference $D - \bar{D}$ mixing still limits NP contributions in a stringent way. Furthermore, a CP phase in the neutral D system can directly be attributed to NP.

In the most analysis which have been performed in order to constrain MSSM parameters the neutralino and chargino contributions to the box digrams shown in fig. 4.3 have been neglected [62, 79–84]. The main argument for considering only the gluino contribution is the smallness of the weak coupling constant which is involved in the chargino and neutralino vertices in comparison with the strong coupling constant. In fact, the contribution to the box diagrams due to the weak interaction is suppressed by a factor g_2^4/g_3^4 compared to the gluino contribution. However, the off-diagonal elements in the LL block of the squark mass matrices cause an enhancement of the flavour changing effects induced by the quark-squark-chargino and quark-squark-neutralino vertices. Moreover, for certain configuration of the MSSM parameters, especially if the gluino is heavier than the squarks, the gluino contribution can be suppressed due to the cancellation between the crossed and uncrossed box diagrams. This effect cannot occur in box diagrams involving charginos because they are Dirac fermions and the crossed box diagrams are not present. Because of the reasons mentioned above, we can conclude that the neglecting of the electroweak contributions is a good approximation only for light gluinos and cannot be justified in regions where the gluinos are heavier than the squarks.

In our analysis we consider the strong as well as the electroweak SUSY contributions to the $K - \bar{K}$ and $D - \bar{D}$ mixing processes in the general MSSM. In particular, we calculate the gluino, gluino-neutralino, neutralino and chargino contributions. Our aim is to obtain

constraints on the mass-splitting between the first two generations of left-handed squarks. As already discussed in the previous section the SU(2) gauge symmetry of the left-handed fermion sector creates a relation between the up-type and down-type squark mass matrices, in particular $M_{uLL}^2 = VM_{dLL}^2V^\dagger$.

Both squark mass matrices can be simultaneously diagonal only if they are proportional to the unit matrix. This is realised in the naive minimal flavour violating MSSM. In case one of the squark mass matrices does not contain only equal diagonal elements, the SU(2) relation eq. (6.15) generates off-diagonal elements in the other one. These entries are proportional to the off-diagonal elements in the squark mass matrix on which the CKM rotation is performed and on the difference between the diagonal elements. In this analysis we are interested in the mass insertions δ_{12}^{uLL} and δ_{12}^{dLL} which cause flavour violation between the first two generations in the up-type and in the down-type squark sector, respectively, and therefore can sizeably affect the $D-\bar{D}$ and $K-\bar{K}$ mixing processes. Assuming a diagonal down-type squark mass matrix with non-degenerate diagonal elements, we obtain for the mass insertion δ_{12}^{uLL} from the SU(2) relation

$$\delta_{12}^{uLL} = V_{us}V_{cs}^* \left[\frac{(M_{dLL}^2)_{22} - (M_{dLL}^2)_{11}}{\tilde{M}^2} \right] + V_{ub}V_{cb}^* \left[\frac{(M_{dLL}^2)_{33} - (M_{dLL}^2)_{11}}{\tilde{M}^2} \right]. \quad (6.27)$$

In the opposite case of a diagonal up-type squark mass matrix the mass insertion δ_{12}^{dLL} induced through the SU(2) relation is given by

$$\delta_{12}^{dLL} = V_{cs}V_{cd}^* \left[\frac{(M_{uLL}^2)_{22} - (M_{uLL}^2)_{11}}{\tilde{M}^2} \right] + V_{ts}V_{td}^* \left[\frac{(M_{uLL}^2)_{33} - (M_{uLL}^2)_{11}}{\tilde{M}^2} \right]. \quad (6.28)$$

The CKM matrix elements in eq. (6.27) and eq. (6.28) can be expressed through the parameters A , λ , ρ and η of the Wolfenstein parametrisation eq. (4.4). We find

$$\delta_{12}^{uLL} = \lambda \left(1 - \frac{\lambda^2}{2} \right) \left[\frac{(M_{dLL}^2)_{22} - (M_{dLL}^2)_{11}}{\tilde{M}^2} \right] + \mathcal{O}(\lambda^5), \quad (6.29)$$

respectively

$$\delta_{12}^{dLL} = -\lambda \left(1 - \frac{\lambda^2}{2} \right) \left[\frac{(M_{uLL}^2)_{22} - (M_{uLL}^2)_{11}}{\tilde{M}^2} \right] + \mathcal{O}(\lambda^5). \quad (6.30)$$

The generated mass insertions mostly depend on the mass difference between the first two generations in the up or down sector and differ from each other only by their overall sign. If we choose the squark mass matrices to be proportional to the unit matrix we find that all MSSM Wilson coefficients are complex numbers with negligible phase: the imaginary

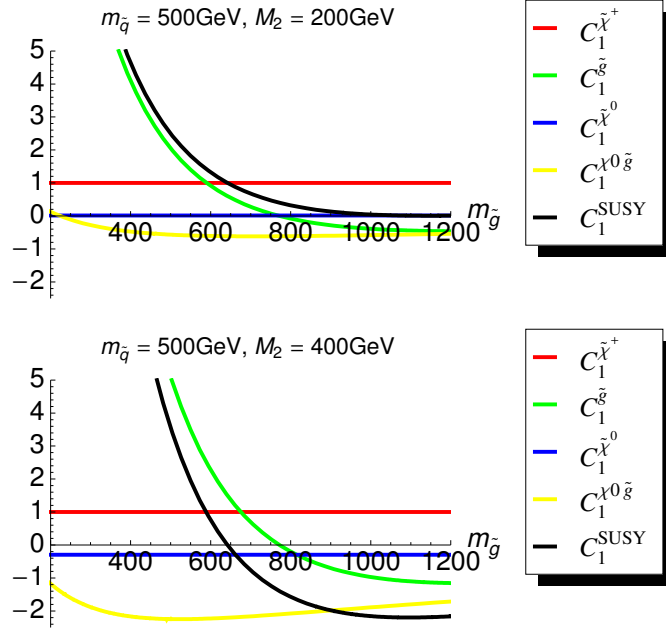


Figure 6.5: Size of the real part of the Wilson coefficients of the different SUSY contributions to the $D-\bar{D}$ or $K-\bar{K}$ mixing process normalised to the chargino contribution. C_1^{SUSY} is the sum of all considered contributions from SUSY particles. Plots for squark masses of 1000 GeV can be found in [77].

part is several orders of magnitude smaller than the real part for large regions of the MSSM parameter space. In fig. 6.5 we show the real part of the SUSY Wilson-Coefficients $C_1^{\tilde{\chi}^\pm}$, $C_1^{\tilde{\chi}^0}$, $C_1^{\tilde{g}}$, $C_1^{\tilde{g}\tilde{\chi}^0}$ contributing to the $K-\bar{K}$ or $D-\bar{D}$ mixing process as a function of the gluino mass. All Wilson coefficients are normalised to $C_1^{\tilde{\chi}^\pm}$. For light gluino masses the gluino contribution dominates over the other ones by far. However, $C_1^{\tilde{g}}$ decreases fast with increasing gluino mass. For heavy gluino masses the most important contribution originates always from chargino boxes. Further, we notice that for some configuration of the MSSM parameters, i.e. in case of heavy gluino and light squark masses around and below 500 GeV, and big values of M_2 around 400 GeV and more, the mixed gluino-neutralino contribution becomes the second dominant one after the chargino contribution. In almost all regions of the MSSM parameter space the contribution to the FCNC meson mixing process due to the neutralino-neutralino boxes is negligible compared to the ones of the other SUSY particles involved in the box diagrams.

In recent analyses [79,84] NP has been constrained by requiring that the NP contribution to

the mass difference of neutral Kaons and D mesons has to be smaller than the corresponding experimental values $\Delta M_K/M_K = (7.01 \pm 0.01)10^{-15}$ [85] and $\Delta M_D/M_D = (8.6 \pm 2.1)10^{-15}$ [86]. CP violation in mixing stemming from NP phenomena is restricted through the parameter $\epsilon_K^{\text{NP}} \leq 0.6\epsilon_K^{\text{exp}}$ [79]. Thus, the following upper bounds on the Wilson coefficients C_1^K and C_1^D have been obtained [79]:

$$\begin{aligned} |C_1^K| &\leq 8.8 \cdot 10^{-13} \left(\frac{\Lambda_{\text{NP}}}{\text{GeV}} \right)^2, \\ |C_1^D| &\leq 5.9 \cdot 10^{-13} \left(\frac{\Lambda_{\text{NP}}}{\text{GeV}} \right)^2, \\ \text{Im}(C_1^K) &\leq 3.3 \cdot 10^{-15} \left(\frac{\Lambda_{\text{NP}}}{\text{GeV}} \right)^2, \\ \text{Im}(C_1^D) &\leq 1.0 \cdot 10^{-13} \left(\frac{\Lambda_{\text{NP}}}{\text{GeV}} \right)^2 \end{aligned} \quad (6.31)$$

where Λ_{NP} is the scale of NP. We use the constraints in eq. (6.31) in order to obtain constraints on the mass splitting between the first two generations of left handed down-type squarks from $K - \bar{K}$ mixing and on left handed up-type squarks from the meson mixing in the neutral D meson system.

We first analyse the two extreme cases with diagonal up-type squark or diagonal down-type squark mass matrix and set $(M_{uLL}^2)_{22} = (M_{uLL}^2)_{33}$, respectively $(M_{dLL}^2)_{22} = (M_{dLL}^2)_{33}$. The constraints obtained for these two scenarios correspond to the green and red area in fig. 6.6 where we show the gluino mass and the squark mass of the first generation in a two dimensional region plot. The plot shows that large regions in the MSSM parameter space with non-degenerate squarks are allowed from $K - \bar{K}$ and $D - \bar{D}$ mixing. While the red and green regions correspond to completely alignment either in the up sector or in the down sector either by choosing M_{uLL}^2 diagonal and obtaining the constraints from the Kaon system or by requiring a diagonal form of M_{dLL}^2 and obtaining the constraints from $D - \bar{D}$ mixing, the yellow region describing the maximally allowed mass splitting is obtained in case of intermediate alignment of the up-type and down-type squark mass matrices in the up and down sector. In this case neither M_{uLL}^2 nor M_{dLL}^2 is diagonal. Following the approach in [79] we perform a rotation of the diagonal squark mass matrices by the matrix [79]

$$V_d = \begin{pmatrix} \cos \theta_d & \sin \theta_d & 0 \\ -\sin \theta_d & \cos \theta_d & 0 \\ 0 & 0 & 1 \end{pmatrix}. \quad (6.32)$$

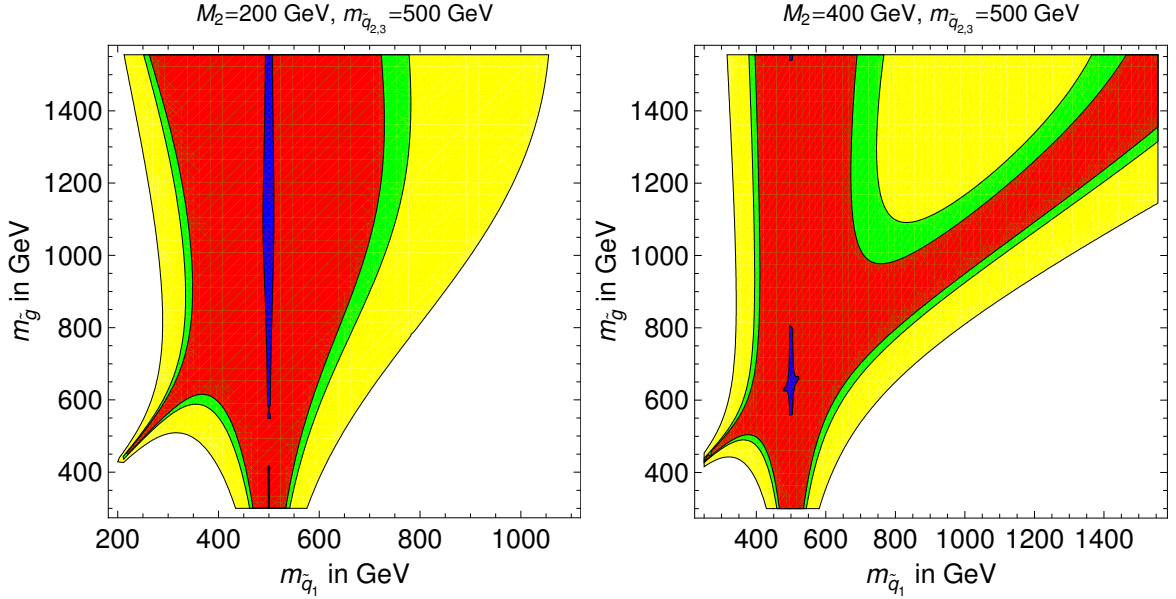


Figure 6.6: Allowed regions in the $(m_{\bar{q}_1}, m_{\bar{g}})$ -plane for $m_{\bar{q}_2} = m_{\bar{q}_3} = 500$ GeV and $M_2 = 200$ GeV, 400 GeV according to eq. (6.31). The green region is the allowed range assuming a diagonal up squark mass matrix. The red region is obtained in case of diagonal down squark mass matrix. The yellow (lightest) area corresponds to the maximally allowed mass splitting assuming intermediate alignment of the squark mass matrices in the up and down LL squark sector. The blue (darkest) area is the minimal region allowed for mass splitting between the left-handed squarks corresponding to a scenario with equal diagonal entries in the down squark mass matrix and an off-diagonal element carrying a maximal phase. Plots for squark masses of 1000 GeV can be found in [77].

The angle θ_d is defined through

$$\tan 2\theta_d = \frac{\sqrt{\left|\frac{C_{\text{exp}}^K}{C_{\text{exp}}^D}\right|} \sin 2\theta_c}{1 + \sqrt{\left|\frac{C_{\text{exp}}^K}{C_{\text{exp}}^D}\right|} \cos 2\theta_c} \quad (6.33)$$

where θ_c denotes the Cabibbo angle. With the numerical constraints given in eq. (6.31) one finds inserting the maximal values of $|C_1^K|$ and $|C_1^D|$ in eq. (6.33) $\theta_d = 6.9^\circ$. Departing from the exact alignment of the LL squark mass matrices either in the up or in the down sector through the rotation by the matrix V_d additional real off-diagonal elements are generated. Looking at the plots in fig. 6.6 one realises that a lot of points in the MSSM parameter space can be found which allow for an even larger mass splitting compared to the cases with

diagonal up-type or down-type squark mass matrix. For a proper value of that off-diagonal elements which in our case of study is given by choosing a value for the angle $\theta_d = 6.9^\circ$ in V_d the allowed mass splitting can be maximised [79].

The blue region in fig. 6.6 shows the minimal region for mass splitting between the left-handed squarks obtained under the assumption that the down squark mass matrix is proportional to the unit matrix and contains an imaginary off-diagonal element carrying a complex phase such that the imaginary part of the Wilson coefficient C_1^K is maximal. The imaginary matrix element of M_{dLL}^2 is an additional source of CP violation in the Kaon system. Using the CP violation parameter ϵ_K as a constraint, i.e. the constraint on the imaginary part of the Wilson coefficient C_1^K given in eq. (6.31) we obtain the most stringent bound on the mass splitting between the left-handed squarks of the first two generations with the maximal amount of CP violation stemming from NP.

Our analysis on the mass splitting between the first two generations of left-handed squarks shows that there are large regions in the MSSM parameter space allowed from $K-\bar{K}$ and $D-\bar{D}$ meson mixing processes where the squarks are not degenerate and for certain scenarios even a large mass splitting of 100% and more is possible. In fact, the most benchmark analysis of the SUSY parameters are performed under the assumption of degenerate squark masses [87,88]. However, in case of different diagonal elements of the mass mixing matrices interesting consequences on the branching ratios can occur [89]. The analysis of the $K-\bar{K}$ and $D-\bar{D}$ mixing processes shows that the up-type and down-type squark mass matrices do not need to be necessarily proportional to the unit matrix at some high scale.

7. NUMERICAL ANALYSIS OF δ_{23}^{uLL} AND δ_{13}^{uLL}

In this chapter we describe the numerical analysis which has been performed in order to constrain the off-diagonal elements $\delta_{23}^{uLL}\tilde{M}^2$ and $\delta_{13}^{uLL}\tilde{M}^2$ of the up-type squark mass matrix. We start with an overview of the main features of the standard analyses of this type. Further, we explain our approach to place bounds on the mass insertions involved in the FCNC processes studied in this work.

As already mentioned at the beginning of Ch. 6, in the past many analyses have been performed in order to constrain off-diagonal elements of the squark mass matrix. The first studies have used the mass insertion approximation (see Ch. 6) while in more recent papers the up-type or down-type squark mass matrices have been fully diagonalised. In order to obtain the most conservative bounds on mass insertions it has been assumed that the flavour changing processes are induced by one mass insertion only. The bounds on the mass insertions are extracted by comparison with the experimental results imposing that the quantities which are calculated taking into account the SUSY contribution to the certain process under study do not exceed the corresponding measured values. In order to perform a test of different SUSY models and to constrain different off-diagonal entries in the squark mass matrices the analyses have been extended and have become more complex and extensive. In previous works on this topic the main focus has been set on $|\Delta F| = 2$ meson mixing processes like $K - \bar{K}$ mixing, $B - \bar{B}$ mixing and $\Delta F = 1$ processes like $B \rightarrow X_s \gamma$, $B \rightarrow X_s l^+ l^-$, $l_i \rightarrow l_j \gamma$ as well as on the CP constraints (see i.e. [71–73], [74] and references therein). Recently, also $|\Delta F| = 0$ processes, in particular the electric dipole moments (EDMs) of quarks and leptons and the anomalous magnetic moment of the muon have been analysed using scatter plot methods [74]. Since the SM predicts very small values for the EDMs they are extremely sensitive to NP contributions. Although the EDMs arise as a result of flavour conserving processes they can be generated by two $|\Delta F| = 1$ transitions. Assuming that SUSY particles are involved in these flavour violating $|\Delta F| = 1$ transitions it is possible to place constraints on the mass insertions. In the most recent

analysis [74] the usually considered set of processes has been extended by rare B decays, $D-\bar{D}$ mixing and time dependent CP asymmetries. By including the full set of SUSY particles which can contribute to the FCNC processes, the charged Higgs, the gluino, the chargino and the neutralino, all theoretically relevant one loop contributions have been taken into account. In [74] bounds on mass insertions are determined in the context of different SUSY models such as the MSSM with minimal flavour violation where the flavour violation even beyond the SM is described by the CKM matrix, a flavour blind MSSM, SUSY models based on abelian and non-abelian flavour symmetries.

Performing an updated analysis of the bounds on the flavour violating terms in the SUSY soft sector in the general MSSM is emphasised as one of the novelties in the most recent work on this subject [74]. The theoretical treatment of the quantities under study is done indeed in the context of the general MSSM. However, for the numerical analysis a spectrum of the so-called constrained MSSM (CMSSM) is assumed. In fact, among various possible sets of boundary conditions which can be imposed on the multidimensional parameter space of the MSSM by far the most popular choice is the CMSSM. In this model at the GUT scale all the sleptons, squarks and Higgs bosons have a common scalar mass m_0 , all the gauginos unify at the common gaugino mass $M_{1/2}$, and so all the tri-linear terms assume a common tri-linear mass parameter A_0 . In addition, at the electroweak scale one selects the ratio of Higgs vacuum expectation values $\tan\beta$ and $\text{sign}(\mu)$, where μ is the higgsino mass parameter of the superpotential.

The aim of our numerical analysis is to obtain constraints on the mass insertions δ_{i3}^{uLL} , $i = 1, 2$ of the up-type squark mass matrix in the general MSSM. We focus on generic relations which are mostly independent on boundary conditions. Such a physical relation stems from chargino boxes which correlate $B_d-\bar{B}_d$ mixing and $B_s-\bar{B}_s$ mixing through the CKM elements involved in the meson mixing processes. Another very important theoretical issue is the relation between the left-handed up-type squark mass matrix and the left-handed down-type one $M_{uLL}^2 = VM_{dLL}^2V^\dagger$ due to $SU(2)$ gauge symmetry in the left handed fermion sector. Since these mass matrices are not independent the only way to avoid flavour off-diagonal mass insertions in the up and in the down sector simultaneously is to choose M_d^2 or M_u^2 proportional to the unit matrix. This is realised in the naive minimal flavour violating MSSM. In a more general definition of MFV [64, 65] flavour violation due to NP is postulated to stem solely from the Yukawa sector resulting in FCNC transitions

(which can now also be mediated by gluinos and neutralinos) proportional to products of CKM elements and Yukawa couplings. In our approach we assume M_{uLL}^2 containing flavour changing non-diagonal entries and calculate the elements of M_{dLL}^2 using the $SU(2)$ relation. In addition, we take into account the numerical relation between the $B_s - \bar{B}_s$ mixing and $B_d - \bar{B}_d$ mixing transition due to ratio of the decay constants and the bag parameters in the B_s and B_d systems. In almost all previous analyses the $B_s - \bar{B}_s$ mixing and $B_d - \bar{B}_d$ mixing were treated independently from each other. However, these two processes are related to each other through the ratio ξ defined in eq. (2.90). In order to obtain the most conservative bounds on mass insertions we assume that the flavour changing processes are induced by one mass insertion only. The bounds on the mass insertions are extracted by comparison with the experimental results imposing that the quantities which are calculated taking into account the SUSY contribution to the certain process under study do not exceed their measured values. In the numerical analysis we consider the chargino, gluino and the charged Higgs contribution to the box diagrams. The box diagrams involving these particles dominate over the ones with a neutralino running in the loop by far. For this reason the neutralino contribution has been neglected in the numerical calculations. Since the box diagrams with charged Higgses do not involve squarks their contribution to the FCNC process of meson-antimeson mixing is not proportional to off-diagonal elements of the squark mass matrix. By exchanging one of the two or both W bosons in the SM box diagrams by a charged Higgs boson the additional contribution to the meson-antimeson decay amplitude depend only on two MSSM parameters, the mass of the charged Higgs boson m_{H^\pm} and $\tan\beta$. For $\tan\beta \leq 7$ the charged Higgs contributions are positive for all allowed values of the charged Higgs mass [59]. They reach small negative values for $\tan\beta = 10$ for very light Higgs bosons (see i.e. Ch. 5.2, iv, fig. 7 in [59]). Therefore, the meson-antimeson transition mediated by H^\pm summarised in the Wilson coefficients $C_i^{H^\pm}$ appears as a small constant shift of the sum of the other Wilson coefficients which is given by the choice of the MSSM parameters m_{H^\pm} and $\tan\beta$. Yet through the resulting shift in the observable quantities the charged Higgs contribution indirectly influences the flavour changing parameters under study. Further, we calculate with the obtained values of δ_{LL}^{u23} and δ_{LL}^{u13} the CP violating parameter $|\epsilon_K|$ which is used as an additional constraint on the studied mass insertions. The constraint from the CP violation in the mixing of neutral Kaons has not been considered by many analyses in the past. However, the value of the non-perturbative parameter \hat{B}_K is known from recent lattice calculations with a good enough precision such that $|\epsilon_K|$ becomes an important quantity for NP searches.

Further, we examine considering the allowed values for the mass insertions δ_{LL}^{u23} and δ_{LL}^{u13} from $B_s - \bar{B}_s$ and $B_d - \bar{B}_d$ mixing whether the branching ratio $\text{Br}(B \rightarrow X_s \gamma)$ which is very sensitive to NP effects satisfies its experimental bounds. In addition, we are using the obtained values for δ_{LL}^{u23} and δ_{LL}^{u13} for the calculation of the $D - \bar{D}$ transition amplitude. Since the $D - \bar{D}$ transition amplitude is proportional to the product $\delta_{LL}^{u23} \delta_{LL}^{u13}$ we tested whether it is possible to obtain an additional constraint on the product of the mass insertions we are studying from the $D - \bar{D}$ system.

7.1. The calculation procedure

In the calculation procedure we first investigate the case in which the SM calculation satisfies the experimental observables inside their 2σ bounds. We take the values of all the input quantities to be in their 2σ experimental regions such that the SM is not experimentally excluded up to 2σ for all observables under study. In this case NP contribution to the calculated quantities is necessary only if their theoretical value has to be equal to a certain value i.e. in the 1σ region, in particular, the central value. The opposite scenario which we investigate under the assumption that the SM is maximally excluded allows us to obtain the maximum amount of NP contribution which is needed in order to satisfy the requirement that the studied observables do not exceed their 2σ experimental bounds. In the maximum NP regime we calculate the entries of the CKM matrix using the values of $|V_{cb}|$ and $|V_{ub}|$ obtained from inclusive semileptonic B decays. In these processes the quark transition $b \rightarrow cl\bar{\nu}_l$, respectively $b \rightarrow ul\bar{\nu}_l$, is realised. Determinations of $|V_{cb}|$ from inclusive decays are currently below 2% relative uncertainty [75]. At present, the inclusive decays provide the most precise determination of $|V_{ub}|$. Unfortunately, the measurement of the total decay rate of $\bar{B} \rightarrow X_u l \bar{\nu}_l$ decay is a very challenging task for experimentalists due to the large background from CKM favoured $\bar{B} \rightarrow X_c l \bar{\nu}_l$ transitions. Taking into account the uncertainty in m_b as well, the total uncertainty on $|V_{ub}|$ is at the 10% level [75]. The maximal value of the angle β corresponds to $\alpha = \pi/2$. Thus, we obtain (cf. fig. 4.1)

$$\beta_{\max} = \arcsin R_b \quad (7.1)$$

where the side of the unitarity triangle R_b is given by

$$R_b = \left(1 - \frac{\lambda^2}{2}\right) \frac{1}{\lambda} \left| \frac{V_{ub}}{V_{cb}} \right|. \quad (7.2)$$

With the numerical values $V_{ub}^{\text{incl}} = (4.12 \pm 0.43) \cdot 10^{-3}$ and $V_{cb}^{\text{incl}} = (41.6 \pm 0.6) \cdot 10^{-3}$ we find the maximal value $\beta_{\max} = 28.34^\circ$ using the upper and lower 1σ bounds on V_{ub}^{incl} and

V_{ub}^{incl} , respectively.

We consider the processes of $B_d-\bar{B}_d$ mixing, $B_s-\bar{B}_s$ mixing, $K-\bar{K}$ mixing, $D-\bar{D}$ mixing as well as the inclusive decay $B \rightarrow X_s\gamma$. For all these transitions we calculate the SUSY contributions from the charged Higgses, gluinos and charginos in the loop diagrams.

7.2. The logical structure of the program

For the extraction of the mass insertions δ_{LL}^{u13} we have used the procedure which logical structure is shown as a flowchart in fig. A.2. In the following we describe the routine. The $B_s-\bar{B}_s$ and $B_d-\bar{B}_d$ transition amplitudes M_{12}^s , M_{12}^d , the $K-\bar{K}$ CP-violating parameter ϵ_K as well as the $B \rightarrow X_s\gamma$ Wilson coefficients C_7 , C_7' , C_8 and C_8' are calculated at previous stages of the program and depend now only on the unknown variables δ_{LL}^{u13} and δ_{LL}^{u23} . The transition amplitudes M_{12}^s and M_{12}^d are functions of the B_s and B_d decay constants f_{B_s} , respectively f_{B_d} , as well. We start with $B_s-\bar{B}_s$ mixing and our first goal is the determination of the allowed values for δ_{LL}^{u23} by scanning over its real and imaginary part and the extraction of the corresponding allowed mass insertion δ_{LL}^{u13} from the $B_d-\bar{B}_d$ mixing process. For this purpose the squark mass eigenvalues are calculated for each value of δ_{LL}^{u23} during the scanning process assuming first $\delta_{LL}^{u13} = 0$. For the following calculation we consider only points in the $(\text{Re } \delta_{LL}^{u23}, \text{Im } \delta_{LL}^{u23})$ -plane for which the numerically smallest squark mass eigenstate is bigger than a certain lower bound which has been chosen to be 350 GeV. When such a point is found during the scanning process it is inserted into the $B_s-\bar{B}_s$ mass difference ΔM_s . Requiring ΔM_s to be equal to the mean value of the experimentally measured mass difference $\Delta M_s^{\text{exp}} = 17.77 \text{ ps}^{-1}$ we find the value of the B_s decay constant f_{B_s} . In case the obtained f_{B_s} satisfies the allowed region $208 \text{ MeV} \leq f_{B_s} \leq 248 \text{ MeV}$ (see table 4.1) the procedure continues with the calculation of the NP phase ϕ_Δ^s . Further, we require the NP phase ϕ_Δ^s to be inside of the 2σ range extracted from the analysis of the CKMfitter group (see table 6.1). In the next step, the decay constant f_{B_d} is determined using the ratio between the decay constants in the B_s and B_d systems given in eq. (2.91) which is known from lattice calculations with a precision up to 4%. Having inserted the found value of f_{B_d} in the $B_d-\bar{B}_d$ mass difference, the mass insertion δ_{LL}^{u13} remains the only unknown parameter in the $B_d-\bar{B}_d$ transition amplitude M_{12}^d . Then, taking into account the SM $B_d-\bar{B}_d$ transition amplitude $M_{12}^{12\text{SM}}$ as well as the measured $B_d-\bar{B}_d$ mass difference ΔM_d^{exp} and mixing phase $2\beta^{\text{exp}}$ the matrix element δ_{LL}^{u13} is calculated by requiring

the theoretical value of the $B_d - \bar{B}_d$ transition amplitude to be equal to the experimental one. Since the mass insertion δ_{LL}^{u13} is a complex quantity, the calculation of its absolute value and phase is performed in an iterative way by starting with a proper value for the phase and solving the equation for the absolute value and then inserting the latter again in M_{12}^{dSM} and extracting the phase once more. This iterative procedure is repeated many times until the calculated values for the absolute value and the phase of δ_{LL}^{u13} are stable. After the determination of δ_{LL}^{u13} it is inserted in the up-type mass mixing matrix which is diagonalised and the check whether the smallest squark mass eigenstate is bigger than the lower bound of 350 GeV has to be passed again. If this is the case the transition amplitude M_{12}^d is calculated by inserting the obtained value of δ_{LL}^{u13} once more in order to be ensured that the equation $M_{12}^d = M_{12}^{d,exp}$ indeed holds. This check is the last confirmation that the mass insertion δ_{LL}^{u13} has been correctly calculated. Then, the whole procedure can be repeated iteratively by using the obtained value of δ_{LL}^{u13} as an input in ΔM_s together with δ_{LL}^{u23} . The decay constant f_{B_s} is determined from the new value of ΔM_s and the procedure continues with the further steps described above. After a certain number of iterations is successfully completed the numerical values of the quantities ϵ_K , $\text{Br}(B \rightarrow X_s \gamma)$ and $|M_{12}^D|$ is calculated with the extracted values of δ_{LL}^{u23} and δ_{LL}^{u13} .

In order to ensure that the routine described above will work for different scenarios and choices of the MSSM input parameters a lot of additional subroutines and checks have been included in the numerical procedure which logical structure has been explained above. In particular, possible divergences in case of equal eigenstates of the squark mass matrices have to be avoided. For special choices of the gluino mass and the mass of the charged Higgs bosons, such that they become accidentally very similar to squark mass eigenstates during the scan over the real and imaginary part of the mass insertion δ_{LL}^{u23} , certain loop functions can diverge as well. In order to ensure the stability of the program it has been necessary to distinguish between several subcases. The analytical diagonalisation of the squark mass mixing turned out to be a difficult and time consuming task for the software Mathematica which has been used in the calculation procedure. In particular, after applying the SU(2) relation in eq. (6.15) to obtain the entries of the down-type squark mass matrix from those of the up-type squark mass matrix its elements become a complex polynomial function of the mass insertions δ_{LL}^{u23} and δ_{LL}^{u13} . From a mathematical point of view the diagonalisation of a complex unitary matrix fails, if its determinant vanishes which means that the inverse matrix does not exist. It turned out that even in the case of a complex unitary 3×3

matrix as an input the calculation of the eigenvectors is not possible with the standard tools of Mathematica in case of matrix elements which are complex polynomial functions of one variable. In our case of study the problem has been easily solved because of the special kind of the transformation defined by the SU(2) relation eq. (6.15), namely, it is an unitary transformation. According to the Sylvester's theorem (which is a special case of the lemma on matrix determinants) lemma the up-type and down-type squark mass matrix have the same characteristic polynomial and therefore the same eigenvalues as well. The eigenvectors are related to each other through the CKM matrix. With the definitions in eq. (4.55) we find

$$(M_D^2)^D = (M_{\tilde{U}}^2)^D, \quad Z_D = Z_U V. \quad (7.3)$$

However, for obtaining the eigenvectors of a general complex matrix which elements are not given as explicit numbers but as complex polynomial functions the standard tools of the software Mathematica cannot be applied in general.

For reason of clarity and a better understanding of the main logic of our procedure for numerical determination of the mass insertions, the additional checks and subroutines which have been included in order to improve the routine concerning the speed, the maintenance of different problems with divergences occurring in special cases and ensuring the correctness of the numerical results have not been explicitly shown on the flowchart in fig. A.2.

7.3. Results of the numerical analysis

The determination of the mass insertions δ_{LL}^{u23} and δ_{LL}^{u13} in the numerical analysis is based on the correlation between the $B_s-\bar{B}_s$ and $B_d-\bar{B}_d$ mixing processes. Then, we place additional constraints on these parameters considering the other processes which involve these off-diagonal elements of the up-type squark mass matrix, in particular, the CP violation parameter ϵ_K , the branching ratio $\text{Br}(B \rightarrow X_s \gamma)$ and the $D-\bar{D}$ transition amplitude $|M_{12}^D|$. Taking into account the experimental bounds on these quantities we investigate which values of the mass insertions are excluded from the processes mentioned above even if they are allowed from $B-\bar{B}$ mixing. This analysis is performed for the region of the $(\bar{\rho}, \bar{\eta})$ -plane compatible with the SM as well as in scenarios in which the NP contribution is maximal. The results are shown as plots of all the combinations of the real part and imaginary part of the mass insertions δ_{LL}^{u23} and δ_{LL}^{u13} in fig. A.5 in the appendix. For the figures we use the following setup of supersymmetric parameters: $M_2 = 500$ GeV, $\mu = 200$ GeV, $\tan \beta = 7$,

$m_{H^\pm} = 500 \text{ GeV}$, $m_{\tilde{g}} = 500 \text{ GeV}$, all diagonal elements in the up-squark mass matrix are set to 500 GeV as well. In following we will comment on the results shown in the plots.

We plot the absolute value of the $D-\bar{D}$ transition amplitude $|M_{12}^D|$ as a function of the absolute value of the mass insertion δ_{23}^{uLL} in fig. A.2. The plot shows that in our scenario with two-step flavour transition $\tilde{c}_L \rightarrow \tilde{t}_L \rightarrow \tilde{u}_L$ not even the lower 2σ experimental bound of the $D-\bar{D}$ transition amplitude can be reached. In order to explain the $D-\bar{D}$ mixing amplitude as a pure supersymmetric effect the mass insertion δ_{12}^{uLL} and/or additional mass insertion in the LR sector would be necessary. As one can see on the plot in fig. A.2 this conclusion is true in the maximal NP regime as well.

In fig. A.5 we show the plots for all the combinations of the real part and imaginary part of the mass insertions δ_{LL}^{u23} and δ_{LL}^{u23} in the SM regime. These simulations have been performed with a CKM elements obtained from a point in $(\bar{\rho}, \bar{\eta})$ -plane such that all observables are compatible with the SM in their 2σ regions. The plots show the regions allowed from $|\epsilon_K|$ and $\text{Br}(B \rightarrow X_s \gamma)$ with different colours. The points for which the 2σ regions of these parameters are not violated lie within the intervals $-0.01 < \text{Re}(\delta_{LL}^{u13}) < 0.025$ and $-0.03 < \text{Im}(\delta_{LL}^{u13}) < 0.01$. These regions correspond to $-0.08 < \text{Re}(\delta_{LL}^{u23}) < 0.180$ and $-0.325 < \text{Im}(\delta_{LL}^{u23}) < 0.125$. In the maximal NP regime we use the CKM matrix elements V_{ub} and V_{cb} determined from inclusive B decays. This leads to an increase of the angle β of the unitarity triangle. In addition, we decrease the experimental value β^{exp} to its lower 2σ bound in order to create a bigger tension with the SM. The plots obtained in this way in the maximal NP regime are shown in fig. A.7.

In addition, we show in fig. A.2 the maximal value of the $B_s-\bar{B}_s$ mixing phase ϕ_Δ^s corresponding to a certain allowed value of the mass insertion δ_{23}^{uLL} for different gluino masses in the maximum NP regime. From this plot we can conclude that in case of small gluino masses when the gluino contribution to the $B_s-\bar{B}_s$ mixing becomes big the value of the negative mixing phase increases. The reason for this is that the gluino contribution directly involves the phase of the mass insertion δ_{23}^{uLL} (see i.e. eqs. (6.17) and (6.26)). The minimum of the curve arises due to cancellation between the crossed and uncrossed gluino box diagrams. This fact has been discussed previously in Ch. 6.1 and illustrated in fig. A.2 and fig. A.3.

8. SUMMARY AND OUTLOOK

With the start of the LHC not only the search for the one only missing particle in the SM, the Higgs boson, but also the direct search for physics beyond the SM has begun. The biggest discovery machine ever built is especially designed for exploring the TeV scale, the region where the masses of the new elementary particles postulated by the most favoured model for manifestation of NP, the minimal supersymmetric extension of the SM, are expected to be. The postulated superpartners of SM particles affect the physical processes and change the values of the observable quantities. The extent to which the theoretical prediction of a certain process is changed under the consideration of the NP particles depends on many parameters of the certain NP model, in particular, considering the MSSM, on the masses of the supersymmetric particles involved in the certain transition or decay process. Unfortunately, these parameters cannot be theoretically predicted from the NP model itself. The prediction of the mass spectrum of the supersymmetric particles is a very important issue from phenomenological point of view as well as an essential topic in regard to the direct search for superparticles at the LHC. Thus, the squark mass matrices have been the object of study of numerous analyses in the past.

With this work we have done a contribution to the understanding of the flavour violation in the MSSM and the constraining of the MSSM parameter space from processes which are well known in the SM but very sensitive to contributions of supersymmetric particles with masses of the weak scale. The aim of this study has been the analysis and the constraint of parameters closely related to the mass spectrum of the MSSM. In particular, the impact of flavour changing elements in the LL sector of the squark mass matrices on FCNC processes has been investigated in detail. The supersymmetric contributions at one loop to the meson mixing processes have been calculated. For the evolution of the Wilson coefficients for the $\Delta F = 2$ meson mixing processes the so called magic numbers from the two loop anomalous dimension matrix in the regularisation independent renormalisation scheme have been calculated using loop results from the literature.

Considering the recent analysis of the CKMfitter collaboration with A. Lenz and U. Nierste concerning the possible amount of NP contribution to the $B_d - \bar{B}_d$ and $B_s - \bar{B}_s$ mixing processes, we could obtain a relation between the allowed regions for the parameters which measure the NP contribution in the B_d and B_s sector. We have found that a big chargino contribution to the $B_s - \bar{B}_s$ mixing process caused by a transition between the second and third squark generation implies an effect of the same order in the $B_d - \bar{B}_d$ system as well. However, the opposite statement is not true. If large flavour violation mediated by charginos between the first and the third squark generation sizeably enhances $B_d - \bar{B}_d$ mixing, the effect on the $B_s - \bar{B}_s$ system is at the per mille level. Taking into account the fact that the NP contribution to the $B_d - \bar{B}_d$ sector characterised by the complex parameter Δ_d is much better constrained than the corresponding parameter Δ_s in the $B_s - \bar{B}_s$ sector, we could link the allowed regions (at 68.3% CL, 95.45% CL and 99.73 CL) in the Δ_d plane to the Δ_s plane provided that the mass insertion δ_{23}^{uLL} is the source of flavour violation. We found that only a small region of the plot related to the $B_s - \bar{B}_s$ is covered in case of an up-type squark mass matrix with equal diagonal elements. However, that region can be enlarged by allowing a mass difference between the diagonal elements of the LL block of the mass mixing matrix or an additional flavour violation stemming from the LR sector. The measurement of the experimental quantities involved in the NP analysis in the $B - \bar{B}$ system of the CKMfitter group is one of the main goals of the LHCb experiment. In future, it will provide data with sufficiently small experimental uncertainty such that the allowed regions for NP would shrink. This would allow the constraining of the difference between the diagonal elements of the LL blocks of the squark mass matrices.

The next topic which has been investigated is the estimation of the maximal possible mass splitting of left handed squarks considering the experimental bounds from the meson mixing process in the neutral $K - \bar{K}$ and $D - \bar{D}$ systems. We analysed four different scenarios taking into account the gluino contribution and the electroweak contributions stemming from neutralino and chargino as well as the mixed neutralino-gluino exchange in the box diagrams. In all MSSM analysis the main focus has been set on gluino contributions. The contributions caused by electroweak interaction effects has been neglected claiming that they are suppressed by a factor g_2^4/g_3^4 in the box diagrams. In fact, in our analysis we found that the gluino contribution is indeed dominant for small gluino masses. However, in the opposite case it can be suppressed because of the cancellation between the crossed

and uncrossed box diagrams. Thus, the usual argument provided by previous analyses that the electroweak contributions can be neglected considering their smallness in comparison to the gluino contribution does not hold anymore in the region where the gluino mass is bigger than the relevant squark mass in the loop function. In the scenario with complete alignment in the up sector the up squark mass matrix is chosen to be diagonal. In the opposite case where the down mass mixing matrix is diagonal there is a complete alignment in the down sector. Further, we obtained the maximal possible mass splitting in a situation with intermediate alignment in the up and down sector where neither the up nor the down mass matrix is diagonal. In the last scenario we have chosen equal diagonal elements and one off-diagonal element with a complex phase which maximises the indirect CP violation in the Kaon system. In this case we obtain the most stringent bound on the mass splitting from $K - \bar{K}$ mixing process. For light gluino masses strong constraints on the mass splitting have been found. However, if the gluino is heavier then the squarks large regions in the MSSM parameter space are allowed from $K - \bar{K}$ and $D - \bar{D}$ mixing where the masses of the left-handed squarks can be highly non-degenerate. This fact can have interesting consequences for LHC benchmark scenarios which usually assume that squarks of the first two generations have the same masses.

The next part of this work has been the numerical analysis on the LL part of the squark mass matrices which aim has been the determination of bounds on the flavour changing parameters δ_{13}^{uLL} and δ_{23}^{uLL} . The simulation is performed in the general MSSM and is mostly independent of boundary conditions. The SUSY contributions from charged Higgs bosons, charginos and gluinos are considered. The inclusion of electroweak contributions to the box diagrams which have been neglected in almost all previous analyses of this type is important especially for the regions in the MSSM parameter space where the gluino mass is bigger than the squark masses. As we have shown, in this regions the gluino contribution suffers from the fact that it is a Majorana particle and a second, crossed box diagram occurs: A cancellation between these two kinds of boxes can appear. Because of this fact the consideration of only strong SUSY contributions to the meson mixing is not justified in general.

Starting with the $B_s - \bar{B}_s$ mixing process and assuming first $\delta_{13}^{uLL} = 0$ a scan over the real and imaginary parts of δ_{23}^{uLL} has been performed. The value determined for δ_{13}^{uLL} is subsequently used as a new input in order to determine a stable value in an iterative way. In many previous analyses the mass insertion approximation has been used in order to

avoid complications which can occur in case of exact diagonalisation of the squark mass matrices. However, the mass insertion approximation is not valid for large off-diagonal elements. We perform the analysis with exact diagonalisation of the squark mass matrices. This has the advantage that we are not restricted to a small mass insertions only but our approach is valid when during the scan over the real part and imaginary part of δ_{23}^{uLL} the calculation is done with big values of this flavour-changing parameter as well. The $B_d - \bar{B}_d$ and $B_s - \bar{B}_s$ mixing are very suitable processes for NP searches and constraints on parameters of different NP scenarios because they belong to the rare processes which are very sensitive to NP effects and are experimentally known to a good accuracy as well. Therefore, the mixing of neutral B mesons have been the object of study of many analyses on MSSM parameter space. However, usually the processes of meson mixing in the B_s and B_d system have been treated independently from each other. In our analysis we have taken into account the correlation between the $B_s - \bar{B}_s$ and $B_d - \bar{B}_d$ mixing processes given by the ratio of the corresponding decay constants. This is an additional constraint in the analysis. Another advantage of our approach is given by the fact that the ratio of the decay constants is determined by calculations on the lattice to a much better precision than the decay constants themselves.

We investigate two cases, the SM regime where the numerical values of all observables have been taken to be in their 2σ experimental regions such that the SM is not excluded as well as the maximal NP regime. In the last the experimental values of the input parameters are chosen in such a way that the maximal tension between the experimental observables and their SM predictions occur. In addition, we test whether the values for the studied mass insertions which are allowed from $B_s - \bar{B}_s$ and $B_d - \bar{B}_d$ mixing satisfy the bounds from the branching ratio of the inclusive $B \rightarrow X_s \gamma$ decay as well as the bounds from the parameter ϵ_K which measures the indirect CP violation in the neutral Kaon system. The indirect CP violation parameter $|\epsilon_K|$ was not considered by many analyses in the past. However, considering recent lattice calculations allow the determination of the non-perturbative part of the $K - \bar{K}$ mixing amplitude with a good enough precision such that $|\epsilon_K|$ becomes an important quantity for NP searches or placing constraints on MSSM parameters. Furthermore, we check the size of the SUSY contribution governed by the determined flavour-changing parameters δ_{23}^{uLL} and δ_{13}^{uLL} to the $D - \bar{D}$ mixing process. For the chosen point in the MSSM parameter space we find that the 2σ regions of the experimental observables are not violated if the real and imaginary parts of the mass insertions do not exceed the intervals $-0.010 < \text{Re}(\delta_{LL}^{u13}) < 0.025$, $-0.03 < \text{Im}(\delta_{LL}^{u13}) < 0.01$, $-0.08 < \text{Re}(\delta_{LL}^{u23}) < 0.18$ and

$-0.325 < \text{Im}(\delta_{LL}^{u23}) < 0.125$ for $m_{\tilde{g}} = 500 \text{ GeV}$ and $m_{\tilde{q}} = 500 \text{ GeV}$. It is found that for the studied points in the MSSM parameter space the flavour violation in the D meson system caused by the product of the mass insertions δ_{23}^{uLL} and δ_{13}^{uLL} is not sufficient to explain the current experimental bounds on the $D - \bar{D}$ transition amplitude. In order to explain the mixing of neutral D mesons as a pure supersymmetric effect the flavour violation has to be enhanced through the mass insertion δ_{12}^{uLL} and/or additional mass insertion in the LR sector of the squark mass matrix.

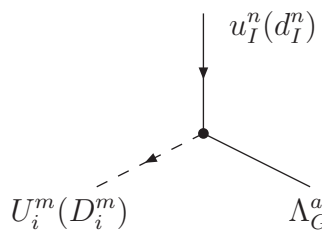
In the future the numerical analysis can be extended to the LR sector of the squark mass matrices. While the LL parts of the up-type and down-type squark mass matrices are related to each other because of the $SU(2)$ gauge symmetry of the left-handed fermion sector their LR blocks are completely independent. If the LL part of the up-type squark mass matrix is not proportional to the unit matrix in the LL part of the down-type squark mass matrix off-diagonal elements are generated which are flavour violating and induce a gluino contribution to the $B - \bar{B}$ meson mixing processes. Practically, a non minimal chargino contribution necessarily leads to a gluino contribution in the $B - \bar{B}$ mixing. However, because of the absent relation between the LR blocks of the squark mass matrices we have the freedom to choose their elements independently. In this way one has better control on the different SUSY contributions to the meson mixing processes and can investigate the limits given by only chargino contribution to the box diagrams and absent gluino ones or vice versa. It would be interesting to investigate the more general case with a flavour violation caused by off diagonal elements in the LL or LR block of the mass mixing matrices in the presence of diagonal elements in the LR block as well. Even if these elements do not affect directly the flavour changing process they allow an additional chirality flip inside the same squark generation. Through the change of the squark mass eigenstates by the presence of these additional flavour-conserving but chirality-changing squark mass matrix elements all supersymmetric contributions to the meson mixing processes would be affected. Furthermore, the obtained bounds on the mass insertions affect single top production processes which is an important topic for the LHC.

A. APPENDIX

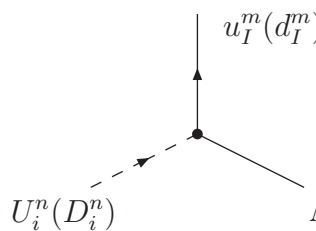
A.1. The Feynman rules for MSSM

In following we write the Feynman rules which have been used in the calculation of the supersymmetric contributions to the considered processes in the MSSM. For the Feynman rules listed below we use the conventions for diagonalising the mass mixing matrices for squarks and gauginos given in Ch. 4.2. The obtained results of the calculation of the Wilson coefficients for the meson mixing processes are in full agreement with the results given in the appendix of [59]. Note that the authors of [59] use the convention of [43].

A.1.1. Quark-squark-gluino vertices

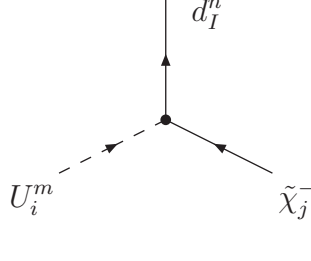


$$= -i\sqrt{2}gY_{mn}^a [(Z_{U(D)})^{iI} P_L - (Z_{U(D)})^{i(I+3)} P_R]$$

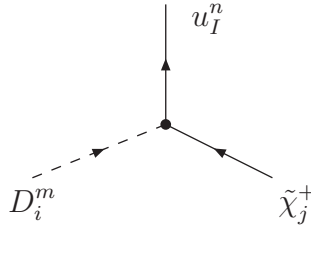


$$= -i\sqrt{2}gY_{mn}^a [(Z_{U(D)}^\dagger)^{Ii} P_R - (Z_{U(D)}^\dagger)^{(I+3)i} P_L]$$

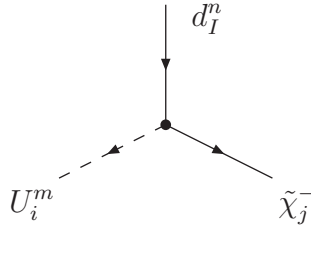
A.1.2. Quark-squark-chargino vertices



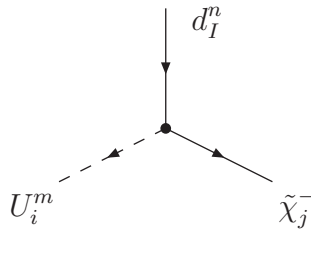
$$= i \frac{e}{s_W} \sum_{J=1}^3 \left[(-Z_U^{\dagger J i} V_{j1} + Z_U^{\dagger (J+3) i} V_{j2} K_U^J) P_R + Z_U^{\dagger J i} U_{2j}^{\dagger} K_D^I P_L \right] K^{IJ} \delta_{mn}$$



$$= i \frac{e}{s_W} \sum_{J=1}^3 \left[(-Z_D^{\dagger J i} U_{j1} + Z_D^{\dagger (J+3) i} U_{j2} K_D^J) P_R + Z_D^{\dagger J i} V_{2j}^{\dagger} K_U^I P_L \right] K^{IJ} \delta_{mn}$$

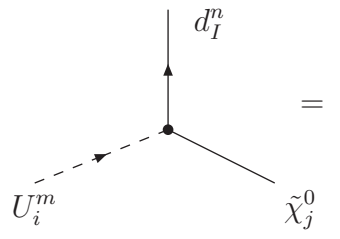


$$= i \frac{e}{s_W} \sum_{J=1}^3 \left[(-Z_U^{iJ} V_{1j}^{\dagger} + Z_U^{i(J+3)} V_{2j}^{\dagger} K_U^J) P_L + Z_U^{iJ} U_{j2} K_D^I P_R \right] K^{JI} \delta_{mn}$$

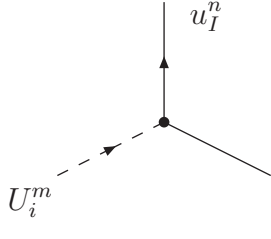


$$= i \frac{e}{s_W} \sum_{J=1}^3 \left[(-Z_U^{iJ} V_{1j}^{\dagger} + Z_U^{i(J+3)} V_{2j}^{\dagger} K_U^J) P_L + Z_U^{iJ} U_{j2} K_D^I P_R \right] K^{JI} \delta_{mn}$$

A.1.3. Quark-squark-neutralino vertices

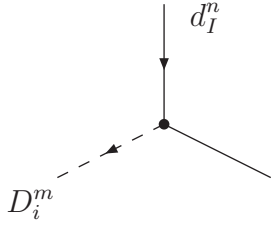


$$= i \frac{e}{s_W} \left\{ \left[\left(-\sqrt{2} (Q_d + \frac{1}{2}) \tan \theta_W Z_N^{j1} + \frac{1}{2} Z_N^{j2} \right) Z_D^{\dagger I i} - Z_D^{\dagger (I+3) i} Z_N^{j4} K_D^I \right] P_L + \left(\sqrt{2} Q_d Z_N^{\dagger 1j} \tan \theta_W Z_U^{\dagger (I+3) i} - Z_D^{\dagger I i} Z_N^{\dagger 4j} K_D^I \right) P_R \right\} \delta_{mn}$$



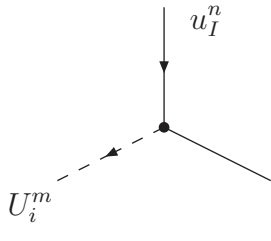
A Feynman diagram showing a vertex with three external lines. A solid line labeled u_I^n enters from the top. A dashed line labeled U_i^m enters from the bottom-left. A solid line labeled $\tilde{\chi}_j^0$ exits to the bottom-right.

$$= i \frac{e}{s_W} \left\{ \left[\left(-\sqrt{2} \left(Q_u - \frac{1}{2} \right) \tan \theta_W Z_N^{j1} - \frac{1}{2} Z_N^{j2} \right) Z_U^{\dagger I i} - Z_U^{\dagger (I+3) i} Z_N^{j4} K_U^I \right] P_L \right. \\ \left. + \left(\sqrt{2} Q_u Z_N^{\dagger 1 j} \tan \theta_W Z_U^{\dagger (I+3) i} - Z_U^{\dagger I i} Z_N^{\dagger 4 j} K_U^I \right) P_R \right\} \delta_{mn}$$



A Feynman diagram showing a vertex with three external lines. A solid line labeled d_I^m enters from the top. A dashed line labeled D_i^m enters from the bottom-left. A solid line labeled $\tilde{\chi}_j^0$ exits to the bottom-right.

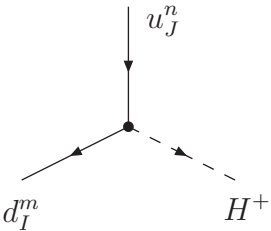
$$= i \frac{e}{s_W} \left\{ \left[\left(-\sqrt{2} \left(Q_d + \frac{1}{2} \right) \tan \theta_W Z_N^{\dagger 1 j} + \frac{1}{2} Z_N^{\dagger 2 j} \right) Z_D^I - Z_D^{i(I+3)} Z_N^{\dagger 4 j} K_D^I \right] P_L \right. \\ \left. + \left(\sqrt{2} Q_d Z_N^{j1} \tan \theta_W Z_U^{i(I+3)} - Z_D^I Z_N^{j4} K_D^I \right) P_R \right\} \delta_{mn}$$



A Feynman diagram showing a vertex with three external lines. A solid line labeled u_I^n enters from the top. A dashed line labeled U_i^m enters from the bottom-left. A solid line labeled $\tilde{\chi}_j^0$ exits to the bottom-right.

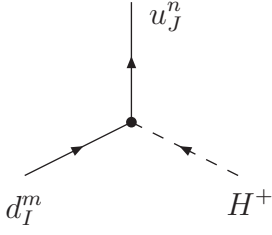
$$= i \frac{e}{s_W} \left\{ \left[\left(-\sqrt{2} \left(Q_u - \frac{1}{2} \right) \tan \theta_W Z_N^{\dagger 1 j} - \frac{1}{2} Z_N^{\dagger 2 j} \right) Z_U^I - Z_U^{i(I+3)} Z_N^{\dagger 4 j} K_U^I \right] P_L \right. \\ \left. + \left(\sqrt{2} Q_u Z_N^{j1} \tan \theta_W Z_U^{i(I+3)} - Z_U^I Z_N^{j4} K_U^I \right) P_R \right\} \delta_{mn}$$

A.1.4. Quark-quark-charged Higgs vertices



A Feynman diagram showing a vertex with three external lines. A solid line labeled u_J^n enters from the top. A solid line labeled d_I^m exits to the bottom-left. A dashed line labeled H^+ exits to the bottom-right.

$$= i \frac{e}{s_W} \left(Z_H^{1i} K_D^I P_L + Z_H^{2i} K_U^I P_R \right) K^{\dagger I J} \delta_{mn}$$



$$= i \frac{e}{s_W} \left(Z_H^{\dagger i1} K_D^I P_R + Z_H^{\dagger i2} K_U^I P_L \right) K^{JI} \delta_{mn}$$

The Yukawa couplings K_D^I and K_U^I used in the Feynman rules listed above are given by

$$K_D^I = \frac{m_d^I}{\sqrt{2} M_W \cos \beta}, \quad K_U^I = \frac{m_u^I}{\sqrt{2} M_W \sin \beta}$$

where m_d^I and m_u^I are the masses of the down-type quarks and up-type quarks of the generation $I = 1, 2, 3$, respectively.

A.2. Plots

In this section we show the flowchart of the program for numerical analysis of δ_{LL}^{u13} and δ_{LL}^{u23} and all the plots which have been described in previous chapters of this work.

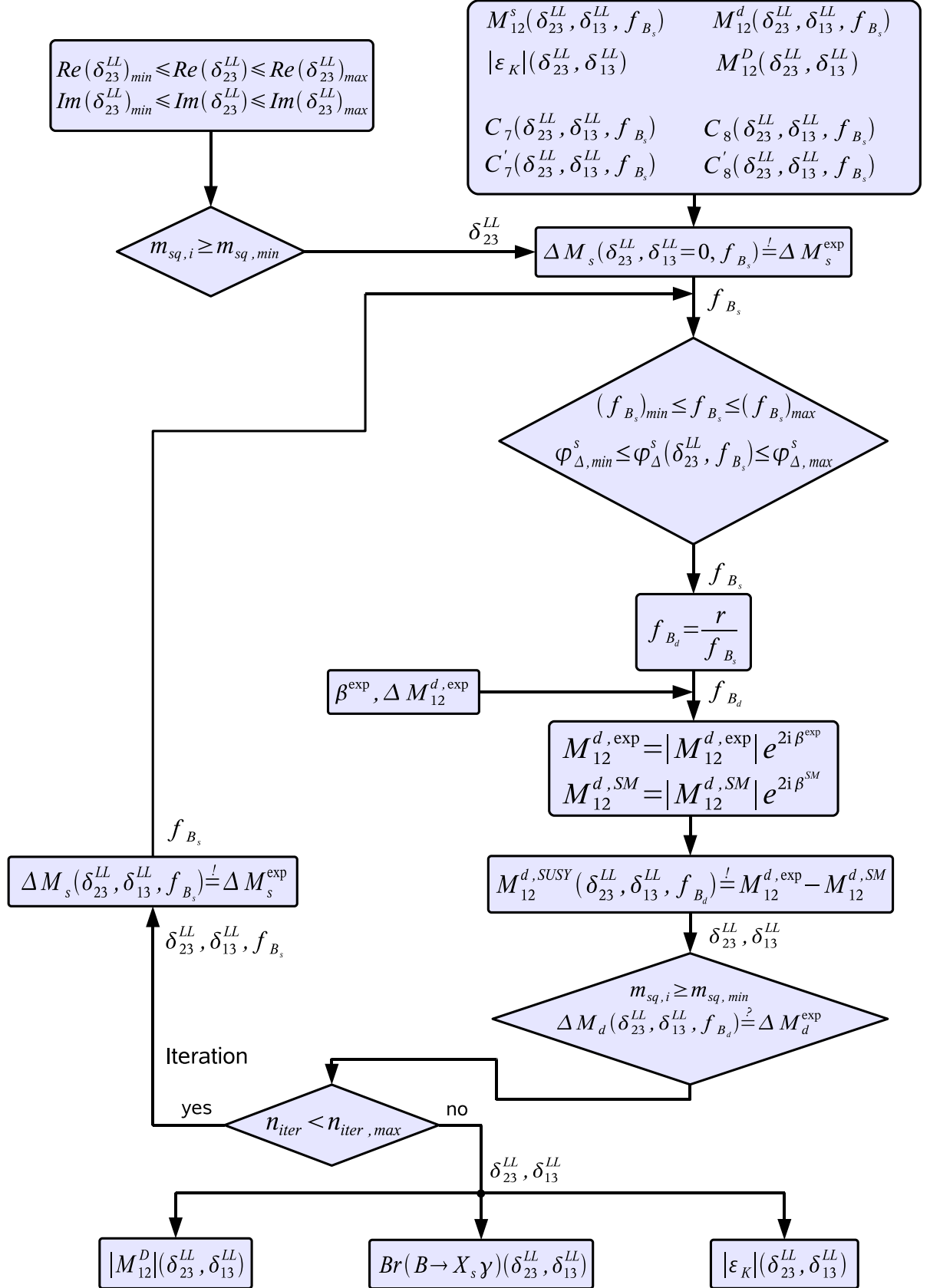


Figure A.1: Logical structure of the program for calculating the matrix elements δ_{13}^{uLL} from δ_{23}^{uLL} (we skip the index "u" in δ_{ij}^{uLL})

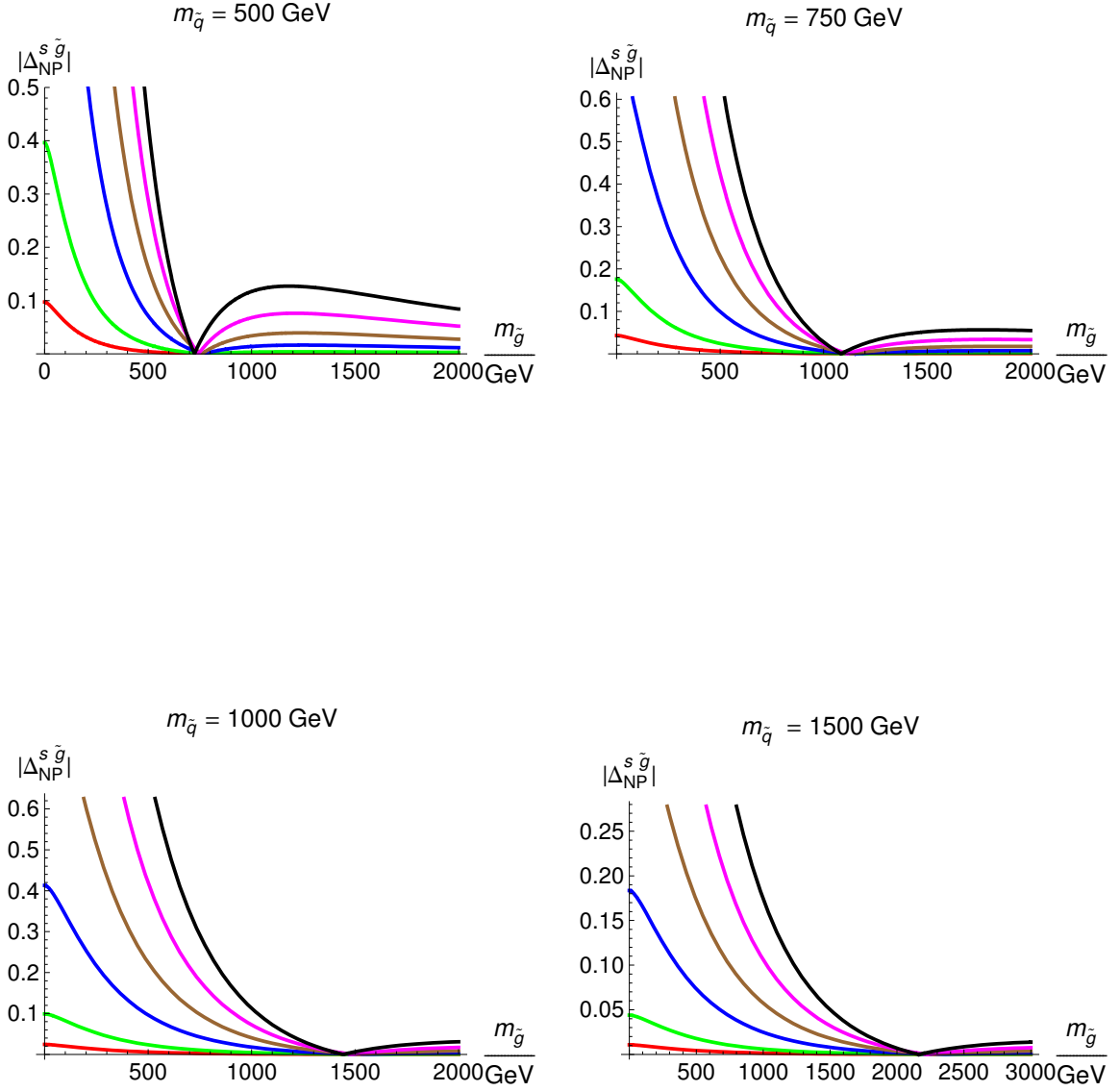


Figure A.2: Relation between the gluino mass $m_{\tilde{g}}$ and $|\Delta_{\tilde{s}}^{\tilde{g}}|$ for different absolute values of the mass insertion $|\delta_{23}^{uLL}|$. From left to right: $|\delta_{23}^{uLL}| = 0.05$ (red), $|\delta_{23}^{uLL}| = 0.1$ (green), $|\delta_{23}^{uLL}| = 0.2$ (blue), $|\delta_{23}^{uLL}| = 0.3$ (brown), $|\delta_{23}^{uLL}| = 0.4$ (magenta), $|\delta_{23}^{uLL}| = 0.5$ (black); $f_{B_s} = 0.228$ GeV.

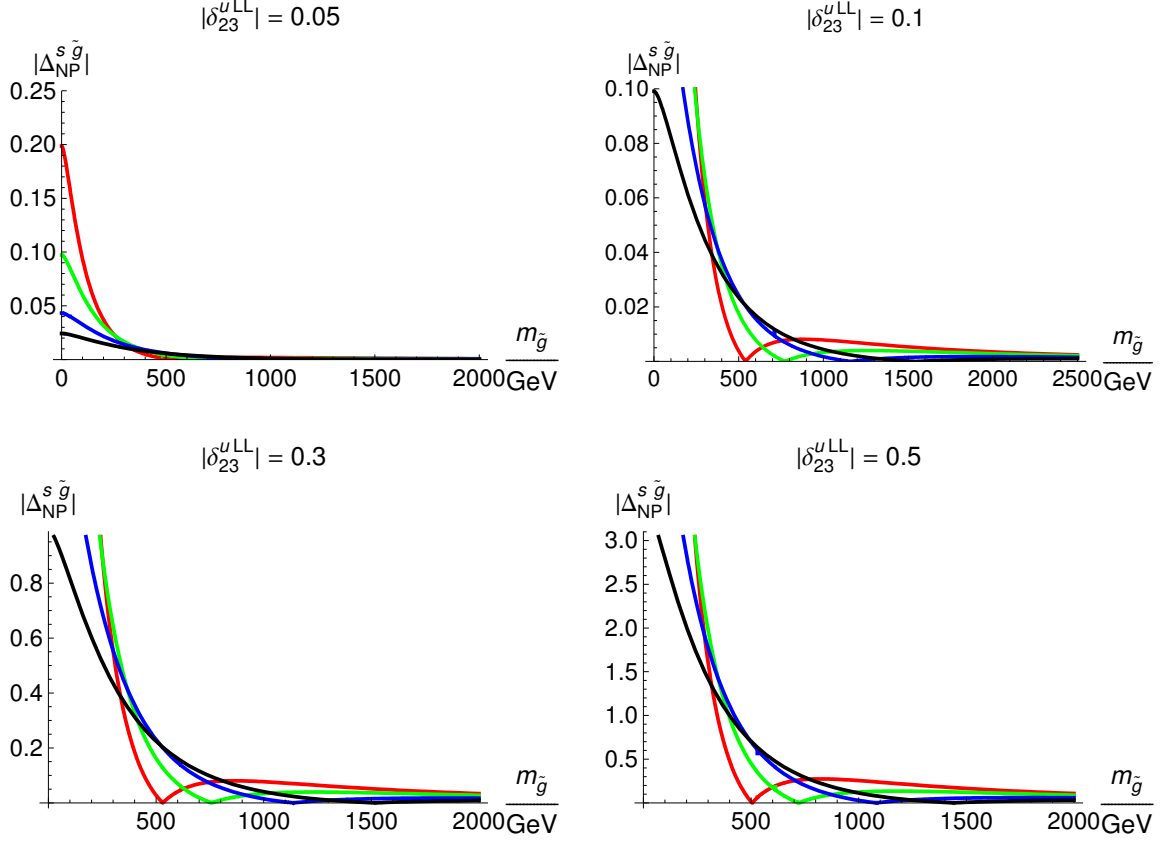


Figure A.3: Relation between the gluino mass $m_{\tilde{g}}$ and $|\Delta_{\text{NP}}^{\tilde{g}}|$ for different squark masses. From left to right according to the minima: $m_{\tilde{q}} = 350$ GeV (red), $m_{\tilde{q}} = 500$ GeV (green), $m_{\tilde{q}} = 750$ GeV (blue), $m_{\tilde{q}} = 1000$ GeV (black); $f_{B_s} = 0.228$ GeV.

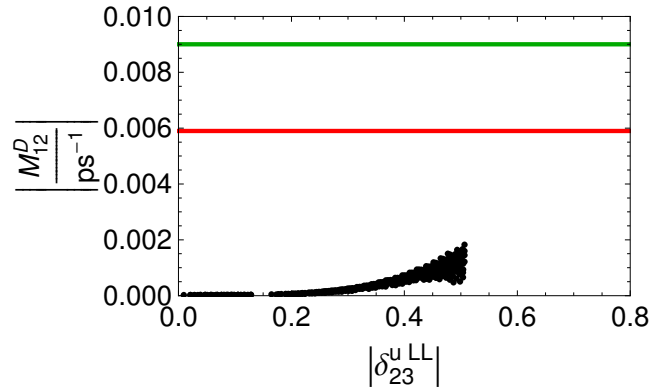


Figure A.4: $|M_{12}^D|$ calculated with the δ_{23}^{uLL} and δ_{13}^{uLL} allowed from $B-\bar{B}$ mixing in the SM allowed regime. Green (upper) line: lower bound 1σ level; Red (lower) line: lower bound 2σ level.

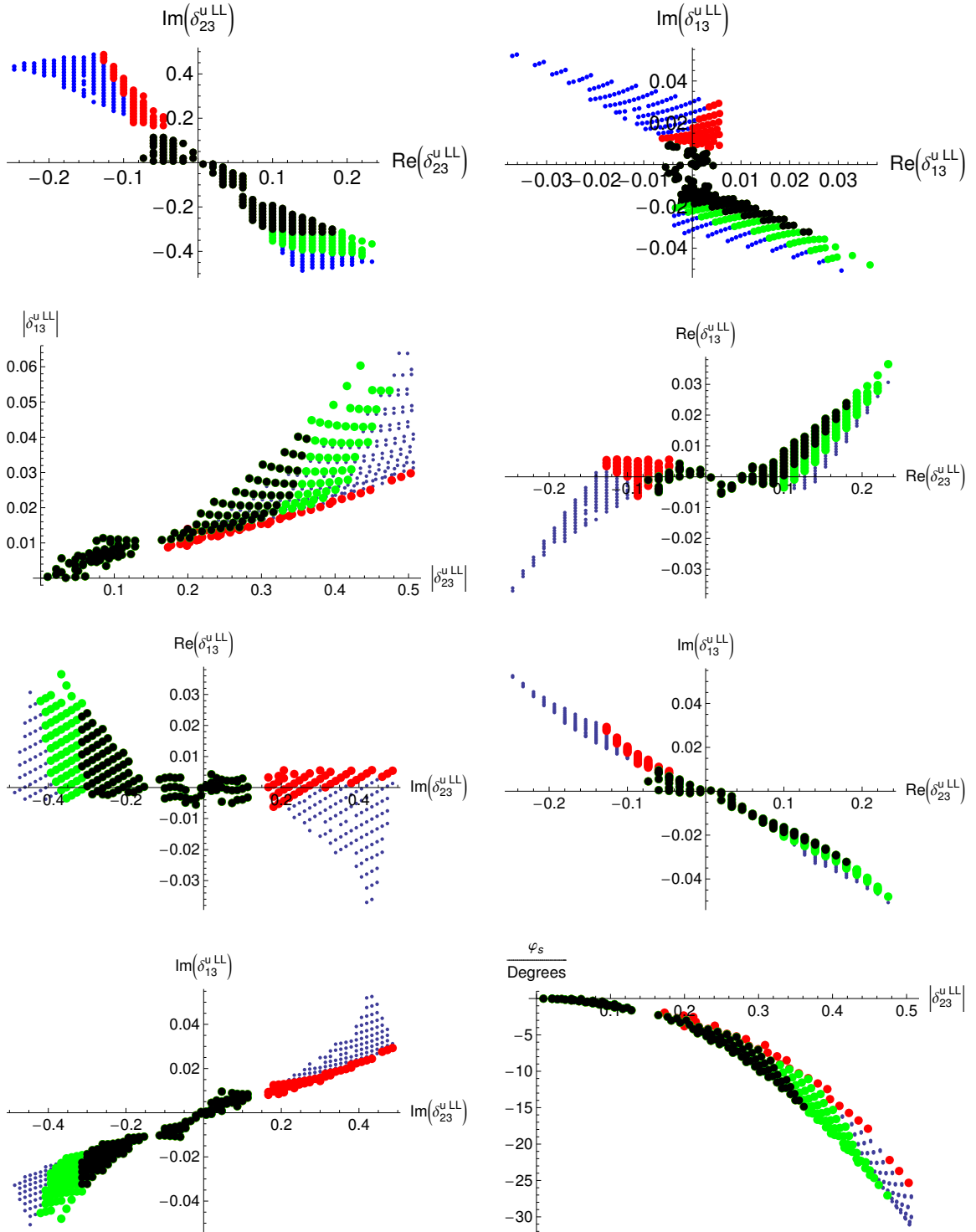


Figure A.5: Bounds on the real part, imaginary part, absolute value of δ_{23}^{uLL} and δ_{13}^{uLL} and φ_s in the SM allowed regime from $B-\bar{B}$ mixing (all points), $K-\bar{K}$ (red), $B \rightarrow X_s \gamma$ (green). The black region is allowed from all processes.

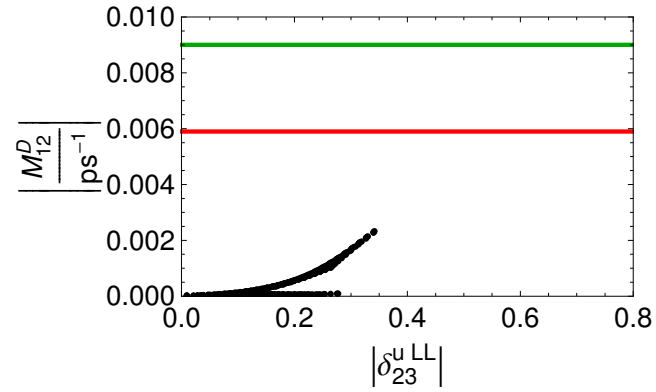
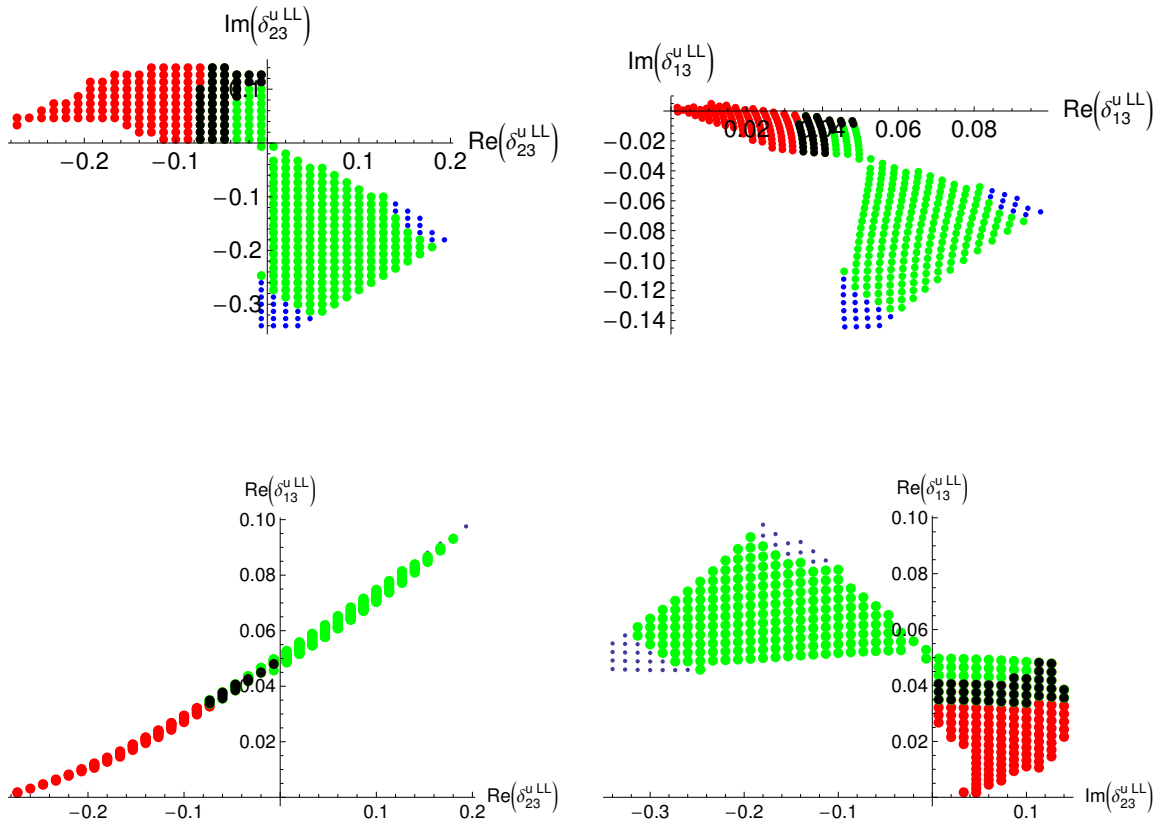


Figure A.6: $|M_{12}^D|$ calculated with the δ_{23}^{uLL} and δ_{13}^{uLL} allowed from $B-\bar{B}$ mixing in the Maximum NP regime. Green (upper) line: lower bound 1σ level; Red (lower) line: lower bound 2σ level.



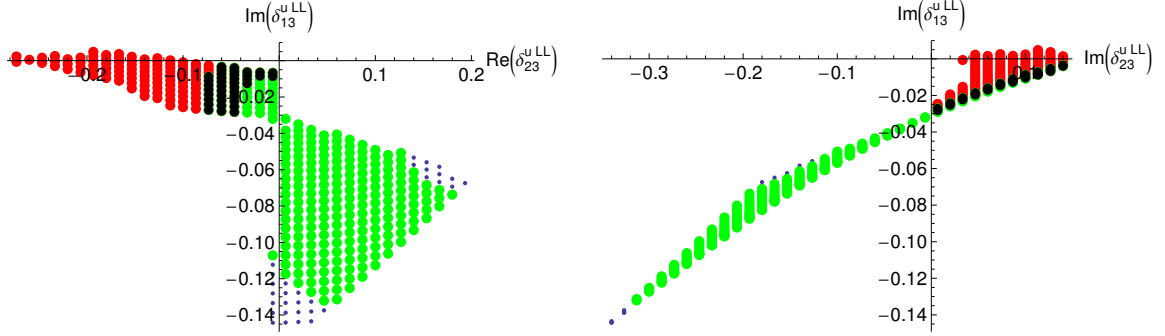


Figure A.7: Bounds on the real part, imaginary part, absolute value of δ_{23}^{uLL} and δ_{13}^{uLL} and ϕ_s in the maximum NP regime from $B-\bar{B}$ mixing (all points), $K-\bar{K}$ (red), $B \rightarrow X_s\gamma$ (green). The black region is allowed from all processes.

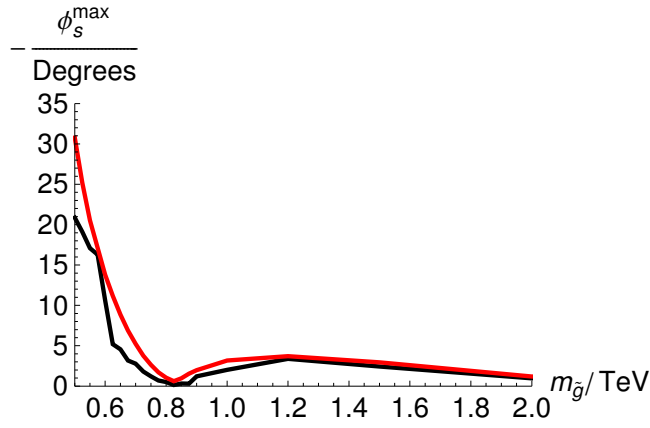


Figure A.8: The maximal value of the mixing phase $-\phi_s$ for different gluino masses. Red (upper) line: from $B-\bar{B}$ mixing; Black (lower) line: points allowed from $B-\bar{B}$ mixing, ϵ_K and $B \rightarrow X_s\gamma$.

BIBLIOGRAPHY

- [1] B. C. Odom, D. Hanneke, B. D'Urso and G. Gabrielse, *Phys. Rev. Lett.* 97 (2006) 030801 [Erratum-*ibid.* 99 (2007) 039902].
- [2] M. Passera, *Nucl. Phys. Proc. Suppl.* 169 (2007) 213 [arXiv:hep-ph/0702027].
- [3] S.L. Glashow (1961). *Nuclear Physics* 22: 579-588.
- [4] F. Englert, R. Brout (1964), *Phys. Rev. Lett* 13: 321-323.
- [5] P. W. Higgs (1964), *Phys. Rev. Lett.* 13: 508-509.
- [6] G. S. Guralnik, C.R. Hagen, T. W. B. Kibble (1964), *Phys. Rev. Lett.* 13: 585-587.
- [7] S. Weinberg (1967), *Phys. Rev. Lett.* 19: 1264-1266.
- [8] A. Salam (1968), N. Svartholm. ed. *Elementary Particle Physics: Relativistic Groups and Analyticity*. Eighth Nobel Symposium. Stockholm: Almquist and Wiksell. pp. 367.
- [9] A. J. Buras, arXiv:hep-ph/9806471.
- [10] G. Martinelli, C. Pittori, C. T. Sachrajda, M. Testa and A. Vladikas, *Nucl. Phys. B* 445 (1995) 81 [arXiv:hep-lat/9411010].
- [11] M. Ciuchini, E. Franco, V. Lubicz, G. Martinelli, I. Scimemi and L. Silvestrini, *Nucl. Phys. B* 523 (1998) 501 [arXiv:hep-ph/9711402].
- [12] M. Ciuchini, E. Franco, G. Martinelli and L. Reina, *Nucl. Phys. B* 415 (1994) 403 [arXiv:hep-ph/9304257].
- [13] A. J. Buras, M. Jamin and M. E. Lautenbacher, *Nucl. Phys. B* 408 (1993) 209 [arXiv:hep-ph/9303284].

-
- [14] F. Gabbiani, E. Gabrielli, A. Masiero and L. Silvestrini, Nucl. Phys. B 477 (1996) 321 [arXiv:hep-ph/9604387].
- [15] M. Beneke, G. Buchalla and I. Dunietz, Phys. Rev. D 54 (1996) 4419 [arXiv:hep-ph/9605259].
- [16] M. Neubert and C. T. Sachrajda, Nucl. Phys. B 483 (1997) 339 [arXiv:hep-ph/9603202].
- [17] A. J. Buras, M. Misiak and J. Urban, Nucl. Phys. B 586 (2000) 397 [arXiv:hep-ph/0005183].
- [18] D. Becirevic, V. Gimenez, G. Martinelli, M. Papinutto and J. Reyes, JHEP 0204 (2002) 025 [arXiv:hep-lat/0110091].
- [19] C. R. Allton *et al.*, Phys. Lett. B 453 (1999) 30 [arXiv:hep-lat/9806016].
- [20] V. Lubicz and C. Tarantino, Nuovo Cim. 123B (2008) 674 [arXiv:0807.4605 [hep-lat]].
- [21] http://ckmfitter.in2p3.fr/plots_Beauty09/latticeinputs280809.pdf.
- [22] http://ckmfitter.in2p3.fr/plots_Beauty09/ckmEval_results_Beauty09.html.
- [23] U. Nierste, arXiv:0904.1869 [hep-ph].
- [24] K. Anikeev *et al.*, arXiv:hep-ph/0201071.
- [25] G. Lüders, Dan. Mat. Phys. Medd. 28 (1954) 5.
- [26] W. Pauli in “Niels Bohr and the Development of Physics”, ed. W. Pauli, L. Rosenfeld and V. Weisskopf (McGraw-Hill, New York, 1955).
- [27] G. Lüders, Ann. Phys. 2 (1957).
- [28] L. Wolfenstein, Phys. Rev. Lett. 51 (1983) 1945.
- [29] S. L. Glashow, J. Iliopoulos and L. Maiani, Phys. Rev. D2 (1970) 1285.
- [30] T. Inami, C. S. Lim, Progr. Theor. Phys. 65 (1981) 297.
- [31] A. J. Buras, M. Jamin and P. H. Weisz, Nucl. Phys. B 347 (1990) 491.
- [32] A. J. Buras and P. H. Weisz, Nucl. Phys. B 333 (1990) 66.

- [33] S. Herrlich and U. Nierste, Nucl. Phys. B 476, 27 (1996) [arXiv:hep-ph/9604330].
- [34] S. Herrlich and U. Nierste, Phys. Rev. D 52, 6505 (1995) [arXiv:hep-ph/9507262].
- [35] S. Herrlich and U. Nierste, Nucl. Phys. B 419, 292 (1994) [arXiv:hep-ph/9310311].
- [36] A. J. Buras and D. Guadagnoli, Phys. Rev. D 78 (2008) 033005 [arXiv:0805.3887 [hep-ph]].
- [37] W.-M. Yao et al., Journal of Physics G 33, 1+ (2006).
- [38] A. J. Schwartz, arXiv:0911.1464.
Online update at <http://www.slac.stanford.edu/xorg/hfag/charm/>.
- [39] D. Asner, Phys. Lett. B667:1, p. (783-789), 2008.
- [40] G. Burdman and I. Shipsey, Ann. Rev. Nucl. Part. Sci. 53 (2003) 431 [arXiv:hep-ph/0310076].
- [41] M. Drees, R. Godbole and P. Roy, *Hackensack, USA: World Scientific (2004) 555 p*;
- [42] H. E. Haber and G. L. Kane, Phys. Rept. 117 (1985) 75;
- [43] J. Rosiek, arXiv:hep-ph/9511250.
Online update at <http://www.fuw.edu.pl/~rosiek/rosiek.html>.
- [44] M. Misiak and M. Steinhauser, Nucl. Phys. B 764 (2007) 62 [arXiv:hep-ph/0609241].
- [45] S.Chen et al. (CLEO Collaboration), Phys. Rev. Lett. 87 (2001) 251807 [hep-ex/0108032].
- [46] K.Abe et al. (Belle Collaboration), Phys. Lett. B 511 (2001) 151 [hep-ex/0103042].
- [47] P. Koppenburg et al. [Belle Collaboration], Phys. Rev. Lett. 93, 061803 (2004).
- [48] A. Limosani et al. (Belle Collaboration), Phys. Rev. Lett. 103 (2009) 241801 [arXiv:0907.1384].
- [49] B.Aubert et al. (BaBar Collaboration), Phys. Rev. D 72 (2005) 052004 [hep-ex/0508004].

-
- [50] Phys. Rev. Lett. 97 (2006) 171803 [hep-ex/0607071], Phys. Rev. D 77 (2008) 051103 [arXiv:0711.4889].
- [51] E. Barberio et al. [Heavy Flavor Averaging Group], 0704.3575 [hep-ex] and online update available at <http://www.slac.stanford.edu/xorg/hfag/>.
- [52] A. L. Kagan and M. Neubert, Eur. Phys. J. C 7 (1999) 5 [arXiv:hep-ph/9805303].
- [53] G. Degrossi, P. Gambino and G.F. Giudice, JHEP 0012 009 (2000).
- [54] M. Carena, D.Garcia, U. Nierste and C.E. Wagner, Phys. Lett. B 499, 141 (2001).
- [55] W. de Boer, M. Huber, A. V. Gladyshev and D. I. Kazakov, Eur. Phys. J. C 20 (2001) 689 [arXiv:hep-ph/0102163].
- [56] T. Besmer, C. Greub and T. Hurth, Nucl. Phys. B 609 (2001) 359 [arXiv:hep-ph/0105292].
- [57] F. Borzumati, C. Greub, T. Hurth and D. Wyler, Phys. Rev. D 62 (2000) 075005 [arXiv:hep-ph/9911245].
- [58] C. Greub, T. Hurth and D. Wyler, arXiv:hep-ph/9912420.
- [59] W. Altmannshofer, A. J. Buras and D. Guadagnoli, JHEP 0711 (2007) 065 [arXiv:hep-ph/0703200].
- [60] F. Gabbiani and A. Masiero, Nucl. Phys. B 322, 235 (1989).
- [61] J. S. Hagelin, S. Kelley and T. Tanaka, Nucl. Phys. B 415, 293 (1994).
- [62] F. Gabbiani, E. Gabrielli, A. Masiero and L. Silvestrini, Nucl. Phys. B 477, 321 (1996) [arXiv:hep-ph/9604387].
- [63] L. J. Hall, V. A. Kostelecky and S. Raby, Nucl. Phys. B 267 (1986) 415.
- [64] G. D'Ambrosio, G. F. Giudice, G. Isidori and A. Strumia, Nucl. Phys. B 645, 155 (2002) [arXiv:hep-ph/0207036].
- [65] A. J. Buras, P. Gambino, M. Gorbahn, S. Jager and L. Silvestrini, Phys. Lett. B 500, 161 (2001) [arXiv:hep-ph/0007085].

-
- [66] B. Aubert *et al.* [BaBar Collaboration], Phys. Rev. Lett. 98, 211802 (2007) [arXiv:hep-ex/0703020].
- [67] M. Staric *et al.* [Belle Collaboration], Phys. Rev. Lett. 98, 211803 (2007) [arXiv:hep-ex/0703036].
- [68] K. Abe *et al.* [Belle Collaboration], Phys. Rev. Lett. 99, 131803 (2007) [arXiv:0704.1000 [hep-ex]].
- [69] A. Lenz and U. Nierste, JHEP 0706 (2007) 072 [arXiv:hep-ph/0612167].
- [70] A. Lenz *et al.*, arXiv:1008.1593 [hep-ph].
- [71] M. Ciuchini, E. Franco, A. Masiero and L. Silvestrini, Phys. Rev. D 67, 075016 (2003) [Erratum-ibid. D 68, 079901 (2003)] [arXiv:hep-ph/0212397].
- [72] J. Foster, K. i. Okumura and L. Roszkowski, JHEP 0508, 094 (2005) [arXiv:hep-ph/0506146].
- [73] J. Foster, K. i. Okumura and L. Roszkowski, JHEP 0603 (2006) 044 [arXiv:hep-ph/0510422].
- [74] W. Altmannshofer, A. J. Buras, S. Gori, P. Paradisi, D.M. Straub, Nucl. Phys. B830, 17-94, 2010, [arXiv:0909.1333].
- [75] R. Kowalewski, T. Mannel, Review of Particle Physics, Phys. Lett. B667:1, 951 - 965, 2008.
- [76] S. Dimopoulos and H. Georgi, Nucl. Phys. B 193 (1981) 150.
- [77] A. Crivellin and M. Davidkov, Phys. Rev. D 81 (2010) 095004 [arXiv:1002.2653 [hep-ph]].
- [78] Y. Nir and N. Seiberg, Phys. Lett. B 309 (1993) 337 [arXiv:hep-ph/9304307].
- [79] K. Blum, Y. Grossman, Y. Nir and G. Perez, Phys. Rev. Lett. 102 (2009) 211802 [arXiv:0903.2118 [hep-ph]].
- [80] J. S. Hagelin, S. Kelley and T. Tanaka, Nucl. Phys. B 415 (1994) 293.
- [81] O. Gedalia, L. Mannelli and G. Perez, arXiv:1002.0778 [hep-ph].

-
- [82] M. Ciuchini *et al.*, JHEP 9810 (1998) 008 [arXiv:hep-ph/9808328].
- [83] M. Ciuchini, E. Franco, D. Guadagnoli, V. Lubicz, M. Pierini, V. Porretti and L. Silvestrini, Phys. Lett. B 655, 162 (2007) [arXiv:hep-ph/0703204].
- [84] O. Gedalia, Y. Grossman, Y. Nir and G. Perez, Phys. Rev. D 80, 055024 (2009) [arXiv:0906.1879 [hep-ph]].
- [85] C. Amsler *et al.* [Particle Data Group], Phys. Lett. B **667** (2008) 1.
- [86] E. Barberio *et al.* (Heavy Flavour Averaging Group) arXiv: 0808.1297, and online update at <http://www.slac.stanford.edu/xorg/hfag>.
- [87] J. A. Aguilar-Saavedra *et al.*, Eur. Phys. J. C 46 (2006) 43 [arXiv:hep-ph/0511344].
- [88] A. De Roeck, J. R. Ellis, F. Gianotti, F. Moortgat, K. A. Olive and L. Pape, Eur. Phys. J. C 49 (2007) 1041 [arXiv:hep-ph/0508198].
- [89] T. Hurth and W. Porod, JHEP 0908 (2009) 087 [arXiv:0904.4574 [hep-ph]].
- [90] V. M. Abazov *et al.* [D0 Collaboration], Phys. Rev. Lett. 97 (2006) 021802 [arXiv:hep-ex/0603029].
- [91] A. Abulencia *et al.* [CDF Collaboration], Phys. Rev. Lett. 97, 242003 (2006) [arXiv:hep-ex/0609040].
- [92] S. P. Martin, arXiv:hep-ph/9709356.
- [93] I. J. R. Aitchison, arXiv:hep-ph/0505105.
- [94] I. J. R. Aitchison, "Supersymmetry in particle physics: An elementary introduction", Cambridge, UK: Univ. Pr. (2007).
- [95] A. Donini, V. Gimenez, L. Giusti and G. Martinelli, Phys. Lett. B **470** (1999) 233 [arXiv:hep-lat/9910017].
- [96] R. Babich, N. Garron, C. Hoelbling, J. Howard, L. Lellouch and C. Rebbi, Phys. Rev. D **74**, 073009 (2006) [arXiv:hep-lat/0605016].
- [97] M. Beneke, G. Buchalla, C. Greub, A. Lenz and U. Nierste, Phys. Lett. B **459**, 631 (1999) [arXiv:hep-ph/9808385].

- [98] A. J. Buras, M. E. Lautenbacher and G. Ostermaier, *Phys. Rev. D* **50** (1994) 3433 [arXiv:hep-ph/9403384].

ACKNOWLEDGEMENTS

In the first place I would like to thank my advisor, Prof. Dr. Ulrich Nierste, for giving me the opportunity to join his group and for his support and patience on every stage of my work. A man with remarkable physical comprehension, in numerous discussions he helped me find the optimal solution of many expected and unexpected problems which appeared during my PhD study with useful advice and creative ideas. I learnt a lot of physics beyond the current topics on which my work was concentrated as well. I am grateful for the financial support, especially in the last months of my PhD study.

I would like to thank Prof. Dr. Matthias Steinhauser for agreeing to be the second referee of my PhD thesis, for his support and reliability.

I am grateful to Dr. Schedar Marchetti for the help and useful discussions at the beginning of my PhD study.

I would like to thank Dr. Christopher Smith and Dr. Andreas Crivellin for useful discussions and help.

In my field of responsibility at the Institute for Theoretical Particle Physics, the work as a system administrator, I was supported a lot by Dr. Peter Marquard and Dr. Joachim Brod. I would like to acknowledge their help and support. Dr. Peter Marquard was always available for solving all kinds of computer problems. With big patience he shared his rich experience on administrating of Unix systems with a novice like me. I would like to thank Jens Salomon who undertook many system administration tasks and helped me solving computer problems.

I appreciate the support from my parents, my sister, my friends Radoslav Atanasov and Petar Georgiev, and Prof. Dr. Wolfgang Ruppel. These were the people on whom I always

could count. Their support was very important for me to surmount the problems during hard times.

I am grateful to Miglena Hristova for her support in the last months of my PhD study. Her encouraging words in many pleasant conversations have been very important for me in stressful times.

I would like to thank Mrs. Martina Schorn, the secretary of the Institut for Theoretical Particle Physics, for her help and support in solving administrative problems.

Financial support of the State of Baden-Württemberg through *Strukturiertes Promotionskolleg für Elementarteilchenphysik und Astroteilchenphysik* and by DFG through project C6 of the SFB-TR9 and by BMBF through project 05H09VKF at the Karlsruhe Institute of Technology is gratefully acknowledged.

